Defect-Engineered Metal−Organic Frameworks as Bioinspired Heterogeneous Catalysts for Amide Bond Formation

Bayu I. Z. Ahmad,[a] Ronald T. Jerozal,[a,‡] Sijing Meng,[a,‡] Tristan H. Lambert,[a,*] Phillip J. Milner[a,*]

[a]Department of Chemistry and Chemical Biology, Cornell University, Ithaca, NY, 14853, United States

*tristan.lambert@cornell.edu

*pjm347@cornell.edu

[‡]These authors contributed equally.

Supporting Information

Table of Contents

1. General information.

Unless otherwise noted, all chemicals were purchased from commercial vendors (Sigma Aldrich, Matrix Chemical, AKSci, Alfa Aesar, Oakwood chemical or TCI) and used without additional purification. The solvents *N*,*N*-dimethylformamide (DMF), tetrahydrofuran (THF), ethanol (EtOH), toluene, hexanes, and ethyl acetate (EtOAc) were purchased from commercial vendors. Anhydrous toluene was obtained by vigorously sparging with Ar for 30 min, followed by passage through two columns of activated alumina using a Phoenix SDS JC Meyer Solvent System.

^{1}H NMR, ^{13}C NMR spectra, and ^{19}F NMR spectra were recorded at 500 MHz (^{1}H), 126 MHz (^{13}C), and 376 MHz (^{19}F) on a Bruker AV-III400 (400 MHZ) or AMX500 (500 MHz) spectrometer. Chemical shifts were calibrated using residual solvent as an internal reference ($CDCl_3$: 7.26 ppm ^{1}H NMR, 77.00 ppm ^{13}C NMR). Attenuated total reflectance infrared (ATR-IR) spectra were collected using a Bruker Tensor II IR spectrometer equipped with a diamond ATR attachment. UV/Vis absorption spectra were collected using a Shimadzu UV-2600 spectrophotometer. High-resolution mass spectrometry (HRMS) data were obtained on a Thermo Fisher Scientific Exactive series DART Mass Spectrometer. Reactions were monitored by thin-layer chromatography (TLC) carried out on commercial silica gel plates using UV light as a visualizing agent. Flash chromatography was performed on silica gel 60 (200-300 mesh) using a Biotage Isolera Flash Chromatography system. Gas chromatography (GC) yields were measured using a Nesix GC-2030 from Shimadzu Scientific Instruments. Optical rotations were measured on a Rudolph Research Analytical Autopol I Automatic Polarimeter and are reported in degrees.

Powder X-ray diffraction (PXRD) patterns were collected on a Rigaku Ultima IV diffractometer equipped with a Cu K_α source (λ = 1.54 Å) and were baseline-corrected using OriginPro. The broad reflection from 2–7° 2θ in the PXRD patterns as collected is due to air scattering. Thermogravimetric decomposition profiles were collected on a Q500 V6.7 thermogravimetric analyzer (TGA) using a temperature ramp of 3.00 °C/min from room temperature to 600.00 °C under an atmosphere of zero grade air (20–22% O_2 in N_2). Data analysis was performed using the TRIOS software package. In each sample, the dehydroxylated product was identified in the TGA profiles as occurring directly before the onset of major mass loss consistent with linker combustion, as determined by the first derivative d(Weight)/d(T) (%/C).[1,2] The remaining residue at 600 °C was assumed to be pure ZrO_2. Scanning electron microscopy (SEM) images were taken at 1.0 or 2.0 kV using a Zeiss Gemini 500 or LEO 1550 FESEM scanning electron microscope. The powder samples were immobilized on carbon tape mounted on an aluminum stub. The samples were blown using compressed air to remove excess material not stuck to the tape and then were spin-coated with a carbon and/or Au/Pd layer. Surface area data were collected on a Micromeritics ASAP 2020 or ASAP 2460 gas sorption analyzer using ultrapure N_2 (99.999%) and a liquid N_2 bath. Brunauer-Emmett-Teller (BET) surface areas were determined by linear least squares regression analysis using the linearized form of the BET equation.

2. Synthesis of 3,5-dicarboxypyridine-*N*-oxide monohydrate.

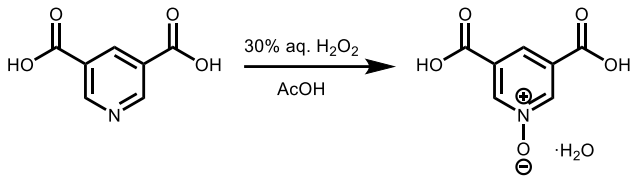

Figure S1. Synthesis of 3,5-dicarboxypyridine-*N*-oxide monohydrate.

Adapted from the literature procedure.[3] A 15 mL screw-cap reaction tube was charged with dinicotinic acid (669 mg, 4.0 mmol), acetic acid (2.5 mL), and 30% aq. H_2O_2 (875 µL). The tube was capped, and the reaction mixture was stirred in a 70 ˚C silicone oil bath for 18 h. At this time, the reaction mixture was allowed to cool to room temperature. The heterogeneous mixture was filtered, and the solid was rinsed with water (10 mL) and EtOAc (10 mL). If impurities remained (as determined by ^{1}H NMR), the solid was further purified by rinsing with additional acetic acid, water, and EtOAc. After drying in a vacuum oven at 110 ˚C overnight, 3,5-dicarboxypyridine-*N*-oxide monohydrate was obtained as a white solid (324 mg, 40% yield). ^{1}H NMR (500 MHz, DMSO-d_6): δ 9.25 (d, J = 2.1 Hz, 2H), 8.64 (t, J = 2.1 Hz, 1H); ^{13}C NMR (126 MHz, DMSO-d_6): δ 166.00, 153.96, 137.79, 127.19. These spectra are consistent with those reported in the literature.[3]

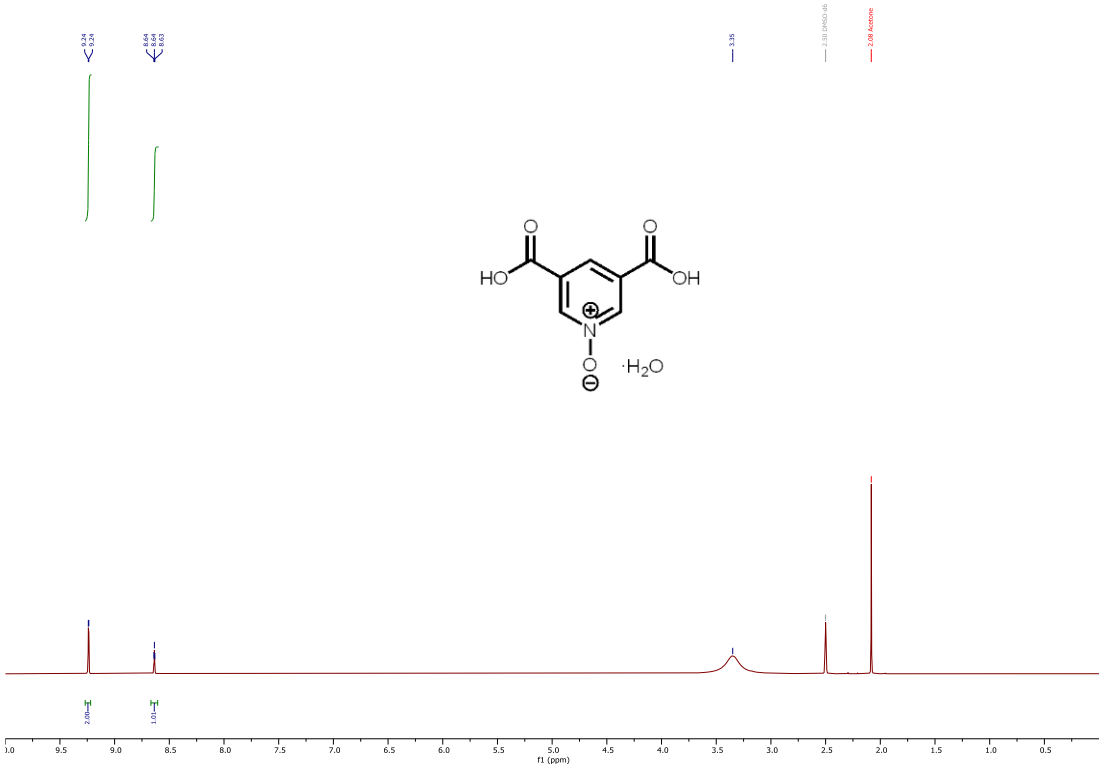

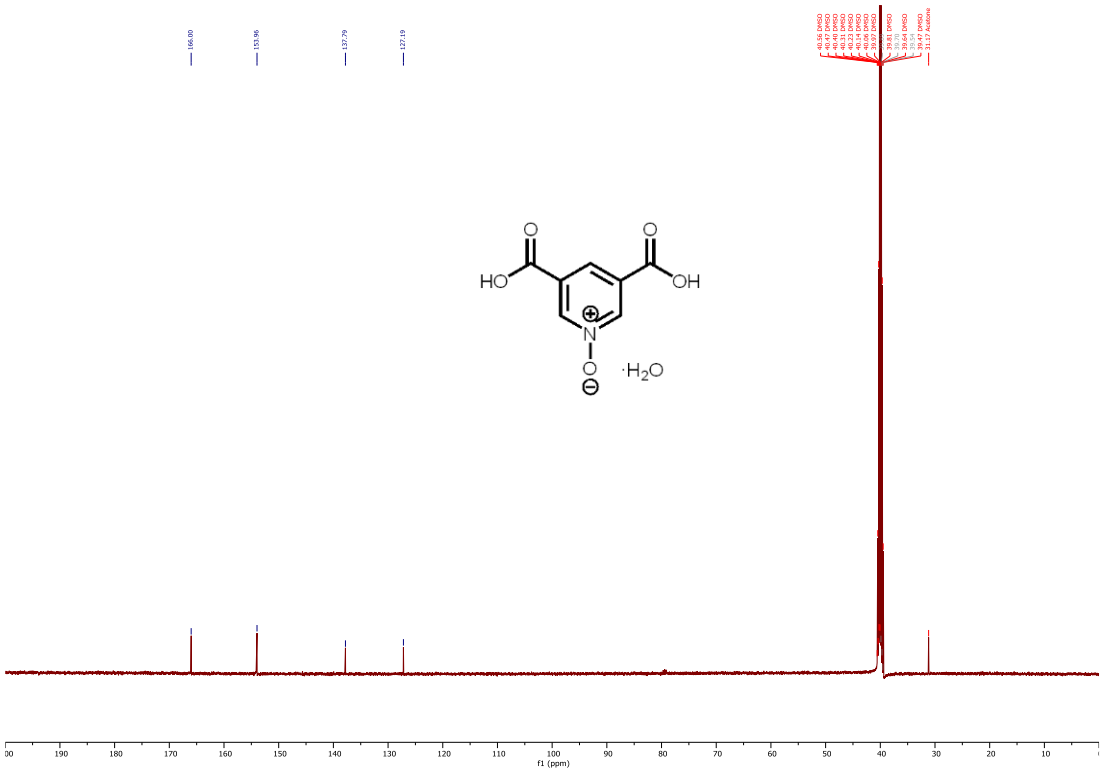

Figure S2. ^{1}H (500 MHz, DMSO-d_6) and ^{13}C (126 MHz, DMSO-d_6) NMR spectra of 3,5-dicarboxypyridine-*N*-oxide monohydrate.

3. Procedures for synthesizing metal−organic frameworks

3.1. General synthetic procedure of pristine and defective metal−organic frameworks.

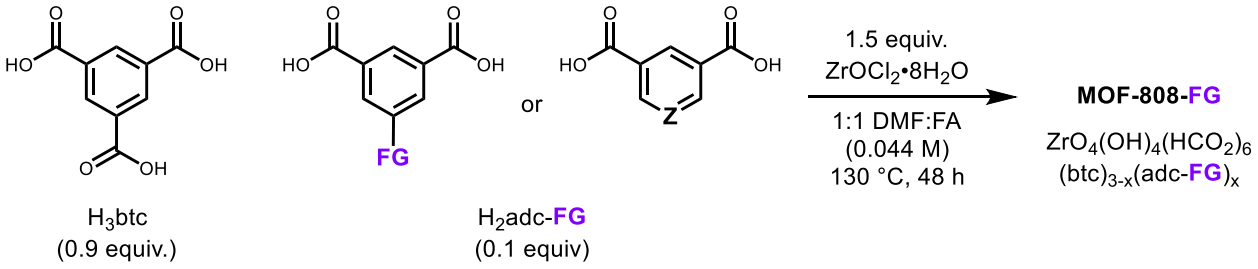

Figure S3. Synthesis of pristine and defective MOF-808 frameworks.

Prepared according to the literature procedure.[4] A 35-mL screw-cap high-pressure flask was charged with $ZrOCl_2 \cdot 8H_2O$ (241.5 mg, 0.75 mmol, 1.5 equiv.) and organic linker(s). For **MOF-808-DF**, the organic linker is only composed of trimesic acid (105.0 mg, 0.5 mmol, 1.0 equiv). For **MOF-808-FG**, the organic linkers are composed of trimesic acid (94.5 mg, 0.45 mmol, 0.9 equiv.) and the corresponding isophthalic acid derivative (0.05 mmol, 0.1 equiv.). Subsequently, a 1:1 mixture of formic acid (FA) and DMF (11.25 mL each, 22.5 mL total) was added to the flask. Once tightly capped, the flask was placed in an oven that had been pre-heated to 130 ˚C. The flask was allowed to stand at 130 ˚C for 48 h. At this time, the reaction mixture was allowed to cool to room temperature. The resulting heterogeneous mixture was centrifuged at 4000 rpm for 10 min, and the supernatant was decanted. The recovered solid was washed by heating in fresh DMF (20 mL) at 130 ˚C for three days, with the solvent replaced with fresh DMF (20 mL) once a day. The solid was next washed with 200-proof EtOH (20 mL) at 70 ˚C for three days, with the solvent replaced with fresh EtOH (20 mL) once a day. The resulting solid was activated under high vacuum (<100 mTorr) at 110 ˚C overnight, yielding the desired MOF as a white solid. All MOFs were stored in a N_2-filled glovebox when not in use.

3.2. Large scale synthesis of MOF-808-py-Nox.

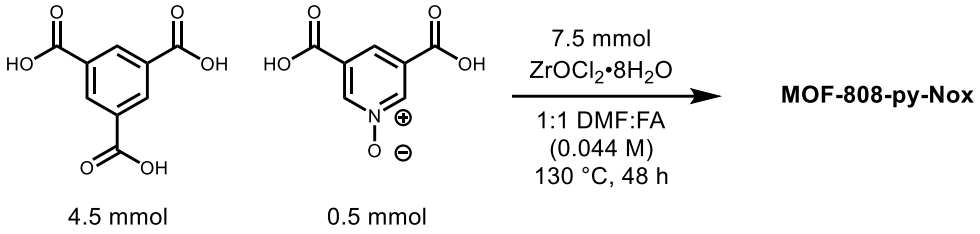

Figure S4. Synthetic scheme of **MOF-808-py-Nox** on gram scale.

The procedure outlined above was scaled up ten-fold to synthesize **MOF-808-py-Nox** on gram scale. A 350-mL pressure flask was charged with trimesic acid (945 mg, 4.5 mmol, 0.9 equiv.), 3,5-dicarboxypyridine-*N*-oxide (100.6 mg, 0.5 mmol, 0.1 equiv.), and $ZrOCl_2 \cdot 8H_2O$ (2.42 g, 7.5 mmol, 1.5 equiv.). Subsequently, a 1:1 mixture of formic acid and DMF (112.5 mL each, 225 mL total) was added to the flask. Once tightly capped, the flask was placed in an oven that had been pre-heated to 130 ˚C. The flask was allowed to stand at 130 ˚C for 48 h. At this time, the reaction mixture was allowed to cool to room temperature. The resulting heterogeneous mixture was centrifuged at 4000 rpm for 10 min, and the supernatant was decanted. The recovered solid was washed by heating in fresh DMF (200 mL) at 130 ˚C for three days, with the solvent replaced with fresh DMF (200 mL) once a day. The solid was next washed with 200-proof EtOH (200 mL) at 70 ˚C for three days, with the solvent replaced with fresh EtOH (200 mL) once a day. The resulting solid was activated under high vacuum (<100 mTorr) at 110 ˚C overnight, yielding the desired MOF as a white solid (1.276 g, 75%). The MOF was stored in a N_2-filled glovebox when not in use.

4. Characterization of metal−organic frameworks.

All synthesized metal−organic frameworks (MOFs) were characterized by PXRD and ^{1}H NMR after acidic or basic digestion, as appropriate. Representative samples were then further characterized by surface area analysis, TGA, ATR-IR spectroscopy, and SEM.

4.1. General procedures.

General procedure for acidic MOF digestion. A 4 mL vial was charged with MOF (~5 mg) and DMSO-d_6 (0.5 mL). Next, 2–5 drops of D_2SO_4 (96-98% wt. in D_2O) were added, and the vial was capped. The vial was heated at 100 °C in a heat block for 12 h until completely homogeneous. The solution was transferred to an NMR tube and analyzed by ^{1}H NMR.

General procedures for basic MOF digestion. A 4 mL vial was charged with MOF (~5 mg) and D_2O (0.5 mL). Next, 2–5 drops of saturated K_3PO_4 solution in D_2O were added, and the vial was capped. The vial was heated at 100 °C in a heat block for 12 h until completely homogeneous. The solution was transferred to an NMR tube and analyzed by ^{1}H NMR.

Calculations for quantifying percent defect incorporation in MOF-808 samples. The integrated signal of a peak of the defect linker is normalized to 1.00. Percent incorporation of the defect linker was determined by the following formula:

$$\text{Percent defect incorporation} = \frac{I_{Defect}}{I_{Defect} + I_{BTC}} \times 100\%$$

where I_{Defect} is the value of the ^{1}H integral of a defect linker divided by the number of equivalent nuclei (1 or 2) contributing to its ^{1}H NMR signal per molecule and I_{BTC} is the ^{1}H integral of trimesic acid divided by the number of equivalent nuclei (3) contributing to its ^{1}H NMR signal per molecule.

Calculating molecular weights of MOF-808 catalysts.

The molecular formula of **MOF-808-DF** is based on the unit cell of the perfect crystal structure of MOF-808, namely $Zr_6O_4(OH)_4(HCO_2)_6[C_6H_3(CO_2)_3]_2$, with a molecular weight of 1363.7 g/mol. Similarly, the generic formula of **MOF-808-FG** is $Zr_6O_4(OH)_4(HCO_2)_6[C_6H_3(CO_2)_3]_{2-x}(adc\text{-}FG)_x$, where x is the percent incorporation of the defective linkers based on ^{1}H NMR analysis upon framework digestion, multiplied by the total number of linkers (2). For example, **MOF-808-py-Nox** with 1% defect incorporation has a formula of $Zr_6O_4(OH)_4(HCO_2)_6[C_6H_3(CO_2)_3]_{1.98}[C_5H_3NO(CO_2)_3]_{0.02}$ and thus a molecular weight of 1363.2 g/mol. This formula does not consider additional charge-balancing ligands, such as formates or hydroxides, to compensate the missing carboxylate of the defective linkers. If it did, **MOF-808-py-Nox** would have a formula of $Zr_6O_4(OH)_{4.2}(HCO_2)_6[C_6H_3(CO_2)_3]_{1.98}$ (M_w = 1366.6 g/mol) or $Zr_6O_4(OH)_4(HCO_2)_{6.2}[C_6H_3(CO_2)_3]_{1.98}$ (M_w = 1372.2 g/mol). These changes have a negligible effect on the calculated molecular weight of the MOF.

4.2. ^{1}H NMR analysis of digested frameworks.

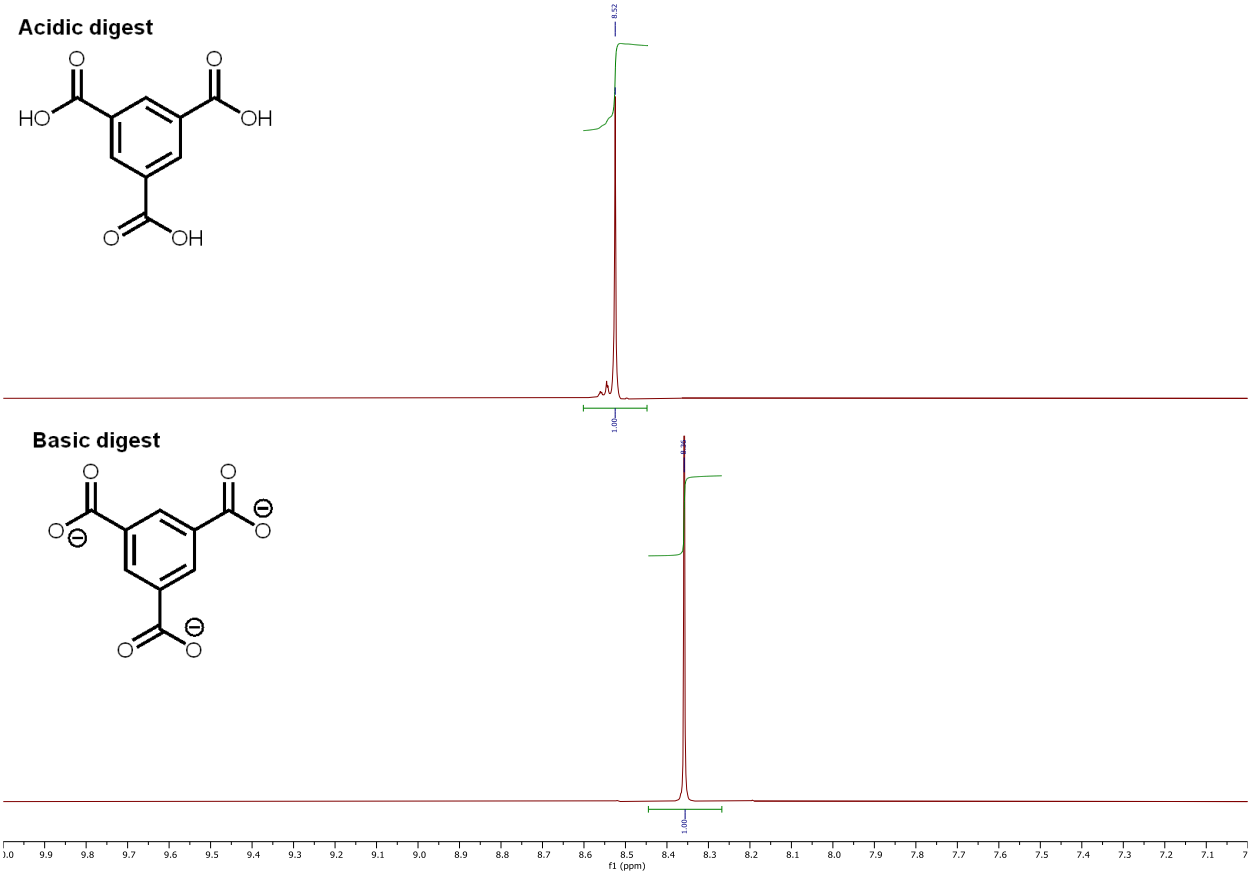

Figure S5. Comparison of ^{1}H NMR spectra of acid and basic-treated trimesic acid for reference.

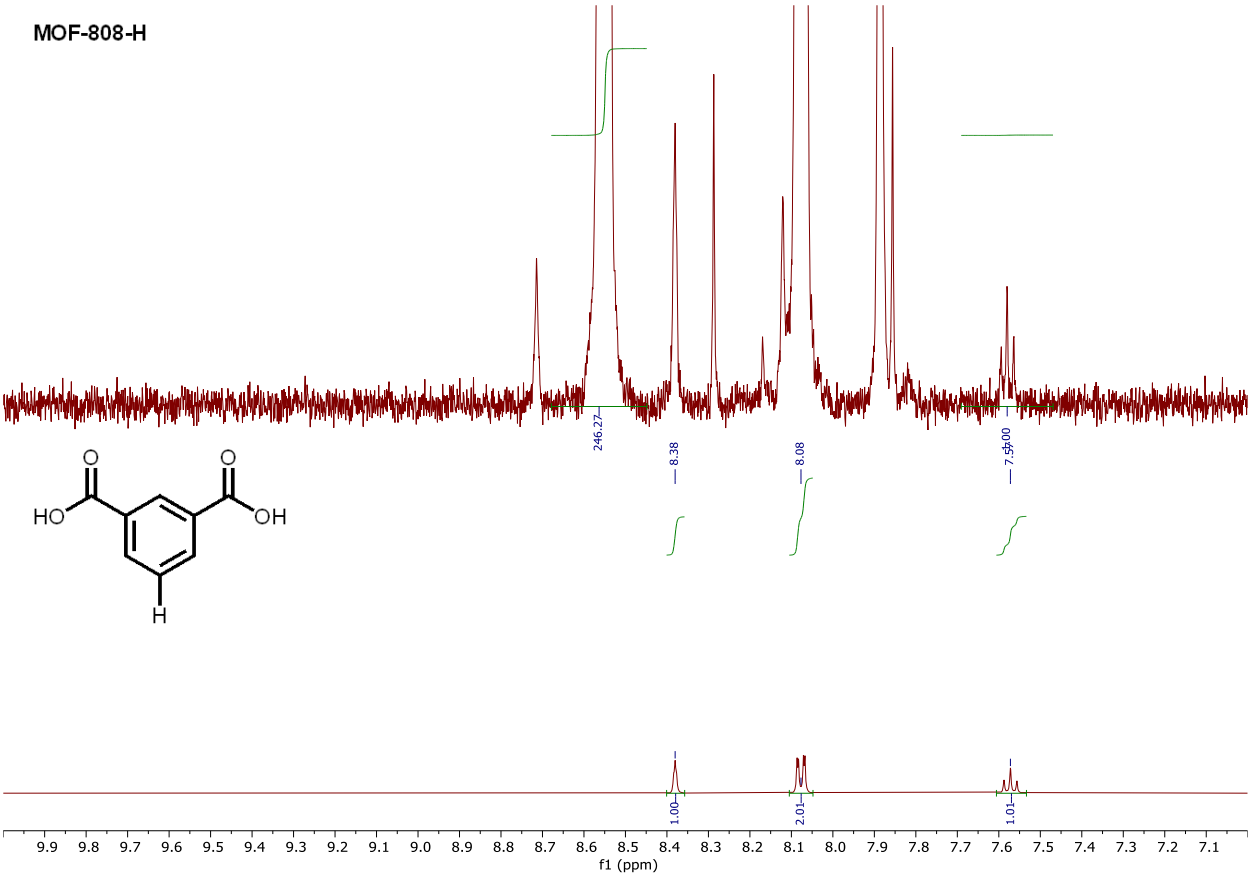

Figure S6. Comparison of ^{1}H NMR spectra of acid-digested isophthalic acid and **MOF-808-H**.

$$\text{Percent defect incorporation} = \frac{I_{Defect}}{I_{Defect}+I_{BTC}} \times 100\% = \frac{1.00}{1.00+\frac{246.27}{3}} \times 100\% \approx 1\%$$

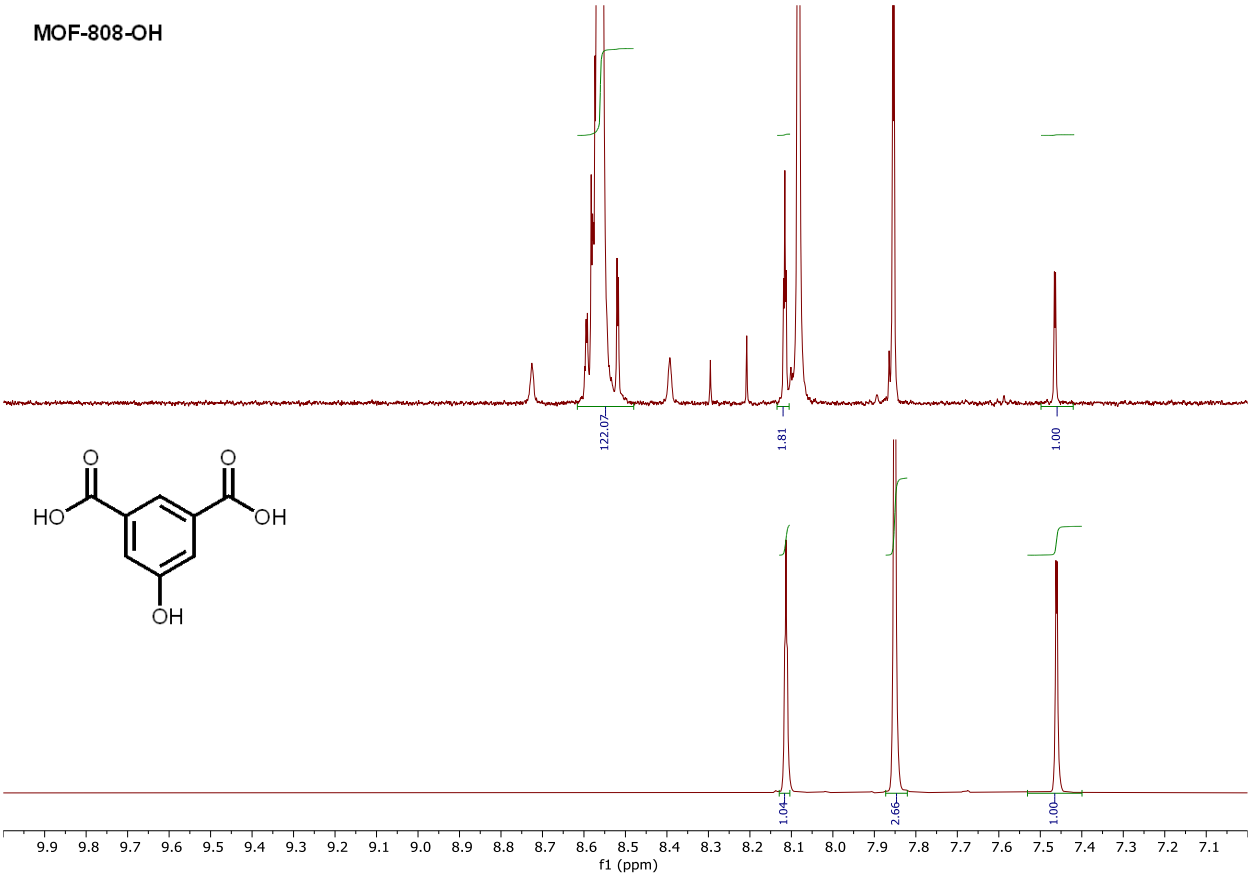

Figure S7. Comparison of ^{1}H NMR spectra of acid-digested 5-hydroxyisophthalic acid and **MOF-808-OH**.

$$\text{Percent defect incorporation} = \frac{I_{Defect}}{I_{Defect}+I_{BTC}} \times 100\% = \frac{1.00}{1.00+\frac{122.07}{3}} \times 100\% \approx 2\%$$

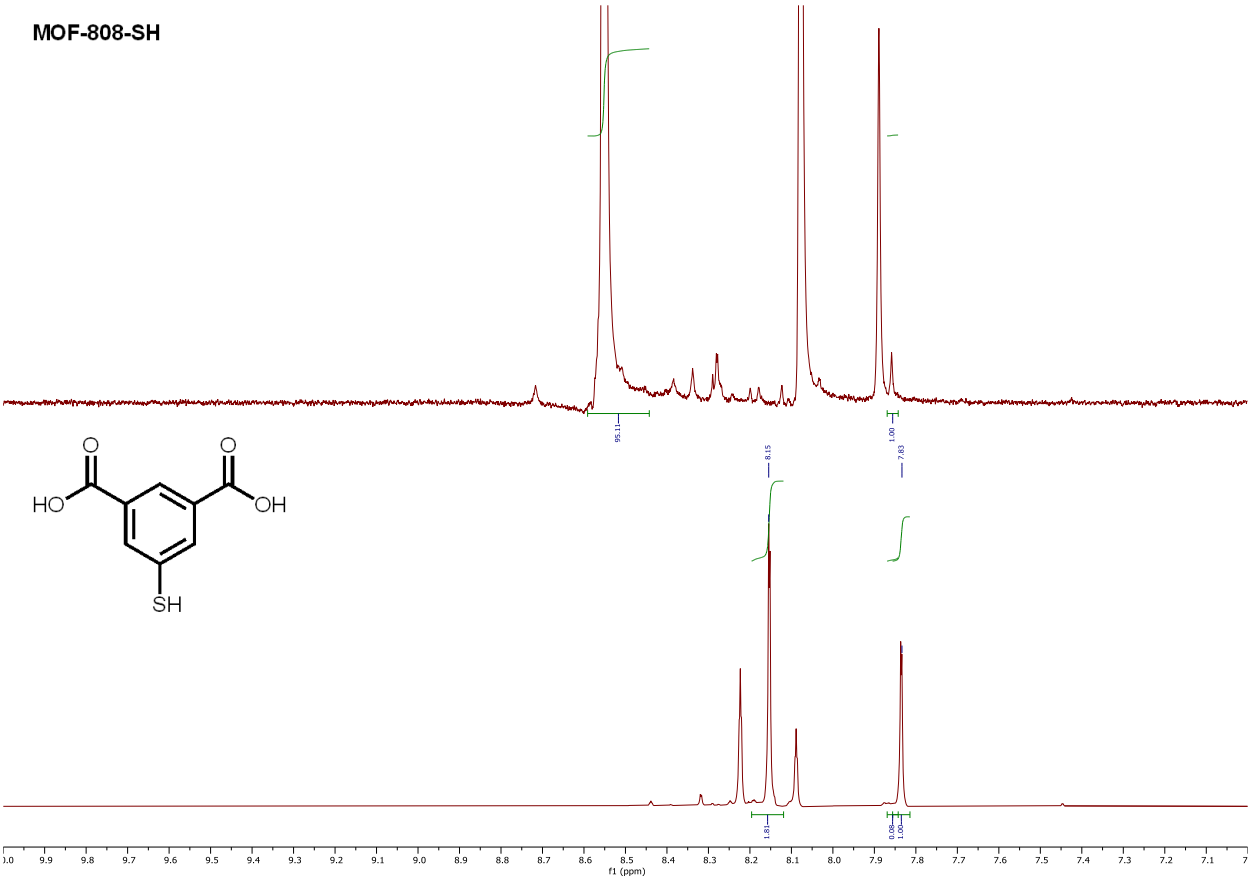

Figure S8. Comparison of ^{1}H NMR spectra of acid-digested 5-mercaptoisophthalic acid and **MOF-808-SH**.

$$\text{Percent defect incorporation} = \frac{I_{Defect}}{I_{Defect}+I_{BTC}} \times 100\% = \frac{1.00}{1.00+\frac{121.97}{3}} \times 100\% \approx 2\%$$

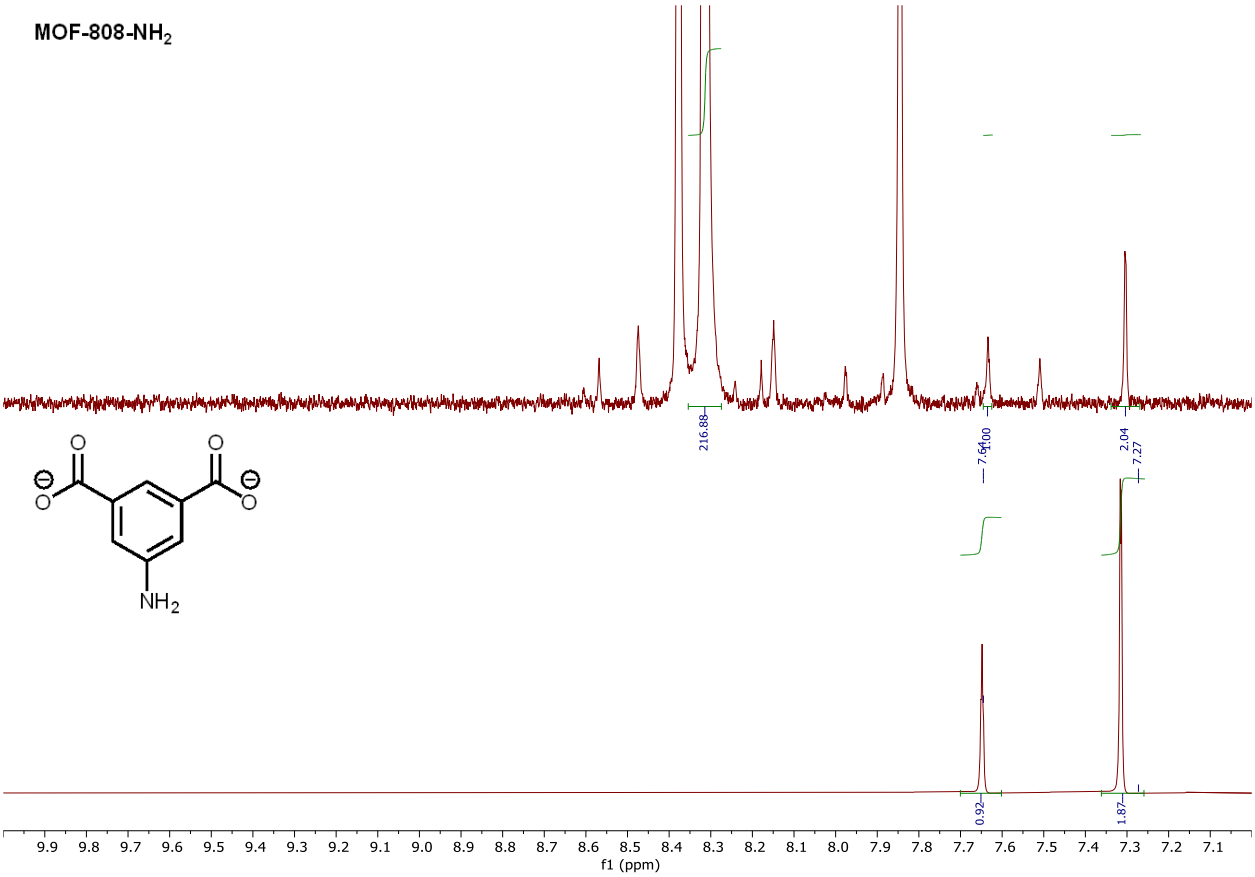

Figure S9. Comparison of ^{1}H NMR spectra of basic-digested 5-aminoisophthalic acid and **MOF-808-NH2**.

$$\text{Percent defect incorporation} = \frac{I_{Defect}}{I_{Defect}+I_{BTC}} \times 100\% = \frac{1.00}{1.00+\frac{216.88}{3}} \times 100\% \approx 1\%$$

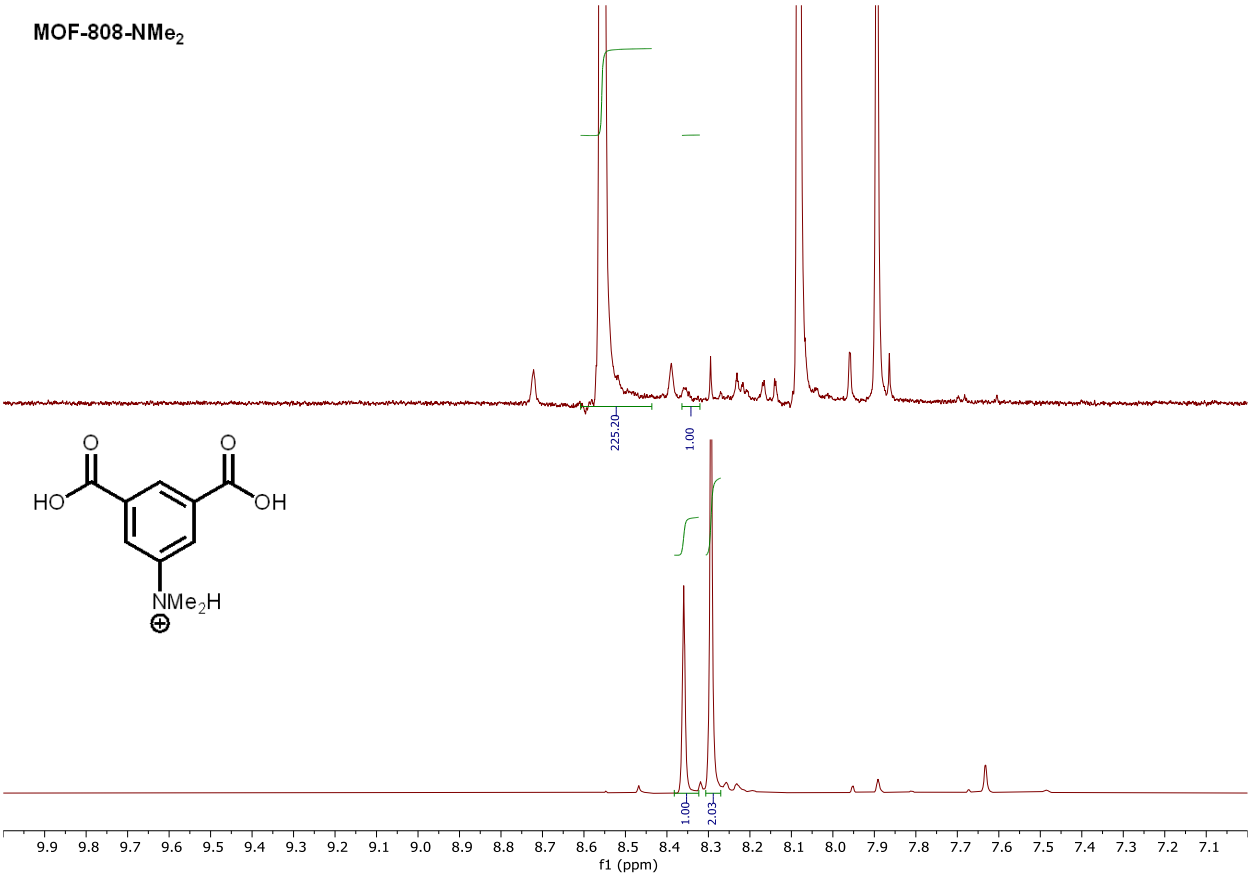

Figure S10. Comparison of ^{1}H NMR spectra of acid-digested 5-(dimethylamino)isophthalic acid and **MOF-808-NMe2**.

$$\text{Percent defect incorporation} = \frac{I_{Defect}}{I_{Defect}+I_{BTC}} \times 100\% = \frac{1.00}{1.00+\frac{225.20}{3}} \times 100\% \approx 1\%$$

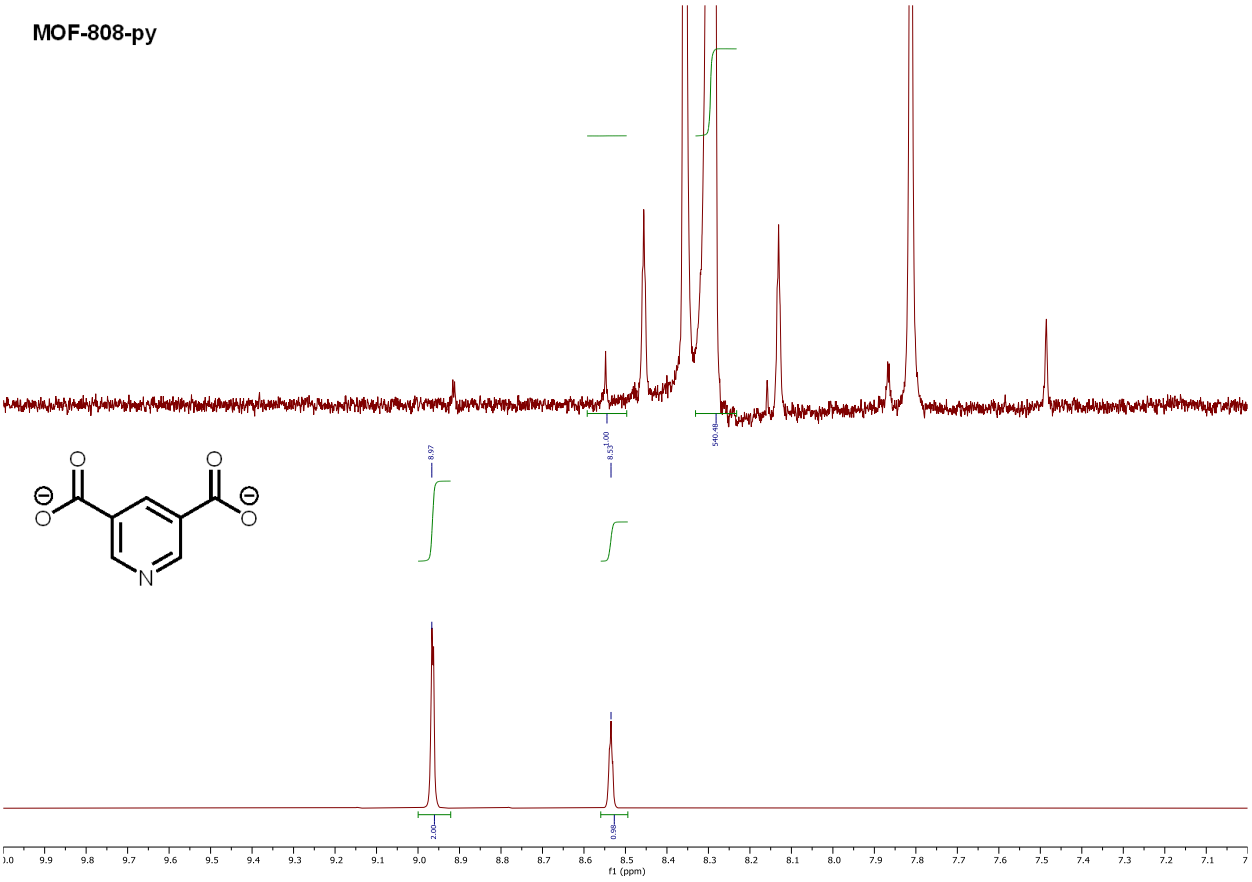

Figure S11. Comparison of ^{1}H NMR spectra of basic-digested dinicotinic acid and **MOF-808-py**.

$$\text{Percent defect incorporation} = \frac{I_{Defect}}{I_{Defect}+I_{BTC}} \times 100\% = \frac{1.00}{1.00+\frac{540.48}{3}} \times 100\% \approx 0.5\%$$

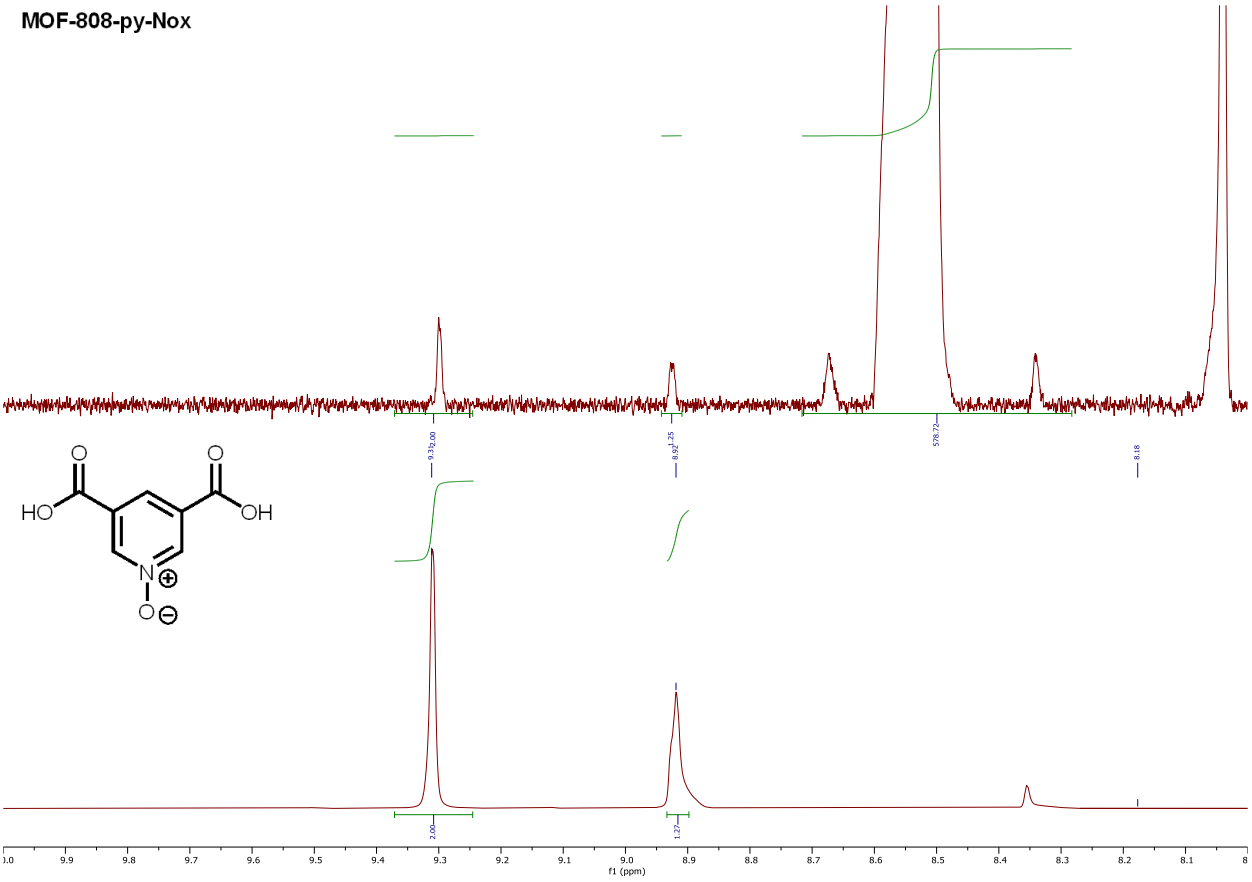

Figure S12. Comparison of ^{1}H NMR spectra of acid-digested dinicotinic acid-*N*-oxide and **MOF-808-py-Nox**.

$$\text{Percent defect incorporation} = \frac{I_{Defect}}{I_{Defect}+I_{BTC}} \times 100\% = \frac{1.00}{1.00+\frac{578.72}{3}} \times 100\% \approx 0.5\%$$

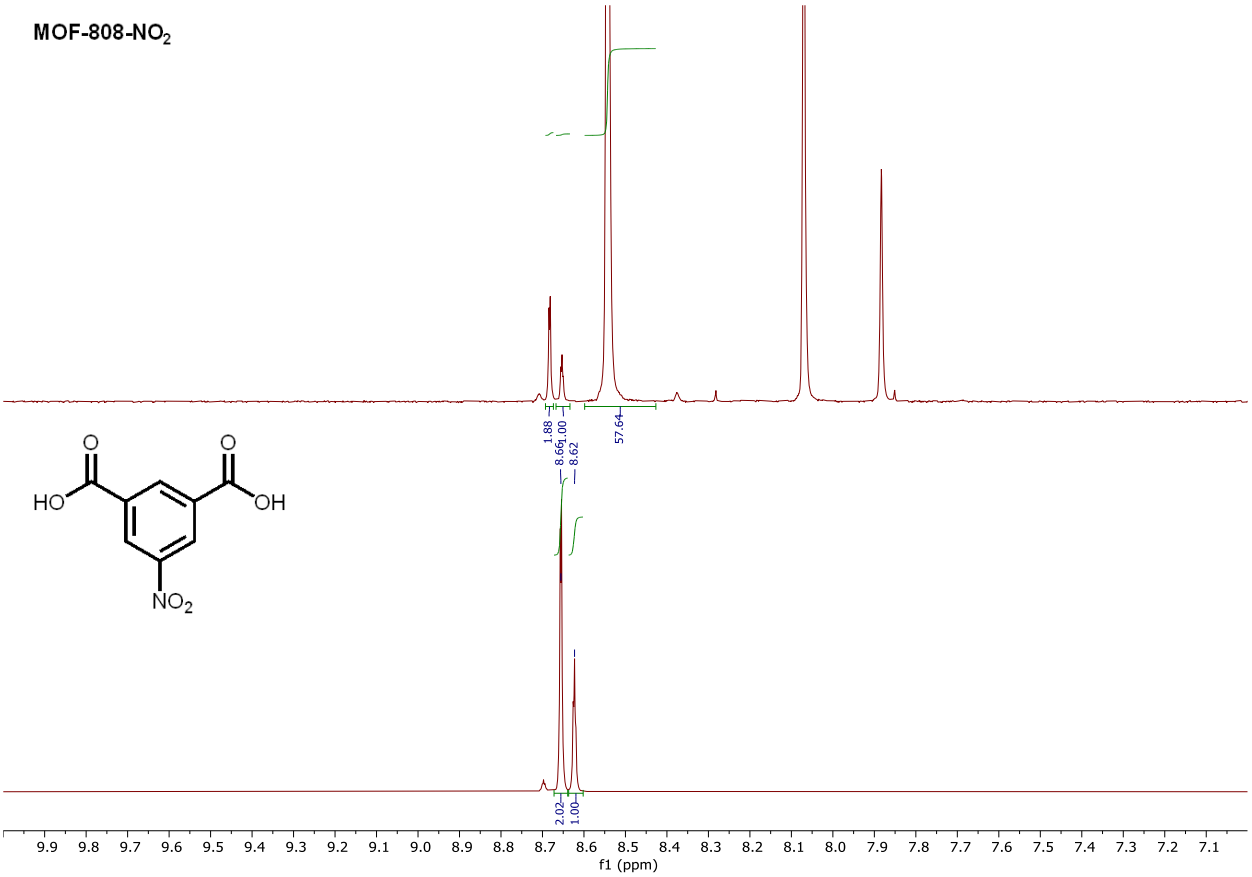

Figure S13. Comparison of ^{1}H NMR spectra of acid-digested 5-nitroisophthalic acid and **MOF-808-NO$_2$**.

$$\text{Percent defect incorporation} = \frac{I_{Defect}}{I_{Defect}+I_{BTC}} \times 100\% = \frac{1.00}{1.00+\frac{57.64}{3}} \times 100\% \approx 5\%$$

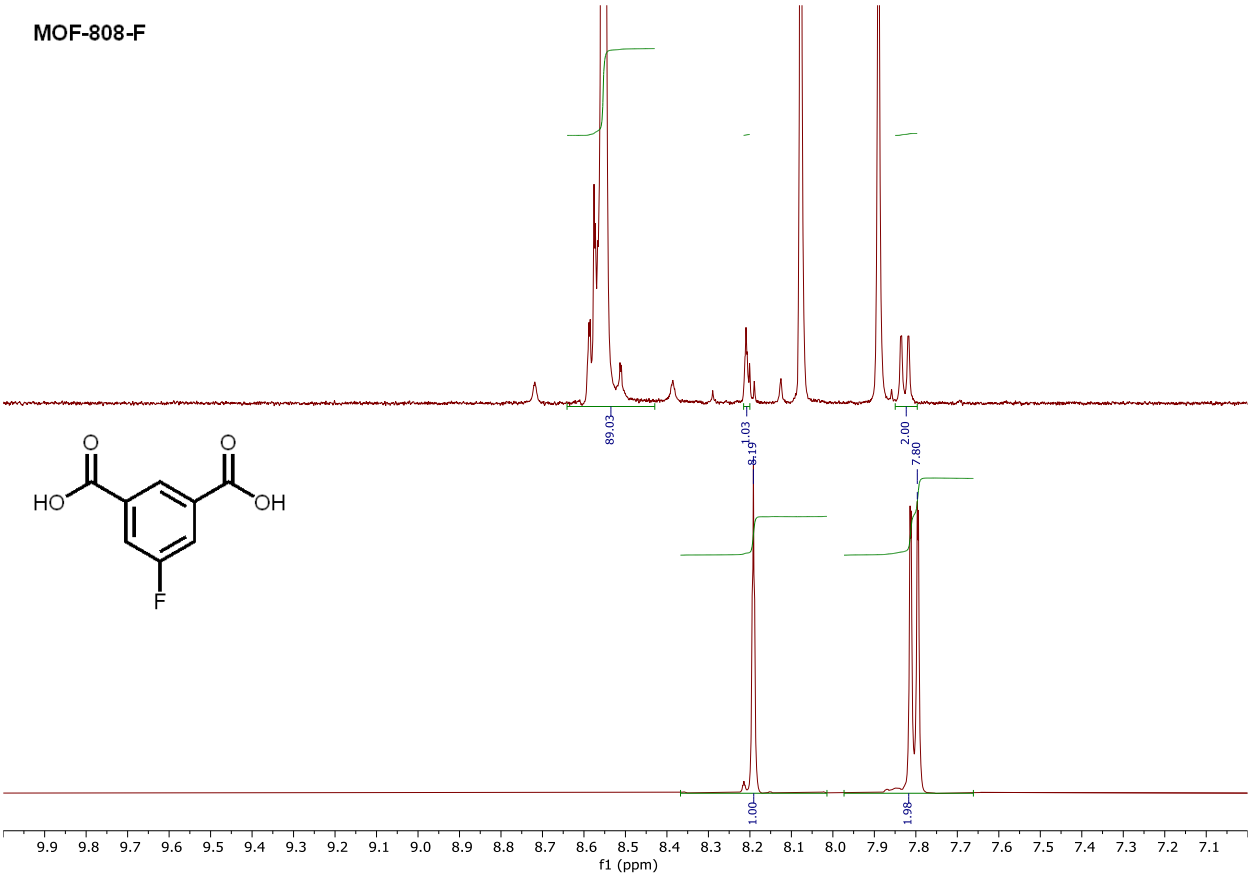

Figure S14. Comparison of ^{1}H NMR spectra of acid-digested 5-fluoroisophthalic acid and **MOF-808-F**.

$$\text{Percent defect incorporation} = \frac{I_{Defect}}{I_{Defect}+I_{BTC}} \times 100\% = \frac{1.00}{1.00+\frac{89.03}{3}} \times 100\% \approx 3\%$$

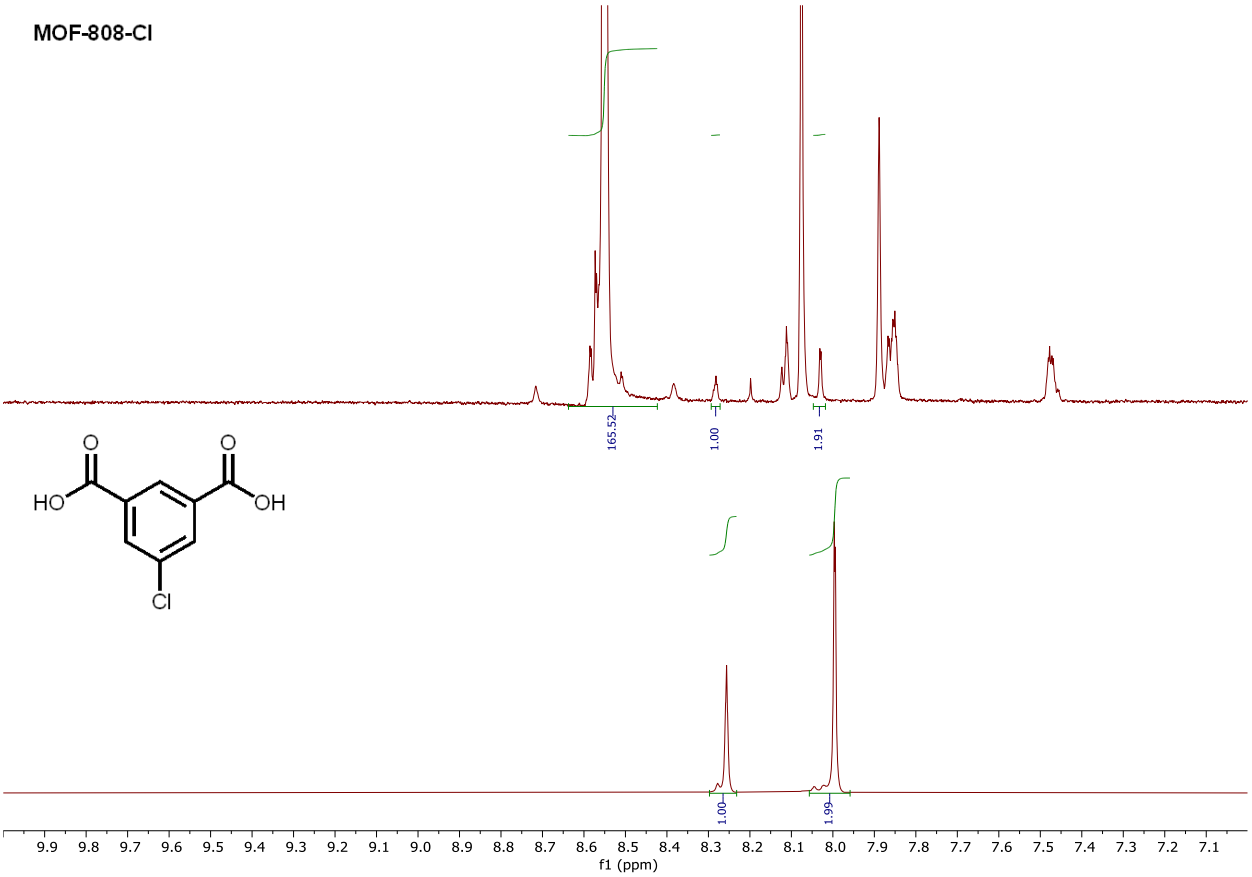

Figure S15. ^{1}H NMR spectra comparison of acid-digested 5-chloroisophthalic acid and **MOF-808-Cl**.

$$\text{Percent defect incorporation} = \frac{I_{Defect}}{I_{Defect}+I_{BTC}} \times 100\% = \frac{1.00}{1.00+\frac{165.52}{3}} \times 100\% \approx 2\%$$

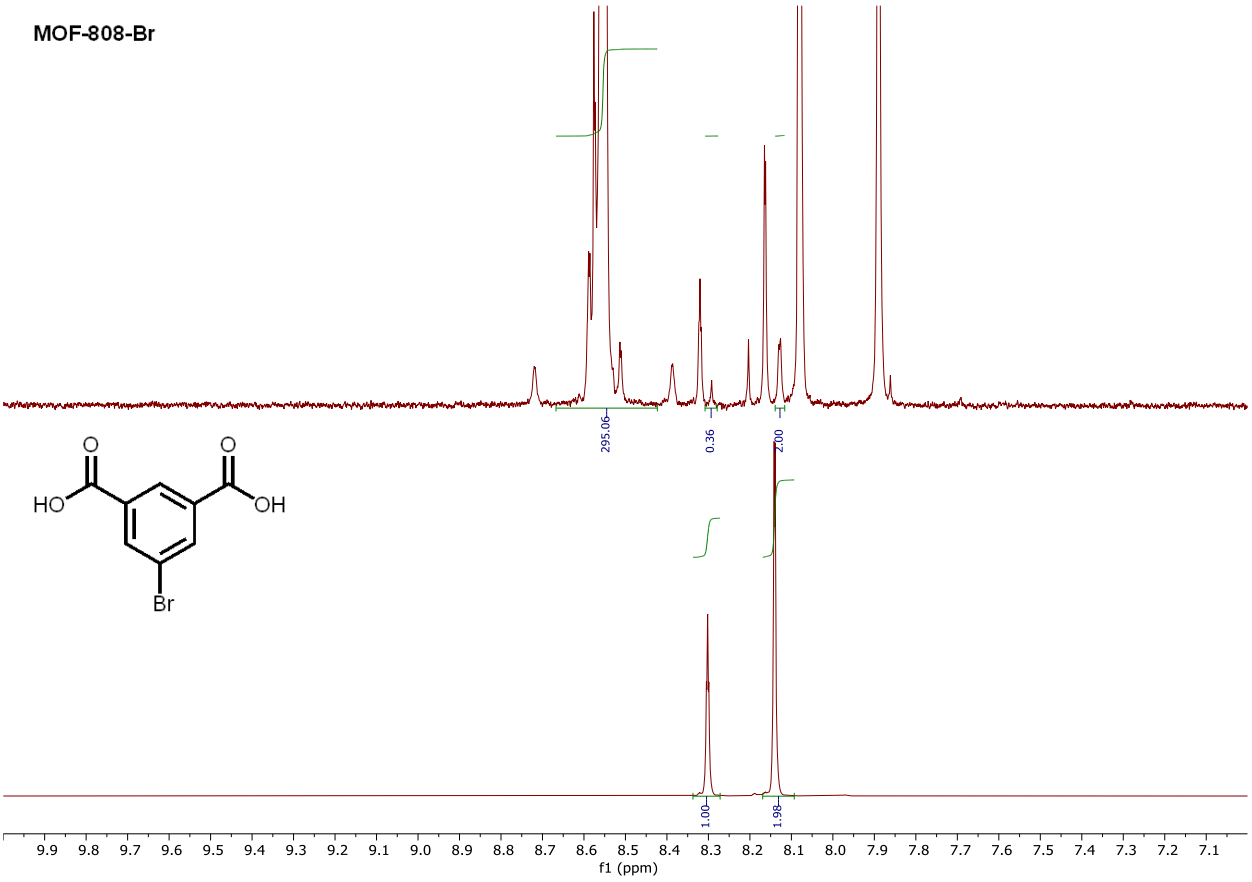

Figure S16. ^{1}H NMR spectra comparison of acid-digested 5-bromoisophthalic acid and **MOF-808-Br**.

$$\text{Percent defect incorporation} = \frac{I_{Defect}}{I_{Defect}+I_{BTC}} \times 100\% = \frac{1.00}{1.00+\frac{295.06}{3}} \times 100\% \approx 1\%$$

Figure S17. ^{1}H NMR spectra comparison of acid-digested 5-iodoisophthalic acid and **MOF-808-I**.

$$\text{Percent defect incorporation} = \frac{I_{Defect}}{I_{Defect}+I_{BTC}} \times 100\% = \frac{\frac{1.00}{3}}{\frac{1.00}{3}+\frac{52.17}{3}} \times 100\% \approx 2\%$$

Table S1. Percent incorporation of defect linkers in defective MOF-808 frameworks as determined by ^{1}H NMR analyses of the digested samples.

Sample	Percent Incorporation (%)
MOF-808-H	1
MOF-808-OH	2
MOF-808-SH	2
MOF-808-NH_2	1
MOF-808-NMe_2	1
MOF-808-py	0.5
MOF-808-py-Nox	0.5
MOF-808-NO_2	5
MOF-808-F	3
MOF-808-Cl	2
MOF-808-Br	1
MOF-808-I	2

4.3. Powder X-ray diffraction.

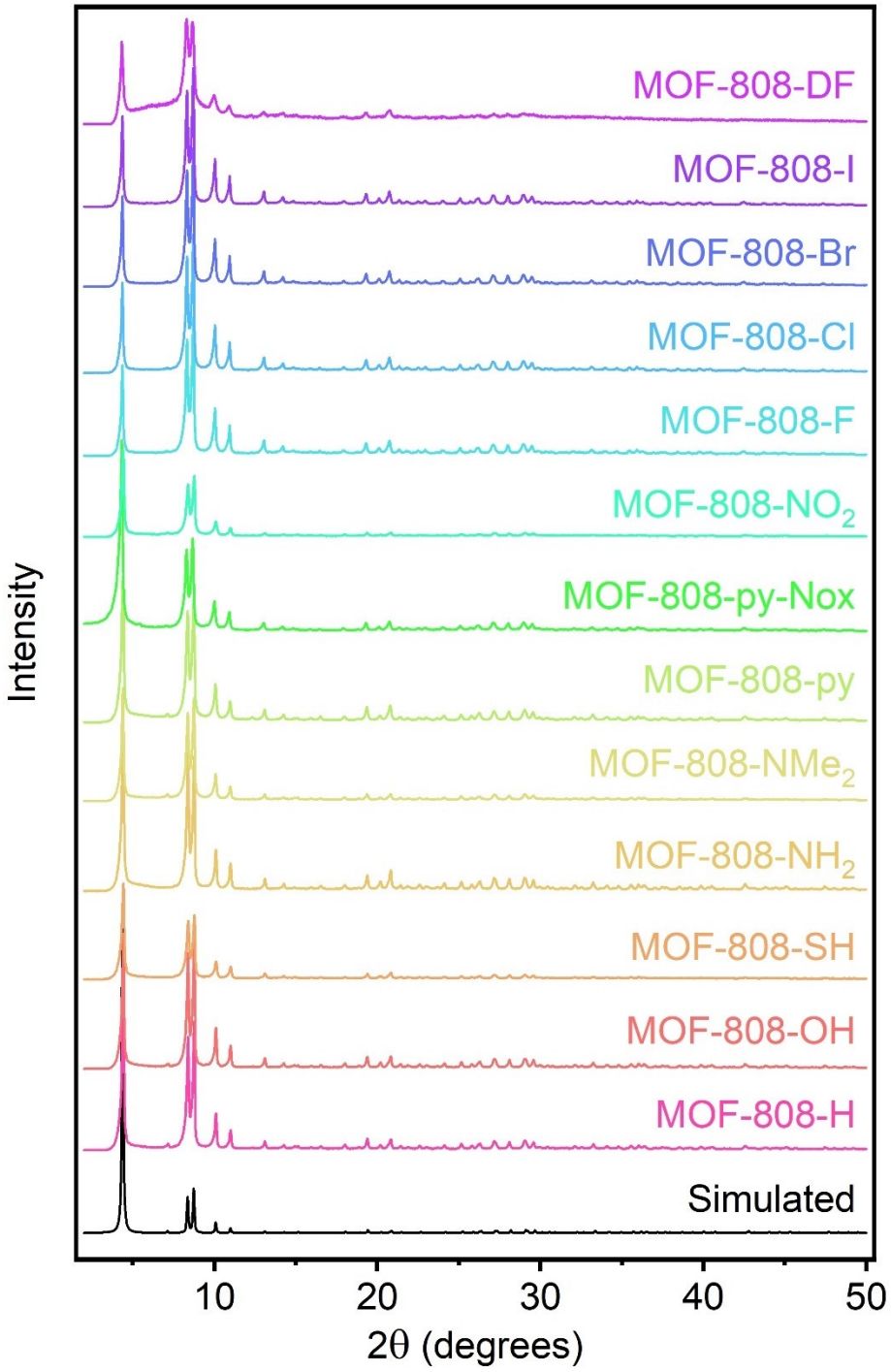

Figure S18. PXRD patterns (λ = 1.54 Å) of pristine and defective MOF-808 frameworks. The simulated pattern based on the single-crystal X-ray diffraction (SCXRD) structure of MOF-808 is included for reference.[5] Several of these PXRD patterns are included in main text Figure 3d for comparison.

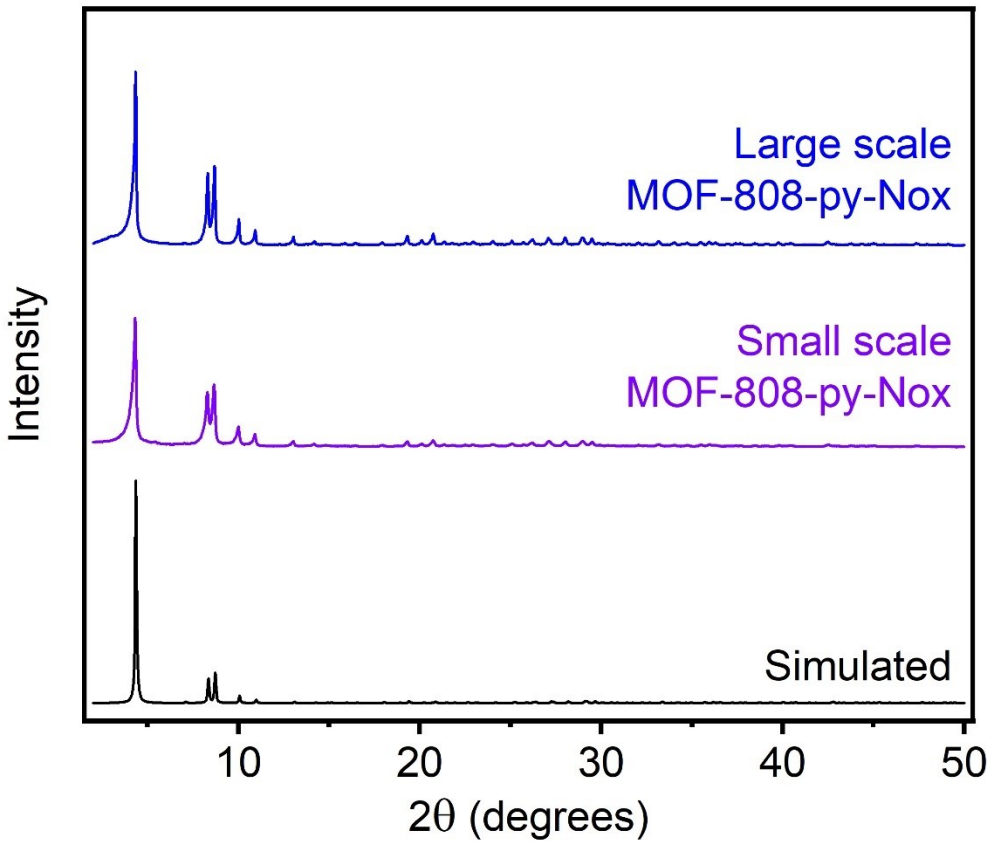

Figure S19. PXRD patterns (λ = 1.54 Å) of **MOF-808-py-Nox** synthesized on small scale and large scale. The simulated pattern based on the SCXRD structure of MOF-808 is included for reference.[5]

4.4. 77 K N_2 adsorption isotherms.

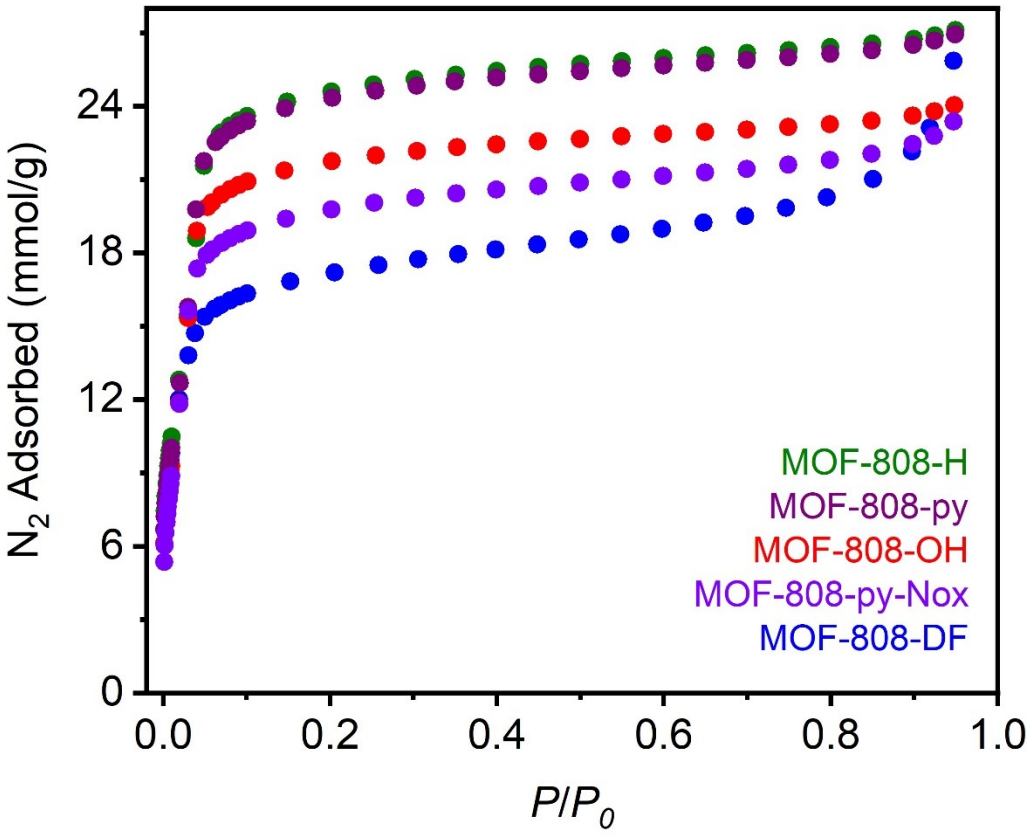

Figure S20. 77 K N_2 adsorption isotherms of representative activated MOF-808 frameworks. The corresponding density functional theory (DFT) calculated pore size distributions are included in main text Figure 2e.

Table S2. BET surface areas of MOF-808 frameworks as determined from 77 K N_2 adsorption isotherms. The reported BET surface area of **MOF-808-DF** is 1409–2060 m^2/g.[4–8]

Sample	BET Surface Area (m^2/g)
MOF-808-DF	1524 ± 21
MOF-808-py-Nox	1855 ± 57
MOF-808-OH	2056 ± 80
MOF-808-py	2280 ± 84
MOF-808-H	2268 ± 83

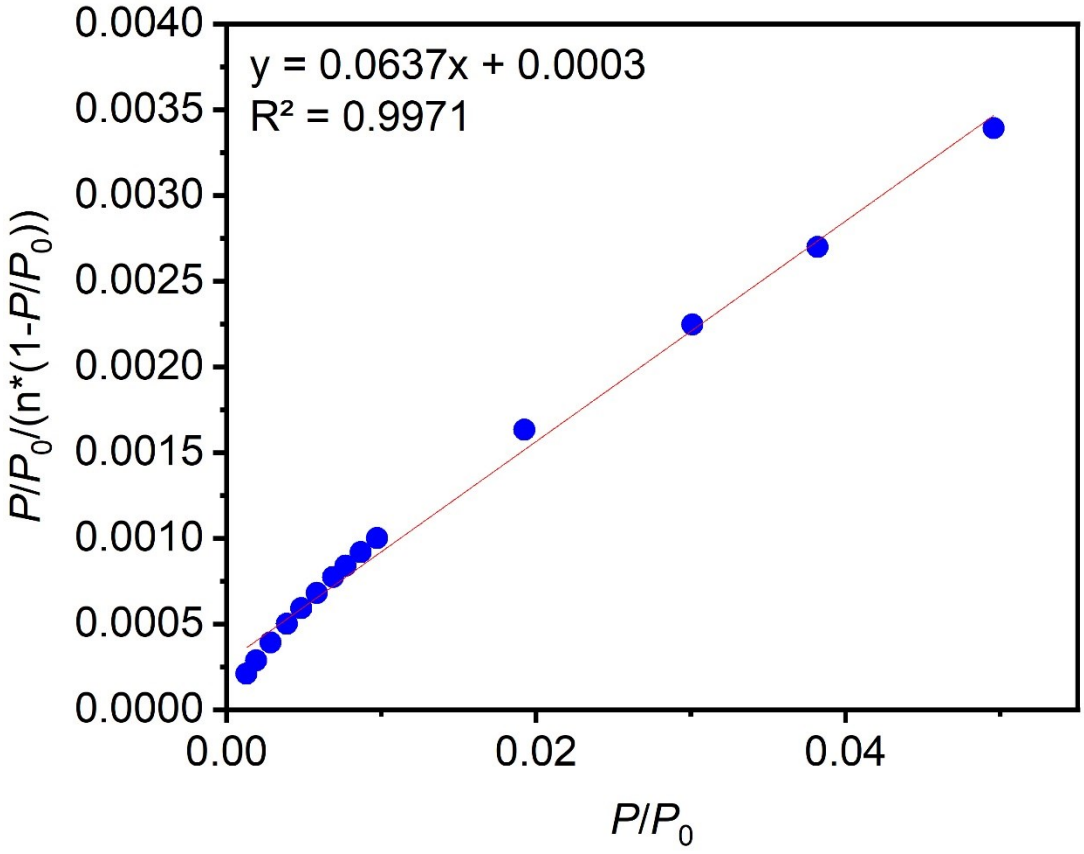

Figure S21. Linearized BET plot of **MOF-808-DF**.

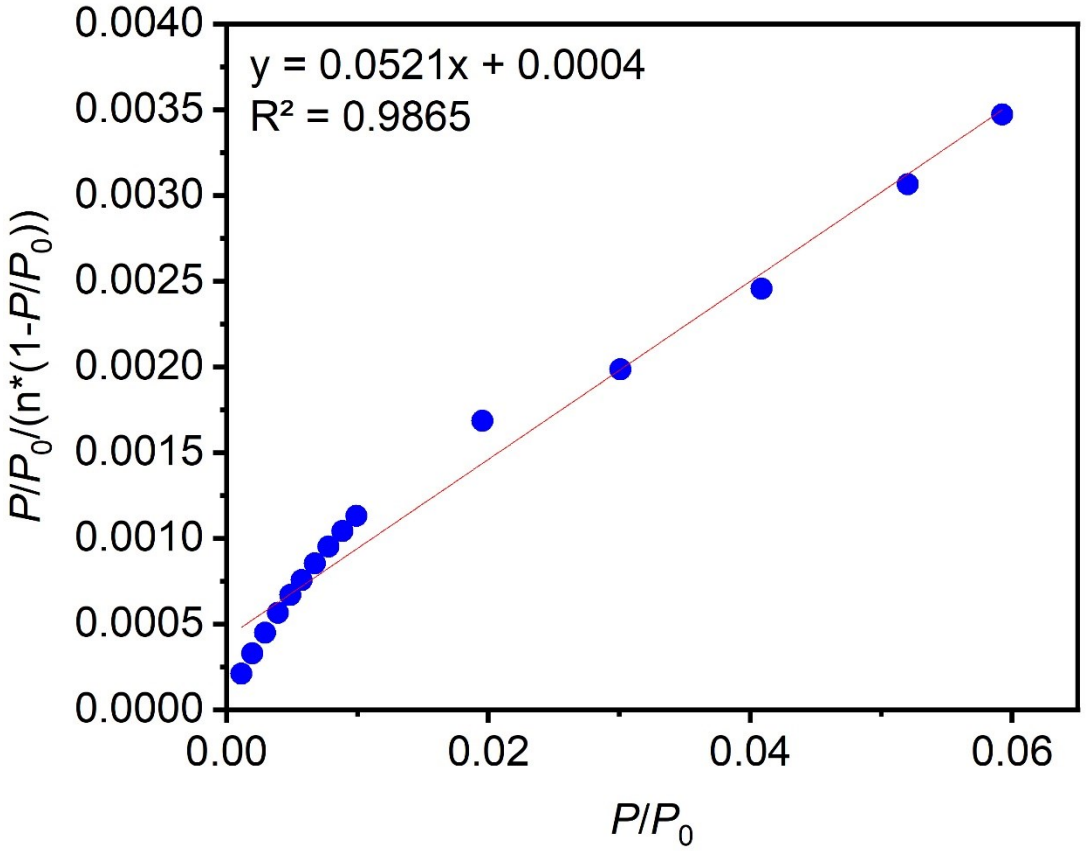

Figure S22. Linearized BET plot of **MOF-808-py-Nox**.

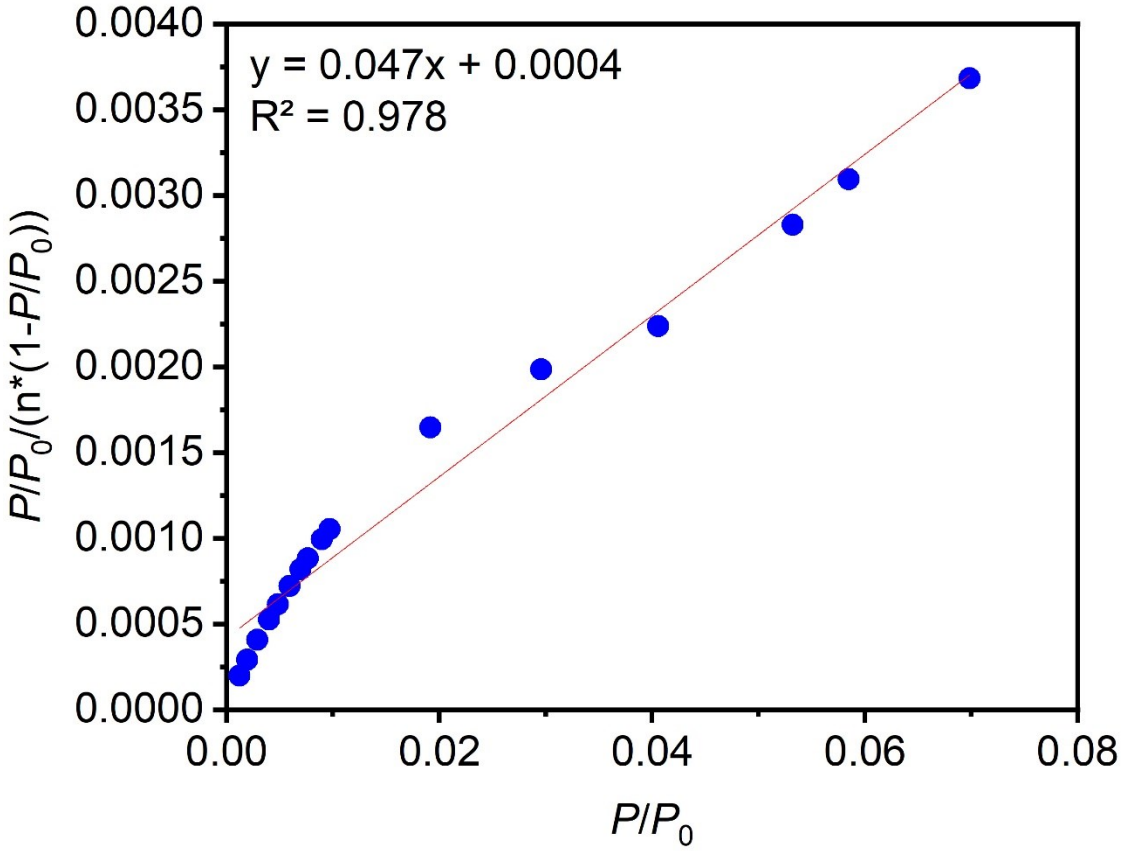

Figure S23. Linearized BET plot of **MOF-808-OH**.

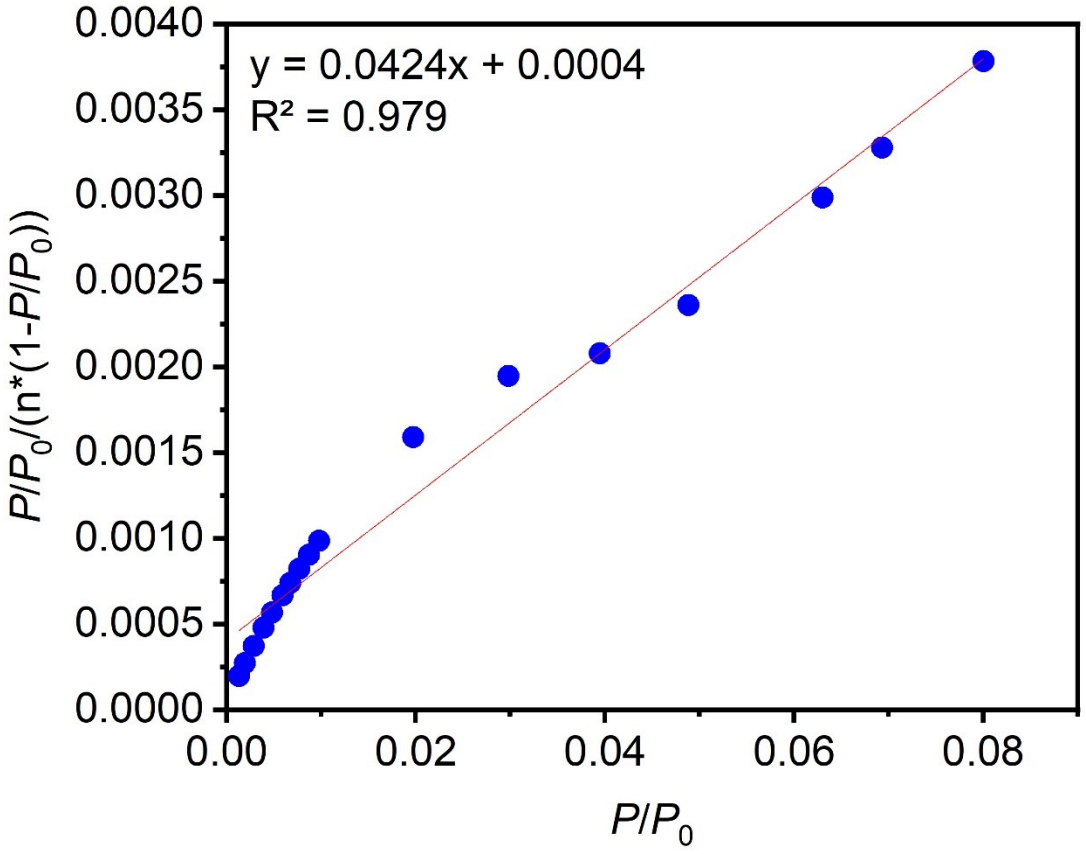

Figure S24. Linearized BET plot of **MOF-808-py.**

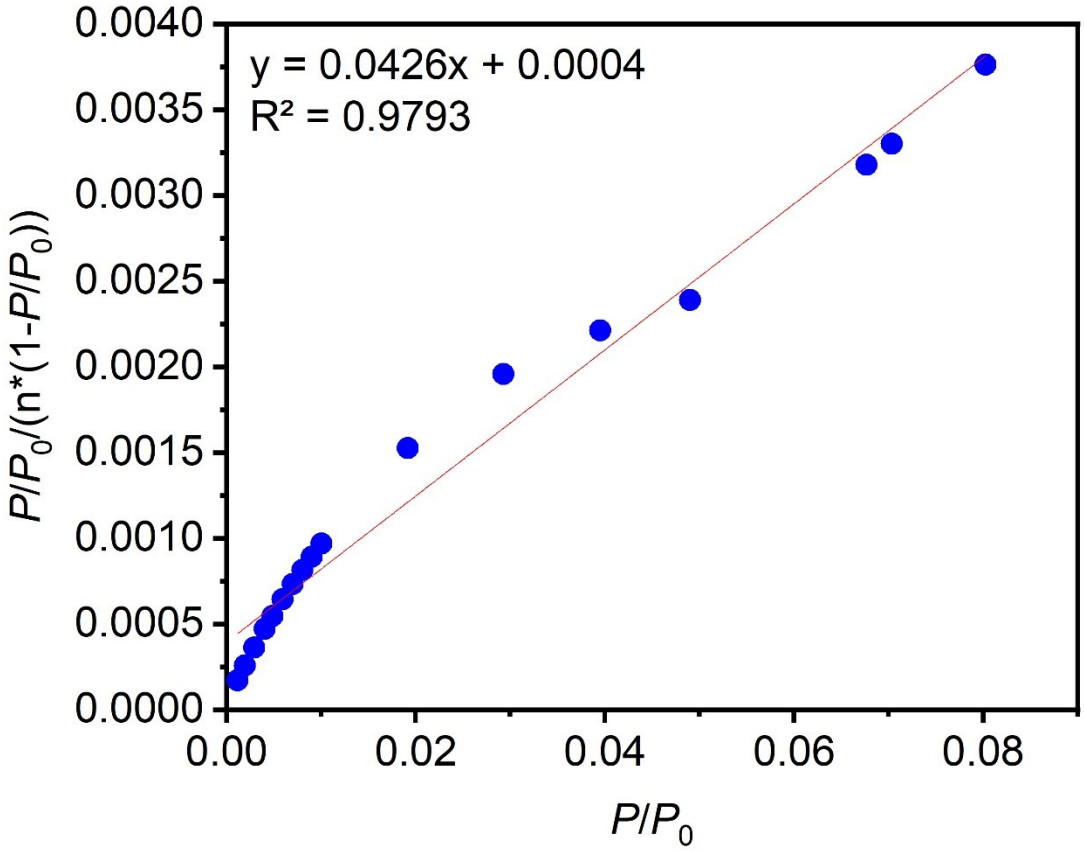

Figure S25. Linearized BET plot of **MOF-808-H**.

4.5. Scanning electron microscopy.

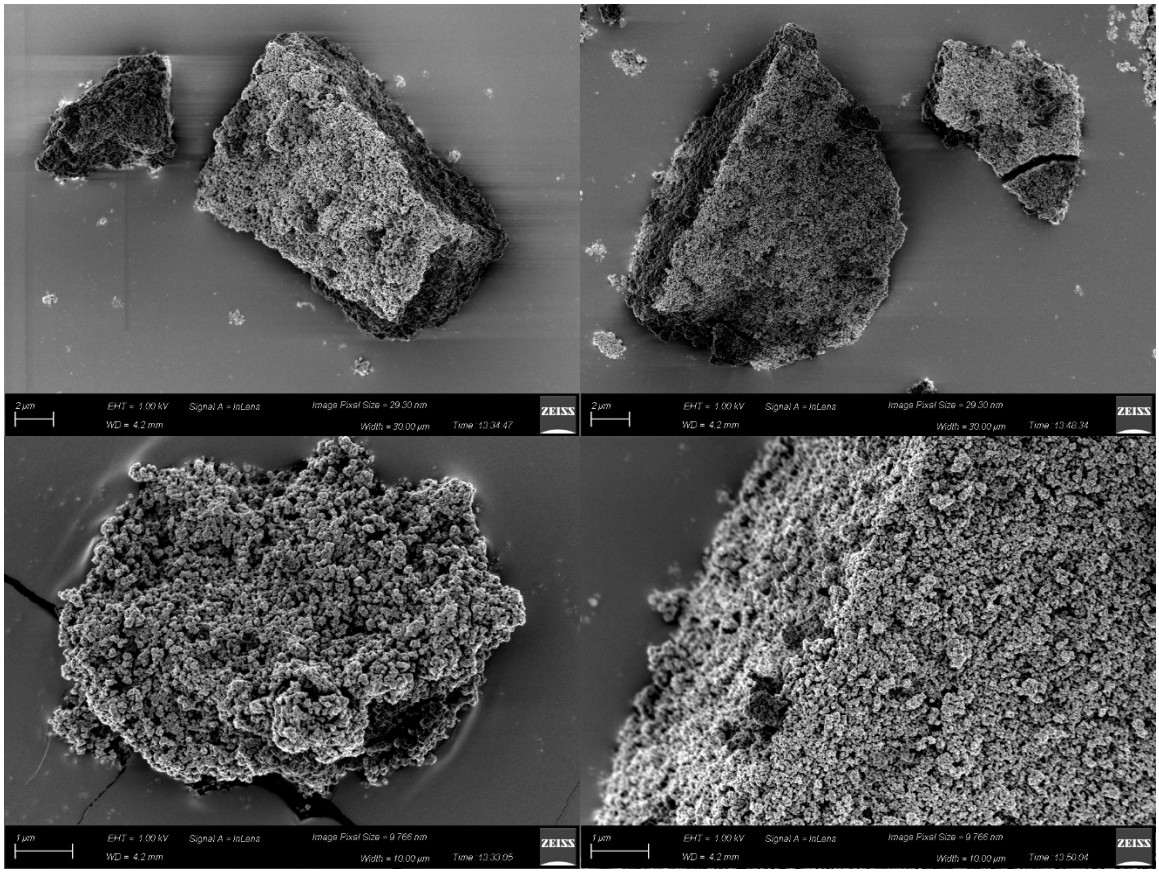

Figure S26. SEM images of **MOF-808-DF**.

The particle size of **MOF-808-DF** was estimated to be 150–200 nm by visual inspection of crystallite images in Figure S26.

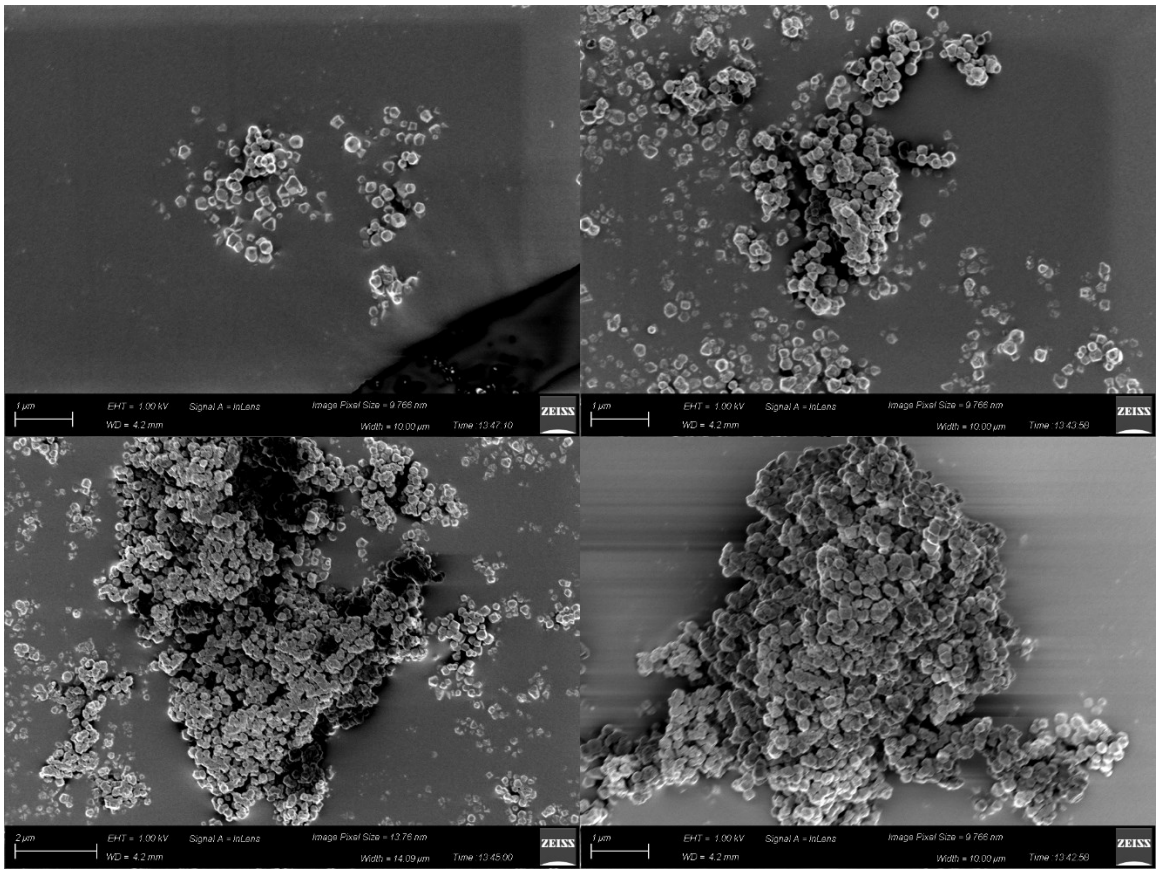

Figure S27. SEM images of **MOF-808-py-Nox**.

The particle size of **MOF-808-py-Nox** was estimated to be 200–300 nm by visual inspection of crystallite images in Figure S27.

4.6. Thermogravimetric analysis.

Quantifying linker-to-cluster ratio.

The quantification employed here follows literature procedures[1,8] but was modified to take into account the gain of oxygen to obtain a more accurate ratio.

MOF-808 frameworks were first decomposed in air using TGA. As the observed weight percentage reaches a plateau near 400 ˚C, a pristine MOF-808 with a formula of $\mathbf{Zr_6O_4(OH)_4(HCO_2)_6(BTC)_2}$ turns into a solvent and modulator free, dehydroxylated MOF with a formula of $\mathbf{Zr_6O_9(BTC)_2}$ and molecular weight of 1105.6 g/mol. In each sample, the dehydroxylated product was identified in the TGA profiles as occurring directly before the onset of major mass loss consistent with linker combustion, as determined by the first derivative *d*(Weight)/*d*(T) (%/C).

As the temperature reaches 600 ˚C, the material decomposes further into $\mathbf{Zr_6O_9O_3}$ or six equiv. of ZrO_2, losing the mass of the combusted linker and gaining the mass of charge-balancing oxygens. The balanced equation of this decomposition is:

$$\mathbf{Zr_6O_9[C_6H_3(CO_2)_3]_2}\,(s) + 21\ \mathbf{O_2}\,(g) \rightarrow \mathbf{Zr_6O_9O_3}\,(s) + 18\ C\mathbf{O_2}\,(g) + 3\ H_2\mathbf{O}\,(g).$$

To quantify the linker-to-cluster ratio, the weight percentage at 600 ˚C ($\%W_{End}$) presumed to be six equiv. of ZrO_2 ($\mathbf{Zr_6O_9O_3}$) was normalized to 100%. For a perfect crystal structure of MOF-808, the normalized weight percentage at the plateau close to 400 ˚C ($\%W_{Ideal,Plat}$) should be $\frac{M_w \text{ of } \mathbf{Zr_6O_9(BTC)_2}}{M_w \text{ of } 6\ ZrO_2} = \frac{1105.6\ \text{g/mmol}}{6 \times 123.2\ \text{g/mmol}} \times 100\% = 149.53\%$. In this case, the weight gain of oxygen or $\%WG_{Oxygen}$ is $\frac{M_w \text{ of } \mathbf{3\ O}}{M_w \text{ of } 6\ ZrO_2} = \frac{3 \times 16.0\ \text{g/mmol}}{6 \times 123.2\ \text{g/mmol}} \times 100\% = 6.49\%$.

Thus, the theoretical weight loss per BTC linker in a perfect crystal of MOF-808 or $\%WL_{Ideal}$ is:

$$\%WL_{Ideal} = \frac{\%W_{Ideal,Plat} - \%W_{End} + \%WG_{Oxygen}}{2} = \frac{149.53 - 100 + 6.49}{2} = 28.01\%$$

where 2 is the number of linkers in an ideal, dehydroxylated sample of $\mathbf{Zr_6O_9(BTC)_2}$.

By replacing 2 and $\%W_{Ideal,Plat}$ with the number of experimental linkers in MOF-808 sample NL_{Exp} and $\%\%W_{Exp,Plat}$ (the experimentally determined plateau prior to linker combustion), respectively, and rearranging the equation to solve for NL_{Exp}, the experimental linker-to-cluster ratio can be determined as:

$$NL_{Exp} = \frac{\%W_{Exp,Plat} - \%W_{End} + \%WG_{Oxygen}}{\%WL_{Ideal}}$$

where $\%W_{End} = 100\%$, $\%WL_{Ideal} = 28.01\%$, $\%WG_{Oxygen} = 6.49\%$.

Example of linker-to-cluster ratio calculation.

The above procedure can be validated with a theoretical, defective MOF-808 framework with a linker-to-cluster ratio of 1.50 and a formula of $\mathbf{Zr_6O_4(OH)_4(HCO_2)_6(BTC)_{1.5}X_{1.5}}$ where X is unspecified charge-compensating ligand, such as formates or hydroxides. As the temperature approaches 400 ˚C, it would decompose into $\mathbf{Zr_6O_9(BTC)_{1.5}}$ with a molecular weight of 1002.0 g/mol. The $\%W_{Exp,Plat}$ for this framework would be $\frac{1002.0\ \text{g/mmol}}{6 \times 123.2\ \text{g/mmol}} \times 100\% = 135.53\%$.

Plugging this value to the equation, the calculated linker-to-cluster ratio would be obtained as:

$$NL_{Exp} = \frac{\%W_{Exp,Plat} - \%W_{End} + \%WG_{Oxygen}}{\%WL_{Ideal}} = \frac{135.53 - 100 + 6.49}{28.01} = 1.50$$

which exactly matches the expected value.

If $\%WG_{Oxygen}$ was not accounted for as previously reported,[1,8] the $\%WL_{Ideal}$ would be:

$$\%WL_{Ideal} = \frac{\%W_{Ideal,Plat} - \%W_{End}}{2} = \frac{149.53 - 100}{2} = 24.77\%$$

and accordingly, the calculated linker-to-cluster ratio would be:

$$NL_{Exp} = \frac{\%W_{Exp,Plat} - \%W_{End}}{\%WL_{Ideal}} = \frac{135.53 - 100}{24.77} = 1.43$$

which does not match the expected value of the theoretical framework.

However, it must be noted that this calculation relies on several assumptions. First, pure white ZrO_2 is assumed to be the solid obtained post-combustion @ 600 ˚C, even though grey solids containing possible impurities were obtained experimentally. Second, it is assumed that weight loss occurring between the onset near 400 ˚C and 600 ˚C is all caused by the complete combustion of only the organic linker. Similarly, incomplete combustion of the organic component may be observed, and leftover solvent or formate capping ligands may contribute to the loss in that range as well. Last, for the defective frameworks, it is assumed that the defect linkers are combusted in the same temperature range as btc^{3-} ligand, when it likely has some variability.

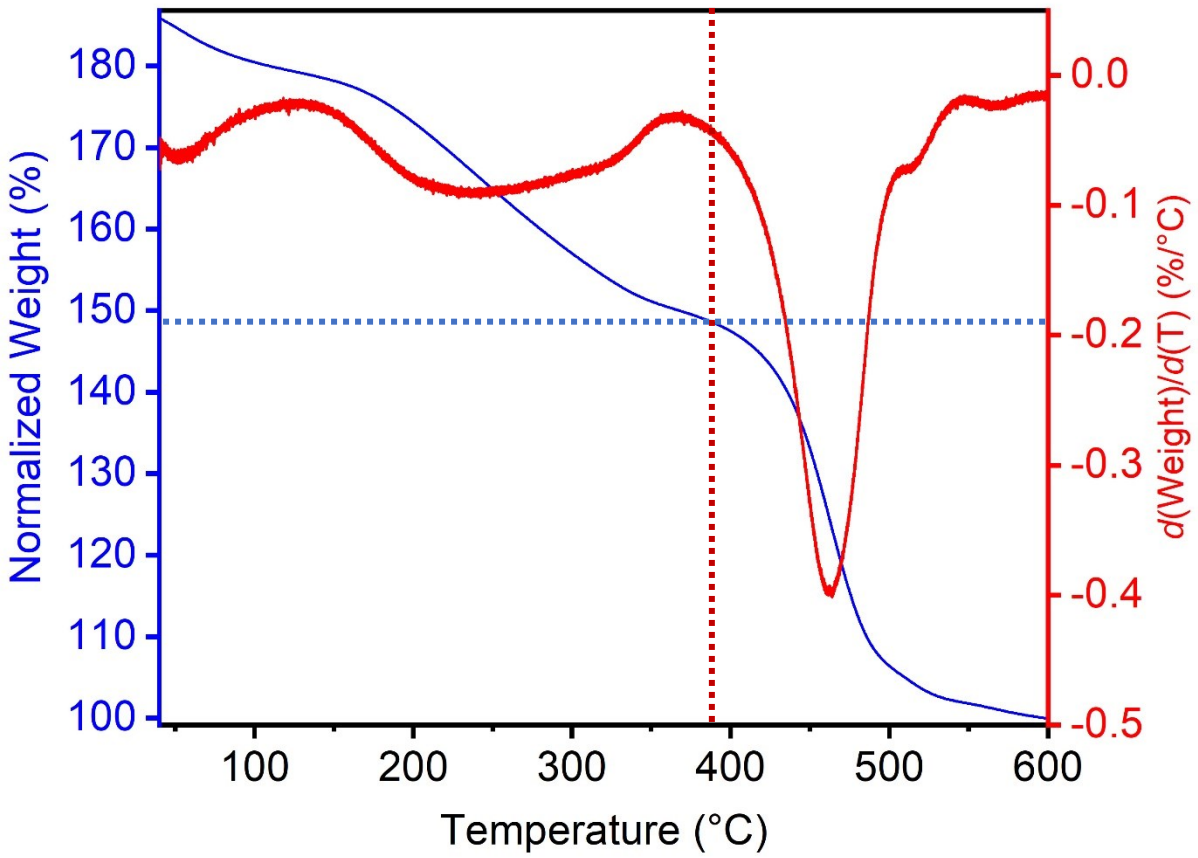

Figure S28. TGA decomposition profile of **MOF-808-DF** under air. Blue and red lines represent the normalized experimental decomposition profile and the derivative *d*(Weight)/*d*(T) (%/C), respectively.

The onset temperature of the major linker combustion near 400 ˚C is determined to be 390 ˚C. Accordingly, the linker-to-cluster ratio of **MOF-808-DF** is obtained as:

$$NL_{Exp} = \frac{\%W_{Exp,Plat} - \%W_{End} + \%WG_{Oxygen}}{\%WL_{Ideal}} = \frac{148.44 - 100 + 6.49}{28.01} = 1.96$$

This value is close to the ideal value of 2 for this framework.

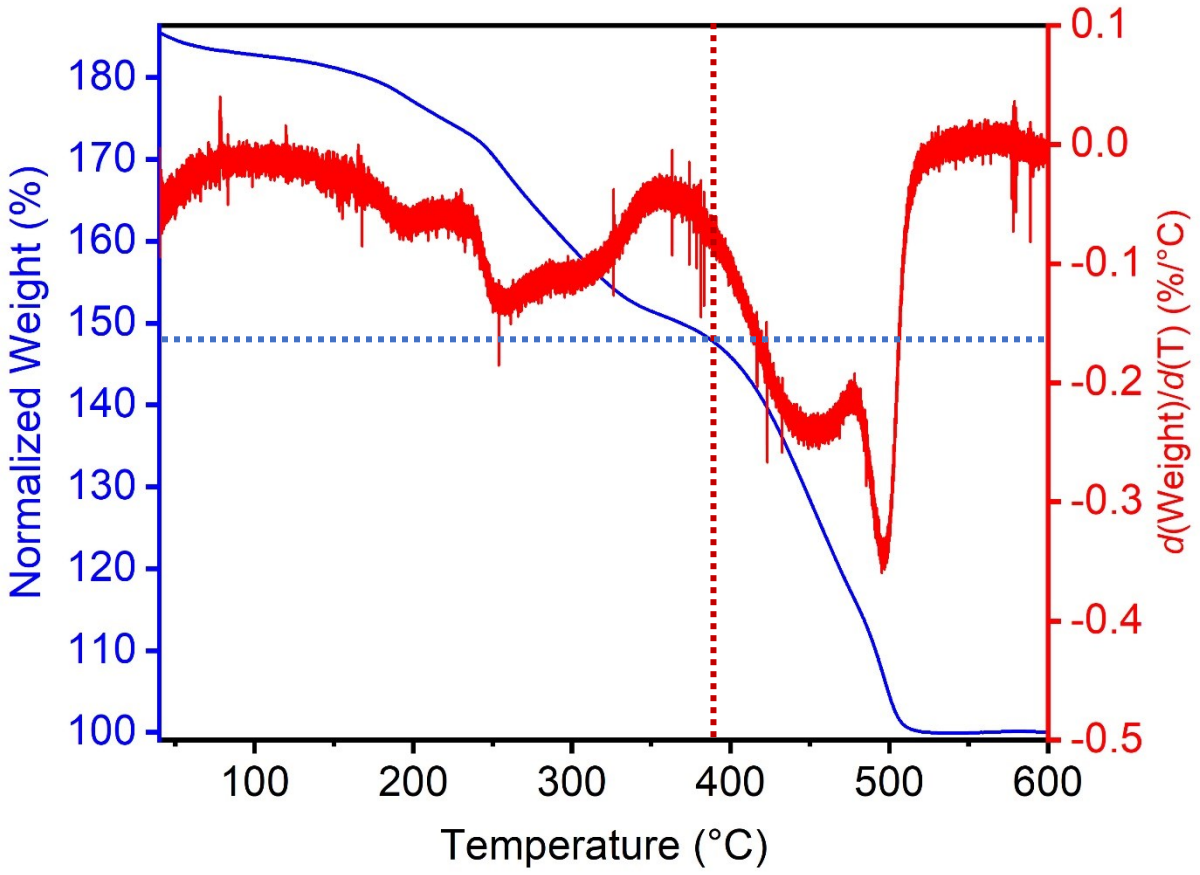

Figure S29. TGA decomposition profile of **MOF-808-py-Nox** under air. Blue and red lines represent the normalized experimental decomposition profile and the derivative *d*(Weight)/*d*(T) (%/C), respectively.

The onset temperature of the major linker combustion near 400 ˚C is determined to be 390 ˚C. Accordingly, the linker-to-cluster ratio of **MOF-808-py-Nox** is obtained as:

$$NL_{Exp} = \frac{\%W_{Exp,Plat} - \%W_{End} + \%WG_{Oxygen}}{\%WL_{Ideal}} = \frac{147.59 - 100 + 6.49}{28.01} = 1.93$$

This is slightly lower than the value obtained for **MOF-808-DF** (1.96), supporting that the addition of defect-introducing linkers leads to a lower linker:cluster ratio and thus additional missing linker defects. This finding is consistent with the presence of mesopores in the pore size distribution of defect-engineered MOF-808 samples (main text Figure 3e), which are absent in **MOF-808-DF**.

4.7. Infrared spectroscopy.

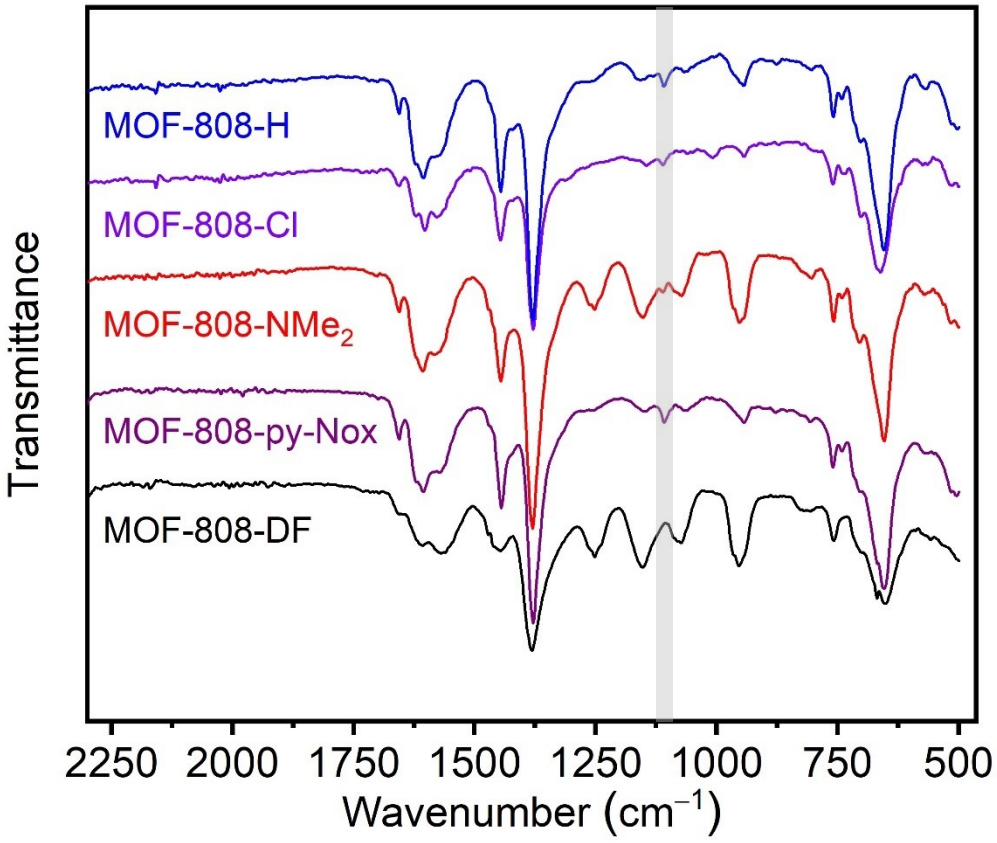

Figure S30. ATR-IR spectra of representative MOF-808 frameworks. Highlighted in gray is the stretch at 1100 cm^{-1} corresponding to hydroxo/water ligands (Zr–OH/OH_2 sites) on the nodes, which are absent in **MOF-808-DF**.[9]

5. Mechanistic considerations.

Given the low percentage incorporation of defects (≤5% in all cases), exact characterization of the defect sites in the MOF-808 variants is challenging. For example, it is assumed here that the defect linker is localized within the framework in the same manner as the btc^{3-} linker (Figure S31, left), resulting in the colocalization of functional groups with Zr centers. Yet, the defect linker can also reside within the framework in other arrangements, such as facing a missing-cluster defect (Figure S31, middle) or replacing a formate capping ligand (Figure S31, right). These other possibilities would lead to alternative mechanisms involving co-localization of functional groups.

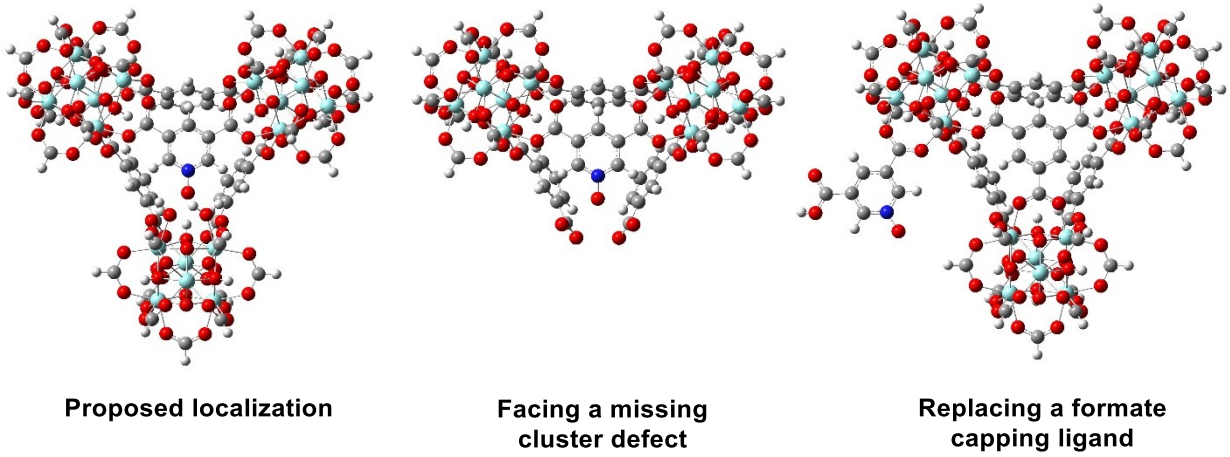

Figure S31. Possible DFT-calculated localizations of defect linkers within MOF-808 frameworks.

However, based on the TGA results in Figure S23, missing-cluster defects in **MOF-808-py-Nox** (Figure S31, middle) are unlikely or would exist in a miniscule quantity because of the lower-than-expected linker-to-cluster ratio (1:93:1), while a missing-cluster defect would be statistically observed when the linker-to-cluster ratio is high (>2:1). On the other hand, a defect linker replacing a formate ligand (Figure S31, right) would likely be removed during the washing procedure because of its labile connection to the node. Overall, the colocalization of the defect linker and the Zr centers is the most likely arrangement.

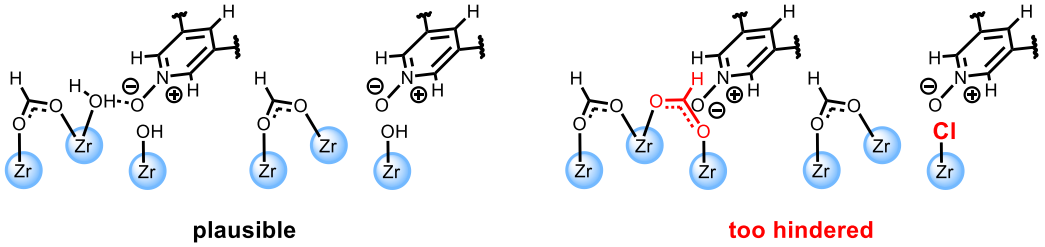

Figure S32. Possible charge-compensating ligands for defective MOF-808 frameworks.

It is also unclear how the frameworks compensate for the missing charge from the defect linkers (2− charge) compared to the linker (3− charge). Formate (HCO_2^-) and chloride (Cl^-) ligands are present during the framework synthesis, but they are likely too sterically bulky to reside

right next to the defect linker (Figure S32, right). On the other hand, hydroxy (OH^-) or water/hydroxy ligands (Zr–OH/OH_2 sites) are common ligands observed for Zr MOFs with relatively small pore sizes (Figure S32).[9–11] Deprotonation of the $Zr_6O_4(OH)_4$ node to $Zr_6O_{4+x}(OH)_{4-x}$ may also be a viable alternative, but given the oxophilic nature of Zr centers, it may require a low pressure or high temperature to remove bound water to achieve this state.

Based on ATR-IR spectra in Figure S30, one particular stretch of interest is at 1100 cm^{-1}, which has been both computationally and experimentally attributed to the collective vibrations of the hydroxo/water ligands (Zr–OH/OH_2 sites) on the node.[9] This peak is observed upon "chemical activation" by methanol (MeOH) wash, removing formate ligands and substituting them with water or MeOH ligands. These ligands are labile and thus ready to exchange with incoming carboxylic acids. This peak is intriguingly observed for all representative defective MOF-808 frameworks in Figure S25 but is absent for **MOF-808-DF**. Accordingly, since all frameworks undergo the same washing procedure, the rise of such a site likely correlates with the introduction of defect linkers.

We hypothesize that these Zr–OH/OH_2 sites arise in defective MOF-808 frameworks because of the increased lability of the formate ligands neighboring a defect linker (Figure S33). Without a carboxylate as an anchor, the defect linkers have some translational flexibility, opening up more space for ligand substitution. If a water molecule is not present, these sites are even less sterically encumbered, lowering the barrier for an associative substitution of the formate ligands. If a water molecule is present, charge-compensating water/hydroxy ligands may facilitate proton transfer that results in the removal of formic acids. Overall, these "chemically activated" sites would engage in catalysis more readily than unsubstituted sites, resulting in the superiority of defective MOF-808 frameworks over **MOF-808-DF**.

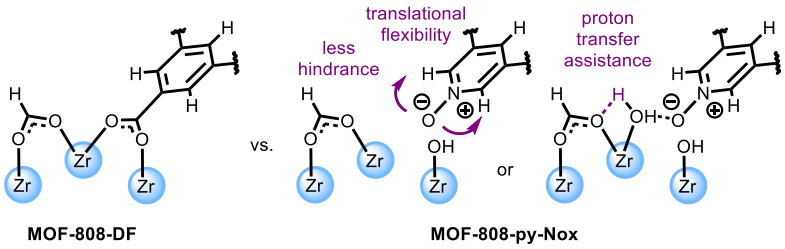

Figure S33. Possible mechanism for observed formate ligand substitution with water/hydroxy ligands in defective MOF-808 variants.

6. General amide bond formation procedure.

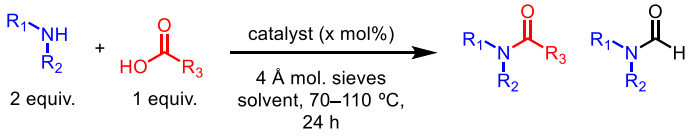

Figure S34. Air-free amide bond formation.

General procedure A. In a N_2-filled glovebox, an oven-dried screw-cap tube was charged with a stir bar, 4 Å molecular sieves pre-activated at 250 ˚C (10 mg or 100 mg/mmol of carboxylic acid), and the catalyst (0.01 mmol, 10 mol %). Once tightly capped, the tube was brought outside the glovebox. Then, 1 mL of stock solution containing the carboxylic acid (0.1 mmol, 1.0 equiv.) and amine (0.2 mmol, 2.0 equiv.) in 200-proof EtOH was added by injection through the Teflon cap under N_2 flow, followed by covering the cap with grease to prevent leaks. The mixture was stirred at 1600 rpm in a 70 ˚C silicone oil bath for 24 h. The reaction mixture was allowed to cool to room temperature. At this time, 1 mL of a 0.1 M solution of 1,3,5-trimethoxybenzene in 200-proof EtOH was added to the reaction mixture. The crude mixture was then filtered through Celite to remove undissolved solids, and 0.1 mL of the filtrate was dissolved in 0.9 mL of dichloromethane for analysis by GC.

This procedure was employed to identify the optimal MOF-808 variants for amide bond formation (main text Figure 3).

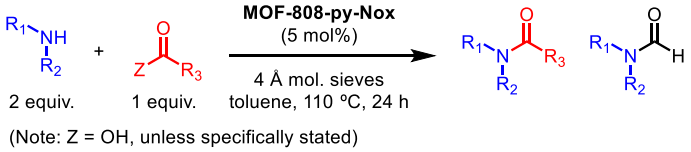

Figure S35. Amide bond formation outside of the glovebox.

General procedure B. An oven-dried screw-cap tube was charged with a stir bar and unactivated 4 Å molecular sieves (50 mg). Once tightly capped, the tube was connected to a Schlenk line and evacuated under high vacuum (<100 mTorr). The tube was flame-dried using a blowtorch three times to activate the molecular sieves and then backfilled with N_2. Anhydrous toluene (1 mL) was added to the activated sieves. The tube was then charged with the carboxylic acid (0.5 mmol, 1.0 equiv.) or its ester/amide derivative, the amine (1.0 mmol, 2.0 equiv.), and **MOF-808-py-Nox** (34 mg, 0.025 mmol, 5 mol%). Additional toluene (4 mL) was then added to the reaction mixture, and once tightly capped, the tube was purged with N_2 for 3 min. The mixture was then stirred at 1600 rpm in a 110 ˚C silicone oil bath for 24 h. At this time, the reaction mixture was allowed to cool to room temperature. The crude reaction mixture was filtered through celite, and the tube was rinsed with additional MeOH (3 × 5 mL) that was filtered through Celite. After concentration under reduced pressure, the product was purified by flash column chromatography on silica gel. For moderately polar amides, the mobile phase was a solvent gradient of 10 → 50% EtOAc in hexanes containing 1% Et_3N, while for highly polar amides, the mobile phase was a solvent gradient of 10 → 100% CH_2Cl_2 in hexanes containing 1% Et_3N, followed by a gradient of 0 → 5% MeOH in CH_2Cl_2. The neutralization of the silica gel by Et_3N was found crucial to minimize decomposition of the amides during chromatography.

This procedure was employed to prepare all of the products in main text Table 2. In cases for which the amine was available as the corresponding HCl salt, Et_3N (2.0 equiv., 1.0 equiv. with respect to the amine) was added.

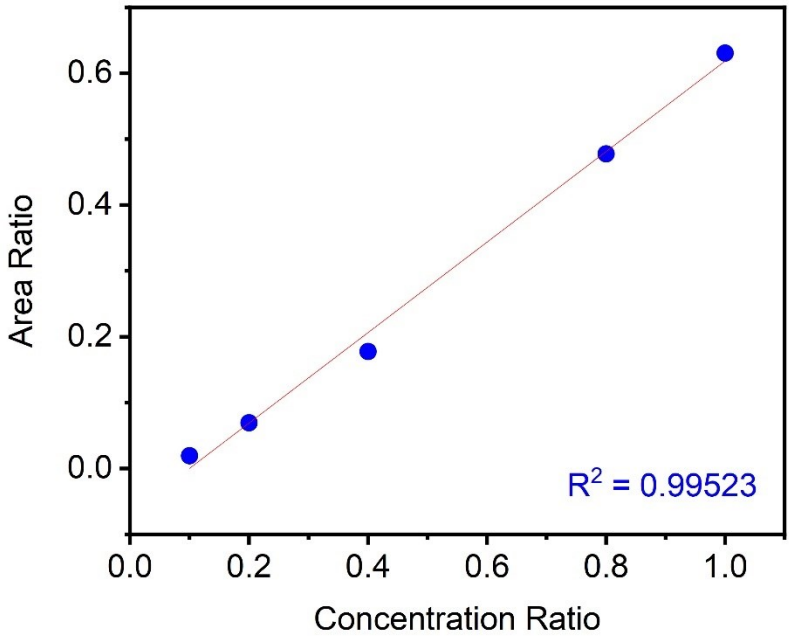

Figure S36. GC calibration curve of *N*-(4-methoxyphenethyl)acetamide (**2**) against internal standard 1,3,5-trimethoxybenzene.

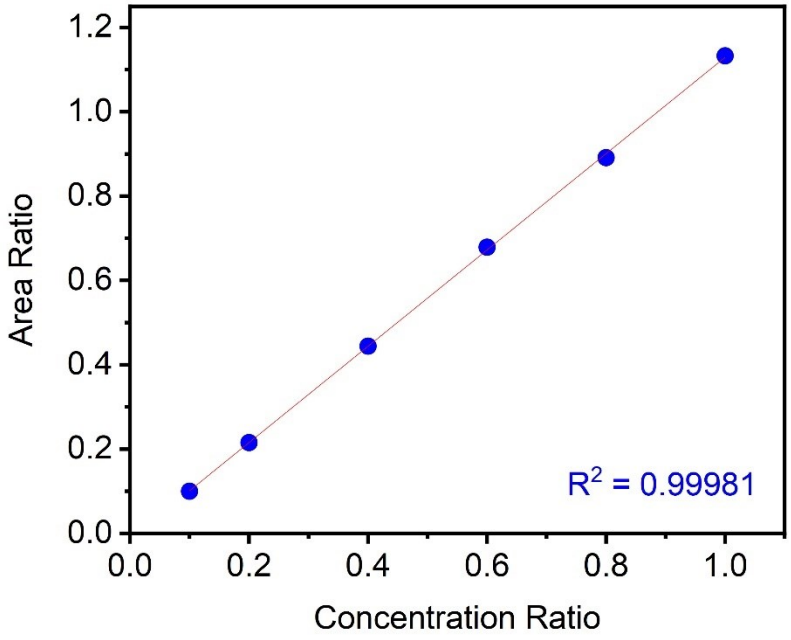

Figure S37. GC calibration curve of *N*-(4-methoxyphenethyl)trifluoroacetamide (**3**) against internal standard 1,3,5-trimethoxybenzene.

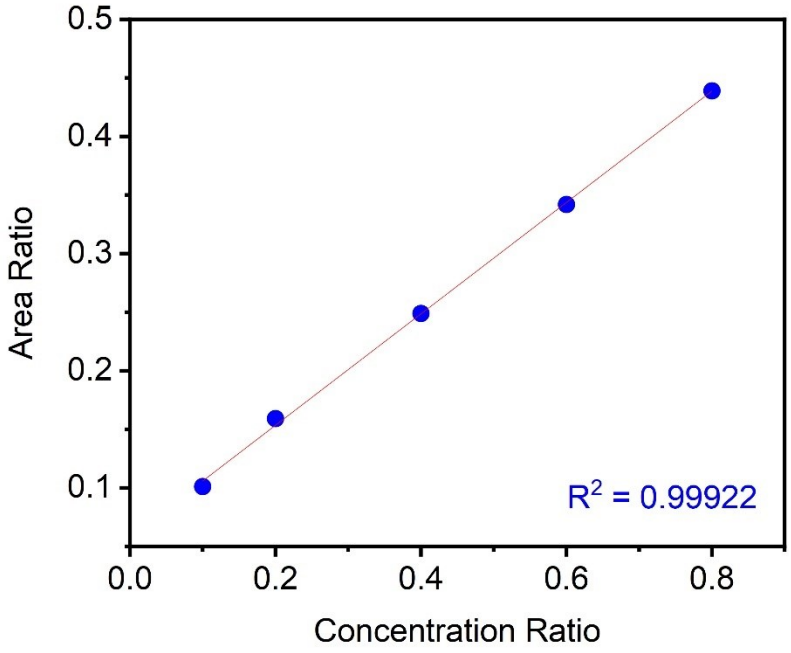

Figure S38. GC calibration curve of *N*-(4-methoxyphenethyl)formamide (**4**) against internal standard 1,3,5-trimethoxybenzene.

7. Procedure for large-scale amide bond formation.

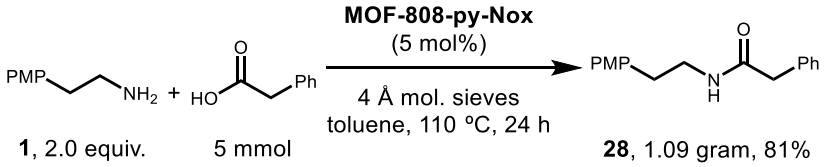

Figure S39. Large-scale amide bond formation.

An oven-dried 100 mL round-bottom flask was charged with a stir bar and unactivated 4 Å molecular sieves (500 mg). The flask was capped with a rubber septum, connected to a Schlenk line, and evacuated under high vacuum (<100 mTorr). The flask was flame-dried with a blowtorch three times to activate the molecular sieves and then backfilled with N_2. Toluene (10 mL) was added to the activated sieves. The tube was then charged with phenylacetic acid (681 mg, 5.0 mmol, 1 equiv.), 2-(4-methoxyphenyl)ethylamine (10.0 mmol, 2 equiv.), and **MOF-808-py-Nox** (340 mg, 0.25 mmol, 5 mol%). Additional toluene (40 mL) was added to the reaction mixture, and once capped, the flask was purged with N_2 for 3 min. The mixture was then stirred at 1600 rpm in a 110 ˚C silicone oil bath for 24 h. At this time, the reaction mixture was allowed to cool to room temperature. The crude reaction mixture was filtered through celite, and the tube was rinsed with additional MeOH (3 × 20 mL) that was filtered through Celite. After concentration under reduced pressure, the product was purified by flash column chromatography on silica gel, affording **28** as a white solid (1.09 g, 81%). The NMR data are consistent with the reported data[12] and with the material prepared on small scale (see below). This yield is comparable to that obtained on small scale (92%).

8. Procedure for recycling MOF-808-py-Nox for multiple amide bond formation cycles.

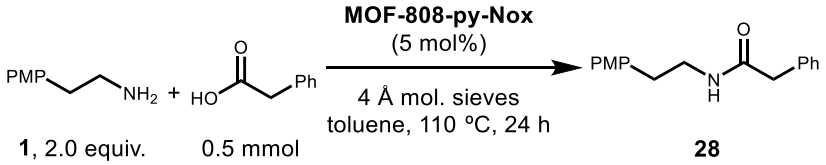

Figure S40. Recycling MOF-808-py-Nox for multiple amide bond formation cycles.

An oven-dried screw-cap reaction tube was charged with a stir bar and unactivated 4 Å molecular sieves (50 mg). Once tightly capped, the tube was connected to the Schlenk line and evacuated under high vacuum (<100 mTorr). The tube was flame-dried using a blowtorch three times to activate the molecular sieves and then backfilled with N_2. A stock solution was prepared by adding 4-methoxyphenethylamine (10 mmol, 1.465 mL, 2.0 equiv.) and phenylacetic acid (5.0 mmol, 681 mg, 1.0 equiv) in anhydrous toluene (10 mL). **MOF-808-py-Nox** (34 mg, 0.025 mmol, 5 mol%) was added to the reaction tube, followed by the addition of the stock solution (1 mL). The remainder of toluene (4 mL) was then added to the reaction mixture, and once tightly capped, the tube was purged with N_2 for 3 min. The mixture was then stirred at 1600 rpm in a 110 ˚C silicone oil bath for 24 h. At this time, the reaction mixture was allowed to cool to room temperature. A 0.5 M solution of 1,3,5-trimethoxybenzene in acetonitrile (1 mL) was added to the crude mixture. The mixture was homogenized by stirring for 15 s, and once the solid was allowed to settle, a portion of the solution (0.1 mL) was dissolved in $CDCl_3$ to obtain the ^{1}H NMR yield of **28** (Table S3).

The crude mixture was centrifuged at 4000 rpm for 10 min, and the supernatant was decanted. To remove adsorbed substrates, the solid was suspended in MeOH (10 mL), allowed to soak for 30 min, and re-collected by centrifugation; this MeOH wash procedure was repeated three times. The solid was then suspended in acetone (5 mL) and transferred to a new oven-dried screw-cap reaction tube. Acetone was then removed under reduced pressure, and the solid was reactivated in a 110 ˚C silicone oil bath under high vacuum (<100 mTorr) overnight. Once backfilled with N_2, the reaction tube was charged with 1 mL of the stock solution described above and anhydrous toluene (4 mL). The reaction was then conducted as described above. The same procedure for preparing ^{1}H NMR samples and activating the solid was followed for a total of five reaction cycles.

Table S3. Results of recycling MOF-808-py-Nox in terms of ^{1}H NMR yield of **28**, as determined by using 1,3,5-trimethoxybenzene as internal standard.

Cycle	^{1}H NMR yield of 28 (%)
1	87
2	90
3	89
4	88
5	91

9. Procedure for amide bond formation in continuous flow.

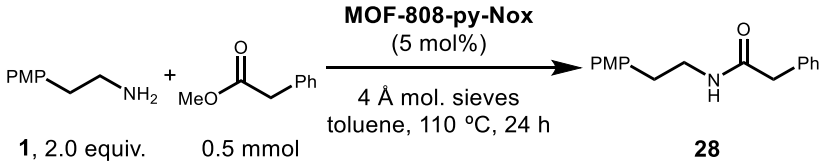

Figure S41. Synthesis of **28** in continuous flow.

The continuous flow amide band formation was performed in a packed-bed flow cell, assembled from 1/4" OD x 1/8" ID stainless-steel housing with 1/8" OD x 1/16" ID stainless steel tubing inlet and outlet (Figure S37). A back-pressure regulator (Cole-Parmer IDEX, 5 atm) was affixed via Luer lock to the 1/8" OD x 1/16" ID tubing. Plastic syringes were affixed using a Luer lock and were used to deliver reagents with a Harvard Apparatus Syringe Infusion Pump 22. The reaction chamber was packed with a ground mixture of **MOF-808-py-Nox** (34 mg, 0.025 mmol, 5 mol%) and pre-activated 4 Å molecular sieves (50 mg) and plugged with glass wool on both ends to immobilize the catalyst. The packed bed was subsequently pre-heated to 110 ˚C using a sand bath. A 5 mL syringe was loaded with a solution of 4-methoxyphenethylamine (146.5 µL, 1 mmol, 2.0 equiv.), methyl phenylacetate (71.2 µL, 0.5 mmol, 1.0 equiv.), and 1,3,5-trimethoxybenzene (84.1 mg, 0.5 mmol, 1.0 equiv. internal standard) in anhydrous toluene (5 mL) and affixed to the reaction chamber. The reaction was conducted for 24 h (0.208 mL/h flow rate, 24 h dwell time, 110 ˚C), collecting into a receiving flask. A 0.1 mL portion of the solution in the receiving flask was dissolved in $CDCl_3$ (0.5 mL) to obtain the ^1H NMR yield of **28** (82%). This yield is comparable to that obtained in batch (93%).

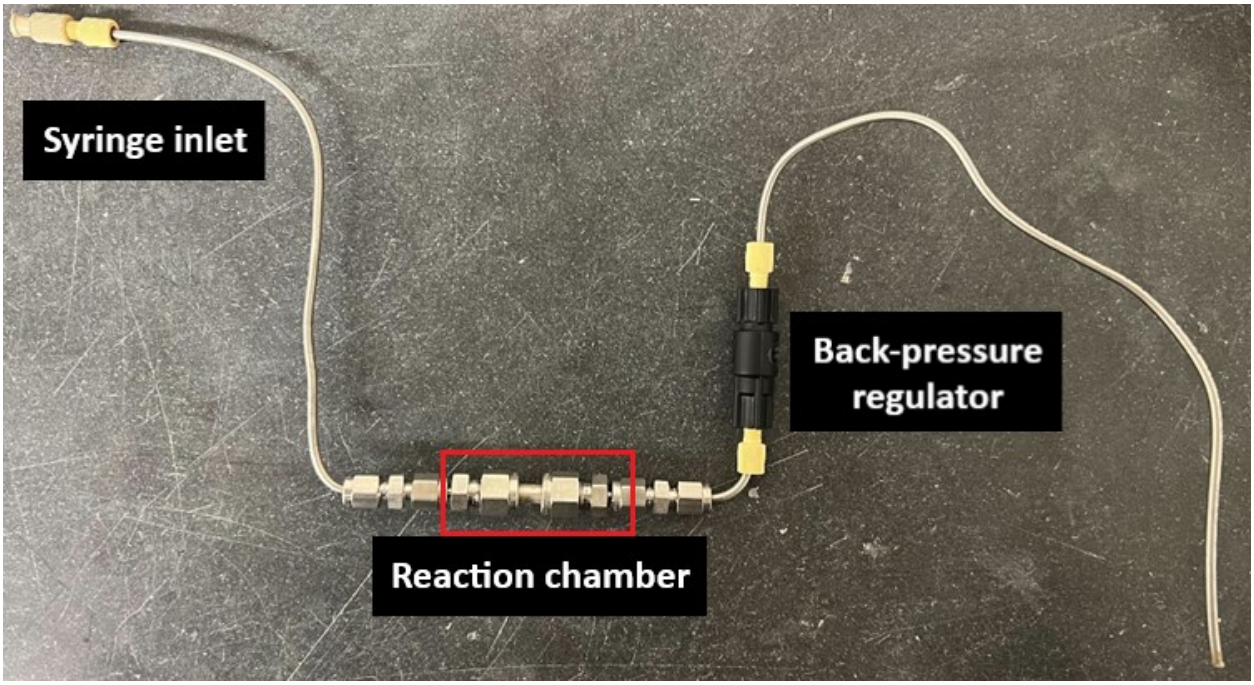

Figure S42. Packed-bed continuous flow reactor used in amide bond formation experiment.

10. Preparation and characterization of amides.

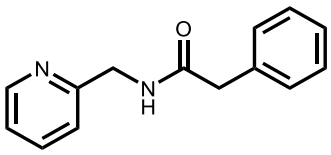

2-phenyl-*N*-(pyridin-2-ylmethyl)acetamide (5)

Following General Procedure B, (pyridin-2-yl)methanamine (103.1 µL, 1.0 mmol, 2.0 equiv.), phenylacetic acid (68.1 mg, 0.5 mmol, 1.0 equiv.), **MOF-808-py-Nox** (34 mg, 0.025 mmol, 0.05 equiv.), and toluene (5 mL) were added to a screw-cap reaction tube containing a stir bar and flame-activated 4 Å molecular sieves. Then, the reaction mixture was stirred in a 110 ˚C silicone oil bath for 24 h. The crude product was purified by silica gel flash chromatography using a Biotage Isolera instrument (gradient of 10% → 50% EtOAc in hexanes containing 1% Et_3N) to afford **5** (89.0 mg, 79%) as a white solid. ^{1}H NMR (500 MHz, DMSO-d_6): δ 8.62 (d, J = 6.1 Hz, 1H), 8.49 (d, J = 4.8 Hz, 1H), 7.73 (td, J = 7.6, 1.8 Hz, 1H), 7.30 (d, J = 5.4 Hz, 4H), 7.26–7.19 (m, 3H), 4.35 (d, J = 5.9 Hz, 2H), 3.51 (s, 2H); ^{13}C NMR (126 MHz, DMSO-d_6): δ 170.79, 159.02, 149.31, 137.15, 136.80, 129.52, 128.68, 126.84, 122.57, 121.40, 44.76, 42.78 ppm. The NMR data are consistent with the reported data.[13]

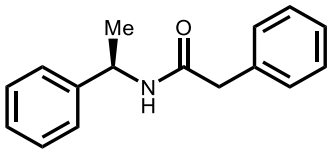

(*R*)-2-phenyl-*N*-(1-phenylethyl)acetamide (6)

Following General Procedure B, (*R*)-(+)-*α*-methylbenzylamine (127.3 µL, 1.0 mmol, 2.0 equiv.), phenylacetic acid (68.1 mg, 0.5 mmol, 1.0 equiv.), **MOF-808-py-Nox** (34 mg, 0.025 mmol, 0.05 equiv.), and toluene (5 mL) were added to a screw-cap reaction tube containing a stir bar and flame-activated 4 Å molecular sieves. Then, the reaction mixture was stirred in a 110 ˚C silicone oil bath for 24 h. The crude product was purified by silica gel flash chromatography using a Biotage Isolera instrument (gradient of 10 → 50% EtOAc in hexanes containing 1% Et_3N) to afford **6** (56.0 mg, 47%) as a white solid. ^{1}H NMR (500 MHz, DMSO-d_6): δ 8.51 (d, J = 8.1 Hz, 1H), 7.34–7.23 (m, 8H), 7.23–7.17 (m, 2H), 4.89 (p, J = 7.2 Hz, 1H), 3.44 (s, 2H), 1.35 (d, J = 7.0 Hz, 3H); ^{13}C NMR (126 MHz, DMSO-d_6): δ 169.58, 145.12, 136.96, 129.41, 128.68, 128.62, 127.06, 126.74, 126.37, 48.34, 42.77, 23.03 ppm; $[\alpha]_D$ +11 (conc. 0.009 g/mL, 20 ºC, $CHCl_3$). The NMR and optical rotation data are consistent with the reported data.[14,15]

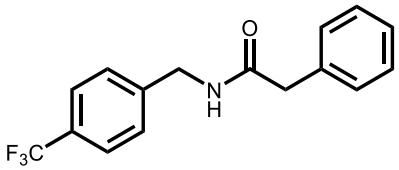

2-phenyl-*N*-(4-(trifluoromethyl)benzyl)acetamide (7)

Following General Procedure B, 4-(trifluoromethyl)benzylamine (142.5 µL, 1.0 mmol, 2.0 equiv.), phenylacetic acid (68.1 mg, 0.5 mmol, 1.0 equiv.), **MOF-808-py-Nox** (34 mg, 0.025 mmol, 0.05 equiv.), and toluene (5 mL) were added to a screw-cap reaction tube containing a stir bar and flame-activated 4 Å molecular sieves. Then, the reaction mixture was stirred in a 110 ˚C silicone oil bath for 24 h. The crude product was purified by silica gel flash chromatography using a Biotage Isolera instrument (gradient of 10 → 50% EtOAc in hexanes containing 1% Et_3N) to afford **7** (89.5 mg, 61%) as a white solid. ^{1}H NMR (500 MHz, $CDCl_3$): δ 7.54 (d, J = 8.0 Hz, 2H), 7.37 (dd, J = 8.1, 6.6 Hz, 2H), 7.33–7.30 (m, 1H), 7.27 (d, J = 1.8 Hz, 4H), 5.76 (s, 1H), 4.46 (d, J = 6.1 Hz, 2H), 3.65 (s, 2H); ^{13}C NMR (126 MHz, $CDCl_3$): δ 171.06, 142.30, 134.57, 129.84, 129.58, 129.47, 129.21, 127.61, 125.65, 125.62, 125.59, 125.56, 125.14, 122.98, 43.82, 43.03; ^{19}F NMR (376 MHz, $CDCl_3$): δ −62.56 ppm. The NMR data are consistent with the reported data.[16]

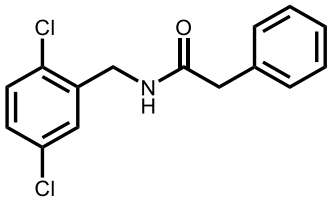

***N*-(2,5-dichlorobenzyl)-2-phenylacetamide (8)**

Following General Procedure B, 2,5-dichlorobenzylamine (133.6 µL, 1.0 mmol, 2.0 equiv.), phenylacetic acid (68.1 mg, 0.5 mmol, 1.0 equiv.), **MOF-808-py-Nox** (34 mg, 0.025 mmol, 0.05 equiv.), and toluene (5 mL) were added to a screw-cap reaction tube containing a stir bar and flame-activated 4 Å molecular sieves. Then, the reaction mixture was stirred in a 110 ˚C silicone oil bath for 24 h. The crude product was purified by silica gel flash chromatography using a Biotage Isolera instrument (gradient of 10 → 50% EtOAc in hexanes containing 1% Et_3N) to afford **8** (84.0 mg, 57%) as a white solid (Note: multiple conformers were observed). ^{1}H NMR (500 MHz, $CDCl_3$): δ 7.53–7.03 (m, 9H), 5.86 (s, 1H), 4.43 (s, 2H), 3.64 (s, 2H); ^{13}C NMR (126 MHz, $CDCl_3$): δ 171.09, 137.21, 134.53, 132.91, 131.52, 130.64, 130.52, 129.47, 129.44, 129.36, 129.20, 129.10, 128.78, 128.59, 128.39, 127.58, 127.11, 43.75, 41.24; HRMS (DART) exact mass calculated for [$C_{15}H_{14}Cl_2NO^+$]: 294.04470, found 294.04753; Melting point: 156.0–158.0 ˚C; IR (neat, cm^{-1}): 3279, 3063, 3030, 2918, 2665, 1660, 1637, 1552, 1496, 1459, 1416, 1398, 1372, 1322, 1273, 1249, 1191, 1148, 1096, 1067, 1041, 1027, 921, 898, 867, 844, 814, 769, 735, 721, 695, 598, 532.

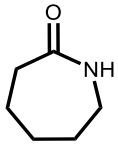

Caprolactam (9)

Following General Procedure B, 6-aminohexanoic acid (131.2 mg, 0.5 mmol, 1.0 equiv), **MOF-808-py-Nox** (34 mg, 0.025 mmol, 0.05 equiv.), and toluene (5 mL) were added to a screw-cap reaction tube containing a stir bar and flame-activated 4 Å molecular sieves. Then, the reaction mixture was stirred in a 110 ˚C silicone oil bath for 24 h. The crude product was purified by silica gel flash chromatography using a Biotage Isolera instrument (gradient of 10 → 50% EtOAc in

hexanes containing 1% Et_3N) to afford **9** (28.0 mg, 50%) as a white solid. ^1H NMR (500 MHz, $CDCl_3$): δ 6.92 (s, 1H), 3.29–3.10 (m, 2H), 2.55–2.39 (m, 2H), 1.76 (qd, J = 5.7, 2.8 Hz, 2H), 1.70 (q, J = 5.3 Hz, 2H), 1.67–1.61 (m, 2H); ^{13}C NMR (126 MHz, $CDCl_3$): δ 179.47, 42.87, 36.80, 30.68, 29.78, 23.29 ppm. The NMR data are consistent with the reported data.[17]

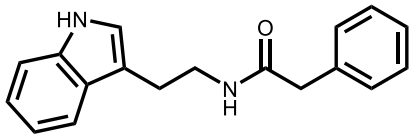

***N*-(2-(1H-indol-3-yl)ethyl)-2-phenylacetamide (10)**

Following General Procedure B, tryptamine (160.2 mg, 1.0 mmol, 2.0 equiv.), phenylacetic acid (68.1 mg, 0.5 mmol, 1.0 equiv), **MOF-808-py-Nox** (34 mg, 0.025 mmol, 0.05 equiv.), and toluene (5 mL) were added to a screw-cap reaction tube containing a stir bar and flame-activated 4 Å molecular sieves. Then, the reaction mixture was stirred in a 110 ˚C silicone oil bath for 24 h. The crude product was purified by silica gel flash chromatography using a Biotage Isolera instrument (gradient of 10 → 100% CH_2Cl_2 in hexanes containing 1% Et_3N, followed by a gradient of 0 → 5% MeOH in CH_2Cl_2) to afford **10** (78.0 mg, 56%) as a brown solid. ^1H NMR (500 MHz, $CDCl_3$): δ 7.93 (s, 1H), 7.54 (d, J = 7.9 Hz, 1H), 7.35 (d, J = 8.1 Hz, 1H), 7.32–7.23 (m, 3H), 7.23–7.16 (m, 1H), 7.15 (d, J = 2.0 Hz, 1H), 7.15–7.07 (m, 2H), 6.78 (d, J = 2.4 Hz, 1H), 5.42 (s, 1H), 3.57–3.50 (m, 4H), 2.89 (t, J = 6.7 Hz, 2H); ^{13}C NMR (126 MHz, $CDCl_3$): δ 170.88, 136.32, 134.97, 129.47, 128.93, 127.23, 127.20, 122.22, 121.93, 119.53, 118.70, 112.84, 111.17, 43.96, 39.73, 25.06 ppm. The NMR data are consistent with the reported data.[18]

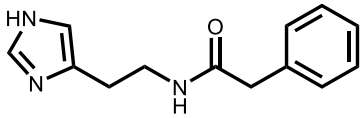

***N*-(2-(1H-imidazol-4-yl)ethyl)-2-phenylacetamide (11)**

Following General Procedure B, histamine (111.1 mg, 1.0 mmol, 2.0 equiv.), phenylacetic acid (68.1 mg, 0.5 mmol, 1.0 equiv), **MOF-808-py-Nox** (34 mg, 0.025 mmol, 0.05 equiv.), and toluene (5 mL) were added to a screw-cap reaction tube containing a stir bar and flame-activated 4 Å molecular sieves. Then, the reaction mixture was stirred in a 110 ˚C silicone oil bath for 24 h. The crude product was purified by silica gel flash chromatography using a Biotage Isolera instrument (gradient of 10 → 100% CH_2Cl_2 in hexanes containing 1% Et_3N, followed by a gradient of 0 → 5% MeOH in CH_2Cl_2) to afford **11** (57.5 mg, 50%) as a faint yellow solid. ^1H NMR (500 MHz, DMSO-d_6): δ 11.78 (s, 1H), 8.08 (s, 1H), 7.50 (s, 1H), 7.28 (t, J = 7.6 Hz, 2H), 7.21 (dd, J = 14.0, 7.1 Hz, 3H), 6.75 (s, 1H), 3.38 (s, 2H), 3.26 (q, J = 6.9 Hz, 2H), 2.61 (t, J = 7.4 Hz, 2H); ^{13}C NMR (126 MHz, DMSO-d_6): δ 170.45, 136.96, 135.09, 129.42, 128.64, 126.74, 42.89, 39.35 ppm. The NMR data are consistent with the reported data.[19]

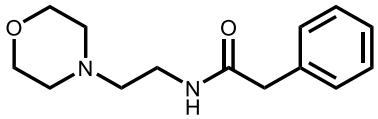

***N*-(2-morpholinoethyl)-2-phenylacetamide (12)**

Following General Procedure B, 4-(2-aminoethyl)morpholine (130.2 mg, 1.0 mmol, 2.0 equiv.), phenylacetic acid (68.1 mg, 0.5 mmol, 1.0 equiv), **MOF-808-py-Nox** (34 mg, 0.025 mmol, 0.05 equiv.), and toluene (5 mL) were added to a screw-cap reaction tube containing a stir bar and flame-activated 4 Å molecular sieves. Then, the reaction mixture was stirred in a 110 ˚C silicone oil bath for 24 h. The crude product was purified by silica gel flash chromatography using a Biotage Isolera instrument (gradient of 10 → 100% CH_2Cl_2 in hexanes containing 1% Et_3N, followed by a gradient of 0 → 5% MeOH in CH_2Cl_2) to afford **12** (66.0 mg, 53%) as a white solid. ^{1}H NMR (500 MHz, $CDCl_3$): δ 7.37 (ddd, J = 7.7, 6.2, 1.5 Hz, 2H), 7.33–7.29 (m, 1H), 7.27 (d, J = 1.7 Hz, 2H), 6.03 (s, 1H), 3.59 (s, 2H), 3.52 (t, J = 4.6 Hz, 4H), 3.28 (q, J = 5.7 Hz, 2H), 2.38 (t, J = 6.1 Hz, 2H), 2.31 (t, J = 4.6 Hz, 4H); ^{13}C NMR (126 MHz, $CDCl_3$): δ 171.13, 135.28, 129.68, 129.13, 127.47, 67.00, 56.45, 53.15, 44.02, 35.78 ppm. The NMR data are consistent with the reported data.[20]

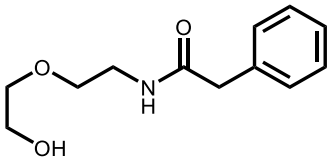

***N*-(2-(2-hydroxyethoxy)ethyl)-2-phenylacetamide (13)**

Following General Procedure B, 2-(2-aminoethoxy)ethanol (100.3 µL, 1.0 mmol, 2.0 equiv.), phenylacetic acid (68.1 mg, 0.5 mmol, 1.0 equiv), **MOF-808-py-Nox** (34 mg, 0.025 mmol, 0.05 equiv.), and toluene (5 mL) were added to a screw-cap reaction tube containing a stir bar and flame-activated 4 Å molecular sieves. Then, the reaction mixture was stirred in a 110 ˚C silicone oil bath for 24 h. The crude product was purified by silica gel flash chromatography using a Biotage Isolera instrument (gradient of 10 → 100% CH_2Cl_2 in hexanes containing 1% Et_3N, followed by a gradient of 0 → 5% MeOH in CH_2Cl_2) to afford **13** (92.5 mg, 83%) as a white solid. ^{1}H NMR (500 MHz, $CDCl_3$): δ 7.39–7.34 (m, 2H), 7.33–7.29 (m, 1H), 7.28 (s, 2H), 5.94 (s, 1H), 3.69–3.62 (m, 2H), 3.59 (s, 2H), 3.49 (dd, J = 6.9, 4.1 Hz, 4H), 3.43 (q, J = 5.3 Hz, 2H), 1.99 (d, J = 185.1 Hz, 1H); ^{13}C NMR (126 MHz, $CDCl_3$): δ 171.23, 134.91, 129.45, 128.95, 127.35, 72.06, 71.99, 69.65, 69.57, 61.70, 43.82, 43.75, 43.67, 39.30; HRMS (DART) exact mass calculated for [$C_{12}H_{18}NO_3^+$]: 224.12812, found 224.13006; Melting point: slightly above room temperature; IR (neat, cm^{-1}): 3247, 3083, 2936, 2874, 1653, 1625, 1568, 1491, 1455, 1428, 1407, 1346, 1316, 1271, 1235, 1160, 1121, 1062, 1026, 961, 936, 890, 871, 759, 712, 692, 616, 556, 537.

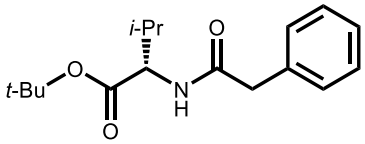

***tert*-butyl (2-phenylacetyl)-*L*-valinate (14)**

Following General Procedure B, *tert*-butyl L-valine ester hydrochloride (151.3 mg, 1.0 mmol, 2.0 equiv.), phenylacetic acid (68.1 mg, 0.5 mmol, 1.0 equiv), triethylamine (139.4 µL, 1.0 mmol, 2.0 equiv.), **MOF-808-py-Nox** (34 mg, 0.025 mmol, 0.05 equiv.), and toluene (5 mL) were added to

a screw-cap reaction tube containing a stir bar and flame-activated 4 Å molecular sieves. Then, the reaction mixture was stirred in a 110 ˚C silicone oil bath for 24 h. The crude product was purified by silica gel flash chromatography using a Biotage Isolera instrument (gradient of 10 → 100% CH_2Cl_2 in hexanes containing 1% Et_3N, followed by a gradient of 0 → 5% MeOH in CH_2Cl_2) to afford **14** (116.0 mg, 80%) as a colorless liquid. ^{1}H NMR (500 MHz, $CDCl_3$): δ 7.39 (dd, J = 8.4, 6.8 Hz, 2H), 7.35–7.29 (m, 3H), 5.87 (d, J = 8.7 Hz, 1H), 4.45 (dd, J = 8.8, 4.5 Hz, 1H), 3.63 (d, J = 3.1 Hz, 2H), 2.11 (pd, J = 6.9, 4.5 Hz, 1H), 1.44 (s, 9H), 0.87 (d, J = 6.9 Hz, 3H), 0.78 (d, J = 6.9 Hz, 3H); ^{13}C NMR (126 MHz, $CDCl_3$): δ 170.79, 170.64, 134.83, 129.40, 129.02, 127.39, 81.94, 57.32, 43.89, 31.45, 30.95, 28.02, 18.83, 17.46 ppm; HRMS (DART) exact mass calculated for [$C_{17}H_{26}NO_3^+$]: 292.19072, found 292.19398; IR (neat, cm^{-1}): 3303, 2966, 2930, 1733, 1649, 1539, 1496, 1455, 1392, 1368, 1313, 1257, 1219, 1150, 1031, 914, 847, 792, 726, 696, 669, 526. $[\alpha]_D$ 0 (conc. 0.008 g/mL, 20ºC, $CHCl_3$).

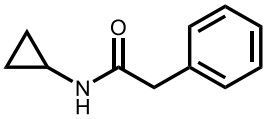

***N*-cyclopropyl-2-phenylacetamide (15)**

Following General Procedure B, cyclopropylamine (69.3 µL, 1.0 mmol, 2.0 equiv.), phenylacetic acid (68.1 mg, 0.5 mmol, 1.0 equiv), **MOF-808-py-Nox** (34 mg, 0.025 mmol, 0.05 equiv.), and toluene (5 mL) were added to a screw-cap reaction tube containing a stir bar and flame-activated 4 Å molecular sieves. Then, the reaction mixture was stirred in a 110 ˚C silicone oil bath for 24 h. The crude product was purified by silica gel flash chromatography using a Biotage Isolera instrument (gradient of 10 → 50% EtOAc in hexanes containing 1% Et_3N) to afford **15** (41.0 mg, 47%) as a white solid. ^{1}H NMR (500 MHz, $CDCl_3$): δ 7.35 (dd, J = 8.1, 6.5 Hz, 2H), 7.32–7.27 (m, 1H), 7.25–7.19 (m, 2H), 5.44 (s, 1H), 3.54 (s, 2H), 2.66 (tq, J = 7.2, 3.5 Hz, 1H), 0.77–0.68 (m, 2H), 0.46–0.32 (m, 2H); ^{13}C NMR (126 MHz, $CDCl_3$): δ 172.51, 135.00, 129.54, 129.19, 127.51, 43.93, 22.89, 6.75 ppm. The NMR data are consistent with the reported data.[21]

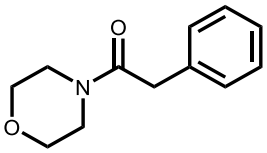

1-morpholino-2-phenylethan-1-one (16)

Following General Procedure B, morpholine (86.2 µL, 1.0 mmol, 2.0 equiv.), phenylacetic acid (68.1 mg, 0.5 mmol, 1.0 equiv), **MOF-808-py-Nox** (34 mg, 0.025 mmol, 0.05 equiv.), and toluene (5 mL) were added to a screw-cap reaction tube containing a stir bar and flame-activated 4 Å molecular sieves. Then, the reaction mixture was stirred in a 110 ˚C silicone oil bath for 24 h. The crude product was purified by silica gel flash chromatography using a Biotage Isolera instrument (gradient of 10 → 100% CH_2Cl_2 in hexanes containing 1% Et_3N, followed by a gradient of 0 → 5% MeOH in CH_2Cl_2) to afford **16** (31.0 mg, 30%) as a off white solid. ^{1}H NMR (500 MHz, $CDCl_3$): δ 7.36–7.30 (m, 2H), 7.29–7.21 (m, 3H), 3.73 (s, 2H), 3.64 (s, 4H), 3.47 (dd, J = 6.1, 4.1 Hz, 2H), 3.43 (dd, J = 5.9, 3.8 Hz, 2H).; ^{13}C NMR (126 MHz, $CDCl_3$): δ 169.64, 134.81, 128.83,

128.54, 126.93, 66.82, 66.47, 46.54, 42.16, 40.89 ppm. The NMR data are consistent with the reported data.[22]

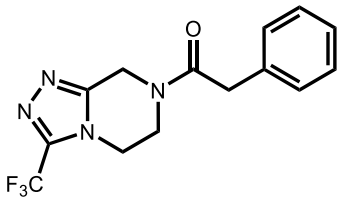

2-phenyl-1-(3-(trifluoromethyl)-5,6-dihydro-[1,2,4]triazolo[4,3-a]pyrazin-7(8H)-yl)ethan-1-one (17)

Following General Procedure B, 3-(trifluoromethyl)-5,6,7,8-tetrahydro-[1,2,4]triazolo[4,3-a]pyrazine (192.2 mg, 1.0 mmol, 2.0 equiv.), phenylacetic acid (68.1 mg, 0.5 mmol, 1.0 equiv), **MOF-808-py-Nox** (34 mg, 0.025 mmol, 0.05 equiv.), and toluene (5 mL) were added to a screw-cap reaction tube containing a stir bar and flame-activated 4 Å molecular sieves. Then, the reaction mixture was stirred in a 110 ˚C silicone oil bath for 24 h. The crude product was purified by silica gel flash chromatography using a Biotage Isolera instrument (gradient of 10 → 100% CH_2Cl_2 in hexanes containing 1% Et_3N, followed by a gradient of 0 → 5% MeOH in CH_2Cl_2) to afford **17** (57.0 mg, 37%) as a white solid. ^{1}H NMR (500 MHz, $CDCl_3$): δ 7.41–7.18 (m, 5H), 5.05 (d, J = 14.3 Hz, 1H), 4.89 (d, J = 7.8 Hz, 1H), 4.19–4.03 (m, 2H), 3.85 (td, J = 23.7, 15.0 Hz, 4H); ^{13}C NMR (126 MHz, $CDCl_3$): δ 170.23, 169.85, 150.35, 149.50, 143.55, 133.70, 133.25, 129.20, 129.05, 128.64, 128.42, 127.47, 121.41, 119.26, 117.11, 114.96, 77.29, 77.04, 76.78, 43.21, 42.96, 42.14, 41.45, 40.98, 39.43, 38.30; ^{19}F NMR (470 MHz, $CDCl_3$) δ −67.82 ppm. HRMS (DART) exact mass calculated for [$C_{14}H_{14}F_3N_4O^+$]: 311.11142, found 311.11427; Melting point: 132.5-134.5 ˚C; IR (neat, cm^{-1}): 3086, 3030, 3063, 2925, 1717, 1656, 1496, 1435, 1273, 1140, 1016, 942, 700, 603.

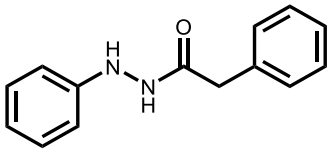

***N*',2-diphenylacetohydrazide (18)**

Following General Procedure B, phenylhydrazine (108.1 mg, 1.0 mmol, 2.0 equiv.), phenylacetic acid (68.1 mg, 0.5 mmol, 1.0 equiv), **MOF-808-py-Nox** (34 mg, 0.025 mmol, 0.05 equiv.), and toluene (5 mL) were added to a screw-cap reaction tube containing a stir bar and flame-activated 4 Å molecular sieves. Then, the reaction mixture was stirred in a 110 ˚C silicone oil bath for 24 h. The crude product was purified by silica gel flash chromatography using a Biotage Isolera instrument (gradient of 10 → 50% EtOAc in hexanes containing 1% Et_3N) to afford **18** (23.0 mg, 20%) as a white solid. ^{1}H NMR (500 MHz, DMSO-d_6): δ 9.90 (d, J = 2.9 Hz, 1H), 7.76 (d, J = 2.9 Hz, 1H), 7.35–7.21 (m, 5H), 7.09 (t, J = 7.6 Hz, 2H), 6.66 (dd, J = 16.3, 7.8 Hz, 3H), 3.49 (s, 2H); ^{13}C NMR (126 MHz, DMSO-d_6): δ 170.44, 149.75, 136.37, 129.47, 129.13, 128.74, 126.98, 118.88, 112.45, 40.93 ppm. The NMR data are consistent with the reported data.[23]

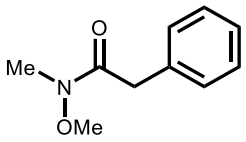

_N_-methoxy-_N_-methyl-2-phenylacetamide (19)

Following General Procedure B, *N*,*O*-dimethylhydroxylamine hydrochloride (97.5 mg, 1.0 mmol, 2.0 equiv.), phenylacetic acid (68.1 mg, 0.5 mmol, 1.0 equiv), triethylamine (139.4 µL, 1.0 mmol, 2.0 equiv.), **MOF-808-py-Nox** (34 mg, 0.025 mmol, 0.05 equiv.), and toluene (5 mL) were added to a screw-cap reaction tube containing a stir bar and flame-activated 4 Å molecular sieves. Then, the reaction mixture was stirred in a 110 ˚C silicone oil bath for 24 h. The crude product was purified by silica gel flash chromatography using a Biotage Isolera instrument (gradient of 10 → 50% EtOAc in hexanes containing 1% Et_3N) to afford **19** (44.0 mg, 49%) as a colorless liquid. ^{1}H NMR (500 MHz, $CDCl_3$): δ 7.35–7.21 (m, 5H), 3.78 (s, 2H), 3.59 (s, 3H), 3.19 (s, 3H); ^{13}C NMR (126 MHz, $CDCl_3$): δ 172.39, 135.00, 129.31, 128.49, 126.77, 61.28, 39.39, 32.20 ppm. The NMR data are consistent with the reported data.[24]

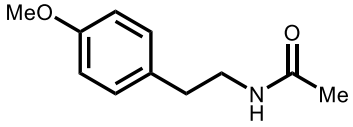

_N_-(4-methoxyphenethyl)acetamide (3)

Following General Procedure B, 4-methoxyphenethylamine (146.5 µL, 1.0 mmol, 2.0 equiv.), acetic acid (28.6 µL, 0.5 mmol, 1.0 equiv), **MOF-808-py-Nox** (34 mg, 0.025 mmol, 0.05 equiv.), and toluene (5 mL) were added to a screw-cap reaction tube containing a stir bar and flame-activated 4 Å molecular sieves. Then, the reaction mixture was stirred in a 110 ˚C silicone oil bath for 24 h. The crude product was purified by silica gel flash chromatography using a Biotage Isolera instrument (gradient of 10 → 50% EtOAc in hexanes containing 1% Et_3N) to afford **3** (61.0 mg, 63%) as a white solid. ^{1}H NMR (500 MHz, $CDCl_3$): δ 7.16–7.06 (m, 2H), 6.88–6.81 (m, 2H), 5.41 (s, 1H), 3.80 (s, 3H), 3.48 (q, J = 6.6 Hz, 2H), 2.77 (q, J = 8.3 Hz, 2H), 1.94 (s, 3H); ^{13}C NMR (126 MHz, $CDCl_3$): δ 170.13, 158.45, 130.95, 129.85, 129.83, 114.22, 55.42, 40.96, 34.85, 23.51 ppm. The NMR data are consistent with the reported data.[25]

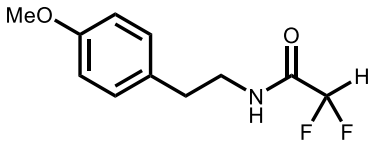

2,2-difluoro-_N_-(4-methoxyphenethyl)acetamide (20)

Following General Procedure B, 4-methoxyphenethylamine (146.5 µL, 1.0 mmol, 2.0 equiv.), difluoroacetic acid (31.5 µL, 0.5 mmol, 1.0 equiv), **MOF-808-py-Nox** (34 mg, 0.025 mmol, 0.05 equiv.), and toluene (5 mL) were added to a screw-cap reaction tube containing a stir bar and flame-activated 4 Å molecular sieves. Then, the reaction mixture was stirred in a 110 ˚C silicone oil bath for 24 h. The crude product was purified by silica gel flash chromatography using a Biotage

Isolera instrument (gradient of 10 → 50% EtOAc in hexanes containing 1% Et_3N) to afford **20** (103.0 mg, 90%) as a faint yellow solid. ^1H NMR (500 MHz, DMSO-d_6): δ 8.83 (t, J = 5.6 Hz, 1H), 7.19–7.08 (m, 2H), 6.92–6.78 (m, 2H), 6.17 (t, J = 53.8 Hz, 1H), 3.72 (d, J = 2.1 Hz, 3H), 3.30 (d, J = 6.9 Hz, 2H), 2.69 (t, J = 7.4 Hz, 2H); ^{13}C NMR (126 MHz, DMSO-d_6): δ 162.55, 158.23, 131.20, 130.06, 114.26, 110.96, 109.00, 107.04, 55.45, 40.76, 34.08; ^{19}F NMR (376 MHz, $CDCl_3$): δ −126.19 (d, J = 1.8 Hz), −126.34 (d, J = 1.7 Hz) ppm; HRMS (DART) exact mass calculated for [$C_{11}H_{14}F_2NO_2^+$]: 230.09871, found 230.10095; Melting point: 59.0–60.5 ˚C; IR (neat, cm^{-1}): 3325, 3117, 3039, 2961, 2865, 2838, 1677, 1613, 1585, 1551, 1511, 1468, 1457, 1374, 1343, 1321, 1302, 1288, 1245, 1187, 1176, 1110, 1081, 1055, 1031, 932, 824, 812, 757, 686, 613, 551, 520.

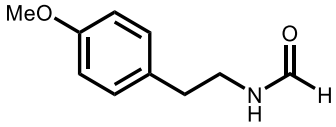

***N*-(4-methoxyphenethyl)formamide (4)**

Following General Procedure B, 4-methoxyphenethylamine (146.5 µL, 1.0 mmol, 2.0 equiv.), formic acid (18.9 µL, 0.5 mmol, 1.0 equiv), **MOF-808-py-Nox** (34 mg, 0.025 mmol, 0.05 equiv.), and toluene (5 mL) were added to a screw-cap reaction tube containing a stir bar and flame-activated 4 Å molecular sieves. Then, the reaction mixture was stirred in a 110 ˚C silicone oil bath for 24 h. The crude product was purified by silica gel flash chromatography using a Biotage Isolera instrument (gradient of 10 → 100% CH_2Cl_2 in hexanes containing 1% Et_3N, followed by a gradient of 0 → 5% MeOH in CH_2Cl_2) to afford **4** (83.0 mg, 93%) as a white solid. Note: the material readily decomposes and loses CO under vacuum. ^1H NMR (500 MHz, $CDCl_3$): δ 8.09 (d, J = 3.0 Hz, 1H), 7.11 (d, J = 8.1 Hz, 2H), 6.87–6.82 (m, 2H), 5.90 (s, 1H), 3.78 (d, J = 1.6 Hz, 3H), 3.51 (qd, J = 6.7, 2.4 Hz, 2H), 2.77 (t, J = 7.1 Hz, 2H); ^{13}C NMR (126 MHz, $CDCl_3$): δ 161.30, 158.32, 130.49, 129.73, 114.08, 55.33, 39.42, 34.59 ppm. The NMR data are consistent with the reported data.[26]

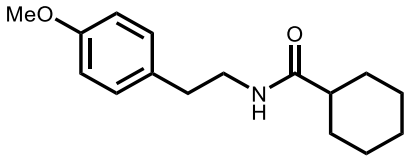

***N*-(4-methoxyphenethyl)cyclohexanecarboxamide (21)**

Following General Procedure B, 4-methoxyphenethylamine (146.5 µL, 1.0 mmol, 2.0 equiv.), cyclohexanecarboxylic acid (64.1 mg, 0.5 mmol, 1.0 equiv), **MOF-808-py-Nox** (34 mg, 0.025 mmol, 0.05 equiv.), and toluene (5 mL) were added to a screw-cap reaction tube containing a stir bar and flame-activated 4 Å molecular sieves. Then, the reaction mixture was stirred in a 110 ˚C silicone oil bath for 24 h. The crude product was purified by silica gel flash chromatography using a Biotage Isolera instrument (gradient of 10 → 50% EtOAc in hexanes containing 1% Et_3N) to afford **21** (52.0 mg, 40%) as a white solid. ^1H NMR (500 MHz, $CDCl_3$): δ 7.10 (d, J = 8.1 Hz, 2H), 6.86 (d, J = 8.1 Hz, 2H), 5.42 (s, 1H), 3.80 (d, J = 1.3 Hz, 3H), 3.47 (q, J = 6.5 Hz, 2H), 2.75 (t, J = 6.8 Hz, 2H), 2.00 (tt, J = 11.9, 3.4 Hz, 1H), 1.90–1.59 (m, 5H), 1.49–1.06 (m, 5H); ^{13}C NMR

(126 MHz, $CDCl_3$): δ 176.02, 158.22, 130.98, 129.76, 114.00, 55.33, 55.24, 45.57, 40.52, 34.79, 29.68, 25.73 ppm. The NMR data are consistent with the reported data.[27]

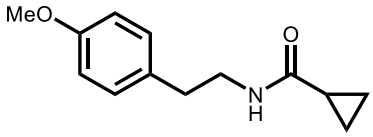

***N*-(4-methoxyphenethyl)cyclopropanecarboxamide (22)**

Following General Procedure B, 4-methoxyphenethylamine (146.5 µL, 1.0 mmol, 2.0 equiv.), cyclopropanecarboxylic acid (39.8 µL, 0.5 mmol, 1.0 equiv), **MOF-808-py-Nox** (34 mg, 0.025 mmol, 0.05 equiv.), and toluene (5 mL) were added to a screw-cap reaction tube containing a stir bar and flame-activated 4 Å molecular sieves. Then, the reaction mixture was stirred in a 110 ˚C silicone oil bath for 24 h. The crude product was purified by silica gel flash chromatography using a Biotage Isolera instrument (gradient of 10 → 50% EtOAc in hexanes containing 1% Et_3N) to afford **22** (47.0 mg, 43%) as a white solid. ^{1}H NMR (500 MHz, $CDCl_3$): 7.16–7.09 (m, 2H), 6.90–6.81 (m, 2H), 3.80 (s, 3H), 3.50 (td, J = 7.0, 5.8 Hz, 2H), 2.76 (t, J = 7.0 Hz, 2H), 1.26 (tt, J = 7.8, 4.6 Hz, 1H), 1.01–0.90 (m, 2H), 0.70 (dq, J = 7.0, 3.9 Hz, 2H).; ^{13}C NMR (126 MHz, $CDCl_3$): δ 173.45, 158.27, 130.95, 129.73, 114.05, 55.28, 40.95, 34.87, 14.76, 7.05 ppm; HRMS (DART) exact mass calculated for [$C_{13}H_{18}NO_2^+$]: 220.13321, found 220.13538; Melting point: 141.0–142.3 ˚C; IR (neat, cm^{-1}): 3303, 3090, 3010, 2942, 2877, 2841, 1635, 1613, 1583, 1548, 1512, 1465, 1442, 1401, 1359, 1303, 1280, 1236, 1185, 1100, 1059, 1028, 939, 833, 819, 754, 687, 650, 568, 520.

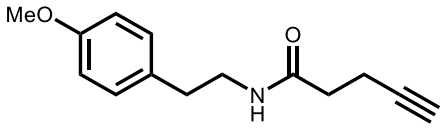

***N*-(4-methoxyphenethyl)pent-4-ynamide (23)**

Following General Procedure B, 4-methoxyphenethylamine (146.5 µL, 1.0 mmol, 2.0 equiv.), 4-pentynoic acid (49.0 mg, 0.5 mmol, 1.0 equiv), **MOF-808-py-Nox** (34 mg, 0.025 mmol, 0.05 equiv.), and toluene (5 mL) were added to a screw-cap reaction tube containing a stir bar and flame-activated 4 Å molecular sieves. Then, the reaction mixture was stirred in a 110 ˚C silicone oil bath for 24 h. The crude product was purified by silica gel flash chromatography using a Biotage Isolera instrument (gradient of 10 → 50% EtOAc in hexanes containing 1% Et_3N) to afford **23** (96.0 mg, 83%) as an off-white solid. ^{1}H NMR (500 MHz, $CDCl_3$): δ 7.15–7.07 (m, 2H), 6.89–6.80 (m, 2H), 5.62 (s, 1H), 3.79 (s, 3H), 3.51 (q, J = 6.7 Hz, 2H), 2.77 (t, J = 6.9 Hz, 2H), 2.50 (td, J = 7.2, 2.6 Hz, 2H), 2.35 (t, J = 7.2 Hz, 2H), 1.95 (t, J = 2.6 Hz, 1H); ^{13}C NMR (126 MHz, $CDCl_3$): δ 170.96, 158.44, 130.89, 129.85, 114.20, 83.13, 69.43, 55.41, 40.95, 35.52, 34.85, 15.00 ppm; HRMS (DART) exact mass calculated for [$C_{14}H_{18}NO_2^+$]: 232.13321, found 232.13553; Melting point: 121.5–122.5 ˚C; IR (neat, cm^{-1}): 3297, 3266, 3066, 3002, 2928, 2875, 2840, 1632, 1614, 1585,1545, 1512, 1466, 1439, 1385, 1303, 1245, 1226, 1179, 1113, 1091, 1027, 958, 819, 754, 666, 592, 566, 517.

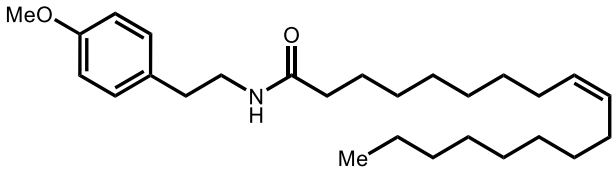

***N*-(4-methoxyphenethyl)oleamide (24)**

Following General Procedure B, 4-methoxyphenethylamine (146.5 µL, 1.0 mmol, 2.0 equiv.), oleic acid (157.8 µL, 0.5 mmol, 1.0 equiv), **MOF-808-py-Nox** (34 mg, 0.025 mmol, 0.05 equiv.), and toluene (5 mL) were added to a screw-cap reaction tube containing a stir bar and flame-activated 4 Å molecular sieves. Then, the reaction mixture was stirred in a 110 ˚C silicone oil bath for 24 h. The crude product was purified by silica gel flash chromatography using a Biotage Isolera instrument (gradient of 10 → 50% EtOAc in hexanes containing 1% Et_3N) to afford **24** (97.5 mg, 47%) as a white solid. ^{1}H NMR (500 MHz, $CDCl_3$): δ 7.17–7.06 (m, 2H), 6.90–6.76 (m, 2H), 5.38 (s, 1H), 5.34 (dt, J = 5.4, 2.7 Hz, 2H), 3.79 (s, 3H), 3.48 (q, J = 6.6 Hz, 2H), 2.75 (t, J = 6.9 Hz, 2H), 2.11 (t, J = 7.7 Hz, 2H), 1.58 (d, J = 7.5 Hz, 3H), 1.44–1.18 (m, 20H), 0.88 (t, J = 6.8 Hz, 3H); ^{13}C NMR (126 MHz, $CDCl_3$): δ 173.18, 158.42, 131.04, 130.15, 129.89, 129.84, 114.18, 55.40, 40.79, 37.01, 34.96, 32.05, 29.92, 29.87, 29.81, 29.67, 29.51, 29.47, 29.47, 29.41, 29.40, 29.29, 27.37, 27.32, 25.89, 22.83, 14.26 ppm. The NMR data are consistent with the reported data.[28]

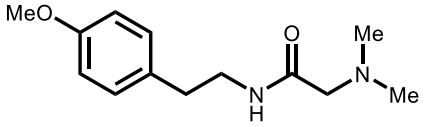

2-(dimethylamino)-N-(4-methoxyphenethyl)acetamide (25)

Following General Procedure B, 4-methoxyphenethylamine (146.5 µL, 1.0 mmol, 2.0 equiv.), dimethylglycine (51.5 mg, 0.5 mmol, 1.0 equiv), **MOF-808-py-Nox** (34 mg, 0.025 mmol, 0.05 equiv.), and toluene (5 mL) were added to a screw-cap reaction tube containing a stir bar and flame-activated 4 Å molecular sieves. Then, the reaction mixture was stirred in a 110 ˚C silicone oil bath for 24 h. The crude product was purified by silica gel flash chromatography using a Biotage Isolera instrument (gradient of 10 → 100% CH_2Cl_2 in hexanes containing 1% Et_3N, followed by a gradient of 0 → 5% MeOH in CH_2Cl_2) to afford **25** (84.0 mg, 71%) as an orange solid. ^{1}H NMR (500 MHz, $CDCl_3$): δ 7.19 (d, J = 8.6 Hz, 1H), 7.14 (d, J = 8.2 Hz, 2H), 6.89–6.84 (m, 2H), 3.81 (s, 3H), 3.53 (q, J = 6.8 Hz, 2H), 2.93 (s, 2H), 2.80 (t, J = 7.1 Hz, 2H), 2.23 (s, 6H); ^{13}C NMR (126 MHz, $CDCl_3$): δ 170.84, 158.21, 134.86, 130.65, 129.63, 129.49, 129.02, 127.32, 114.01, 55.27, 45.57, 43.93, 40.86, 34.57, 8.52 ppm; HRMS (DART) exact mass calculated for [$C_{13}H_{21}N_2O_2^+$]: 237.15975, found 237.16196; Melting point: 54.0–56.0 ˚C; IR (neat, cm^{-1}): 3293, 2999, 2919, 2849, 2816, 2767, 1650, 1611, 1583, 1510, 1454, 1440, 1363, 1319, 1298, 1244, 1175, 1147, 1111, 1087, 981, 862, 810, 749, 638, 602, 555, 525.

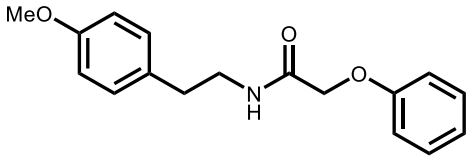

***N*-(4-methoxyphenethyl)-2-phenoxyacetamide (26)**

Following General Procedure B, 4-methoxyphenethylamine (146.5 µL, 1.0 mmol, 2.0 equiv.), 2-phenoxyacetic acid (76.1 mg, 0.5 mmol, 1.0 equiv), **MOF-808-py-Nox** (34 mg, 0.025 mmol, 0.05 equiv.), and toluene (5 mL) were added to a screw-cap reaction tube containing a stir bar and flame-activated 4 Å molecular sieves. Then, the reaction mixture was stirred in a 110 ˚C silicone oil bath for 24 h. The crude product was purified by silica gel flash chromatography using a Biotage Isolera instrument (gradient of 10 → 50% EtOAc in hexanes containing 1% Et_3N) to afford **26** (115.5 mg, 81%) as a faint yellow solid. ^{1}H NMR (500 MHz, $CDCl_3$): δ 7.36–7.28 (m, 2H), 7.09–7.05 (m, 2H), 7.03 (tt, J = 7.3, 1.3 Hz, 1H), 6.91–6.84 (m, 2H), 6.84–6.79 (m, 2H), 6.60 (s, 1H), 4.47 (s, 2H), 3.79 (s, 3H), 3.57 (q, J = 6.7 Hz, 2H), 2.78 (t, J = 7.0 Hz, 2H); ^{13}C NMR (126 MHz, $CDCl_3$): δ 168.13, 158.34, 157.19, 130.51, 129.79, 129.72, 122.10, 114.63, 114.09, 67.33, 55.28, 40.29, 34.80 ppm. The NMR data are consistent with the reported data.[29]

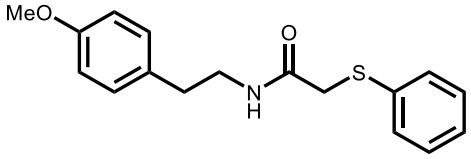

***N*-(4-methoxyphenethyl)-2-(phenylthio)acetamide (27)**

Following General Procedure B, 4-methoxyphenethylamine (146.5 µL, 1.0 mmol, 2.0 equiv.), 2-(phenylthio)acetic acid (84.1 mg, 0.5 mmol, 1.0 equiv), **MOF-808-py-Nox** (34 mg, 0.025 mmol, 0.05 equiv.), and toluene (5 mL) were added to a screw-cap reaction tube containing a stir bar and flame-activated 4 Å molecular sieves. Then, the reaction mixture was stirred in a 110 ˚C silicone oil bath for 24 h. The crude product was purified by silica gel flash chromatography using a Biotage Isolera instrument (gradient of 10 → 50% EtOAc in hexanes containing 1% Et_3N) to afford **27** (122.0 mg, 81%) as a faint yellow solid. ^{1}H NMR (500 MHz, $CDCl_3$): δ 7.28 (t, J = 7.5 Hz, 2H), 7.23–7.15 (m, 3H), 7.00–6.92 (m, 2H), 6.84 (s, 1H), 6.79–6.73 (m, 2H), 3.78 (s, 3H), 3.60 (s, 2H), 3.48 (q, J = 6.6 Hz, 2H), 2.67 (t, J = 6.9 Hz, 2H); ^{13}C NMR (126 MHz, $CDCl_3$): δ 167.73, 158.39, 134.85, 130.58, 129.75, 129.40, 127.91, 126.65, 114.17, 55.37, 41.18, 37.31, 34.69, 1.16 ppm; HRMS (DART) exact mass calculated for [$C_{17}H_{20}NO_2S^+$]: 302.12093, found 302.12353; Melting point: 119.5–120.5 ˚C; IR (neat, cm^{-1}): 3328, 3034, 3007, 2957, 2838, 1643, 1610, 1583, 1509, 1481, 1463, 1442, 1390, 1322, 1292, 1241, 1198, 1177, 1113, 1089, 1046, 1030, 998, 888, 835, 817, 789, 761, 736, 688, 589, 561, 515.

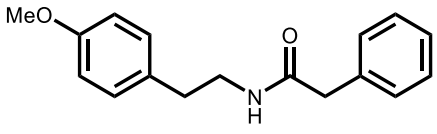

***N*-(4-methoxyphenethyl)-2-phenylacetamide (28)**

Following General Procedure B, 4-methoxyphenethylamine (146.5 µL, 1.0 mmol, 2.0 equiv.), phenylacetic acid (68.1 mg, 0.5 mmol, 1.0 equiv), **MOF-808-py-Nox** (34 mg, 0.025 mmol, 0.05 equiv.), and toluene (5 mL) were added to a screw-cap reaction tube containing a stir bar and flame-activated 4 Å molecular sieves. Then, the reaction mixture was stirred in a 110 ˚C silicone oil bath for 24 h. The crude product was purified by silica gel flash chromatography using a Biotage Isolera instrument (gradient of 10 → 50% EtOAc in hexanes containing 1% Et_3N) to afford **28** (123.5 mg, 92%) as a faint yellow solid. ^{1}H NMR (500 MHz, $CDCl_3$): δ 7.31 (dt, J = 13.3, 6.5 Hz, 3H), 7.22–7.14 (m, 2H), 6.96–6.89 (m, 2H), 6.78–6.73 (m, 2H), 5.45 (t, J = 6.0 Hz, 1H), 3.78 (s, 3H), 3.52 (s, 2H), 3.41 (q, J = 6.5 Hz, 2H), 2.65 (t, J = 6.8 Hz, 2H); ^{13}C NMR (126 MHz, $CDCl_3$): δ 170.87, 158.13, 134.83, 130.63, 129.62, 129.46, 128.95, 127.27, 113.94, 55.28, 43.86, 40.86, 34.54 ppm. The NMR data are consistent with the reported data.[12]

Following General Procedure B, 4-methoxyphenethylamine (146.5 µL, 1.0 mmol, 2.0 equiv.), methyl phenylacetate (71.2 µL, 0.5 mmol, 1.0 equiv), **MOF-808-py-Nox** (34 mg, 0.025 mmol, 0.05 equiv.), and toluene (5 mL) were added to a screw-cap reaction tube containing a stir bar and flame-activated 4 Å molecular sieves. Then, the reaction mixture was stirred in a 110 ˚C silicone oil bath for 24 h. After the reaction mixture was allowed to cool to room temperature, 1 mL of a 0.5 M solution of 1,3,5-trimethoxybenzene in acetonitrile was added to the crude mixture. A portion of the settled solution was then diluted in $CDCl_3$ (0.5 mL) to obtain the ^{1}H NMR yield of **28** (93%).

Following General Procedure B, 4-methoxyphenethylamine (146.5 µL, 1.0 mmol, 2.0 equiv.), phenylacetamide (67.6 mg, 0.5 mmol, 1.0 equiv), **MOF-808-py-Nox** (34 mg, 0.025 mmol, 0.05 equiv.), and toluene (5 mL) were added to a screw-cap reaction tube containing a stir bar and flame-activated 4 Å molecular sieves. Then, the reaction mixture was stirred in a 110 ˚C silicone oil bath for 24 h. After the reaction mixture was allowed to cool to room temperature, 1 mL of 0.5 M solution of 1,3,5-trimethoxybenzene in acetonitrile was added to the crude mixture. A portion of the settled solution was then diluted in $CDCl_3$ (0.5 mL) to obtain the ^{1}H NMR yield of **28** (92%).

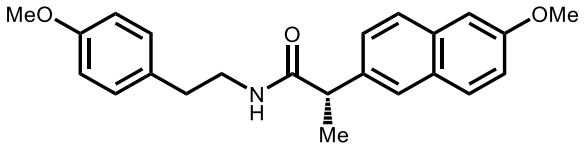

(*S*)-2-(6-methoxynaphthalen-2-yl)-*N*-(4-methoxyphenethyl)propenamide (29)

Following General Procedure B, 4-methoxyphenethylamine (146.5 µL, 1.0 mmol, 2.0 equiv.), (+)-(*S*)-2-(6-methoxynaphthalen-2-yl)propanoic acid (115.1 mg, 0.5 mmol, 1.0 equiv), **MOF-808-py-Nox** (34 mg, 0.025 mmol, 0.05 equiv.), and toluene (5 mL) were added to a screw-cap reaction tube containing a stir bar and flame-activated 4 Å molecular sieves. Then, the reaction mixture was stirred in a 110 ˚C silicone oil bath for 24 h. The crude product was purified by silica gel flash chromatography using a Biotage Isolera instrument (gradient of 10 → 100% CH_2Cl_2 in hexanes containing 1% Et_3N, followed by a gradient of 0 → 5% MeOH in CH_2Cl_2) to afford **29** (74.5 mg, 41%) as a white solid. ^{1}H NMR (500 MHz, DMSO-d_6): δ 7.98 (t, J = 5.6 Hz, 1H), 7.76 (dd, J = 13.9, 8.8 Hz, 2H), 7.69 (d, J = 1.8 Hz, 1H), 7.42 (dd, J = 8.5, 1.8 Hz, 1H), 7.29 (d, J = 2.6 Hz, 1H), 7.15 (dd, J = 8.9, 2.6 Hz, 1H), 6.98–6.92 (m, 2H), 6.72–6.65 (m, 2H), 3.87 (s, 3H), 3.70 (dt, J =

13.9, 6.7 Hz, 1H), 3.66 (s, 3H), 3.30–3.11 (m, 2H), 2.58 (t, J = 7.1 Hz, 2H), 1.39 (d, J = 7.0 Hz, 3H); ^{13}C NMR (126 MHz, DMSO-d_6): δ 173.63, 157.99, 157.43, 137.91, 133.60, 131.74, 130.06, 129.57, 128.84, 127.02, 126.93, 125.80, 118.99, 114.01, 106.14, 55.62, 55.34, 45.51, 40.98, 34.52, 18.82 ppm; HRMS (DART) exact mass calculated for [$C_{23}H_{26}NO_3^+$]: 364.19072, found 364.19426; Melting point: 149.5–151.5 ˚C; IR (neat, cm^{-1}): 3315, 3033, 3004, 2960, 2933, 2917, 2836, 1608, 1581, 1509, 1465, 1374, 1333, 1300, 1271, 1241, 1173, 1111, 1030, 974, 812, 753, 701, 615, 561, 522. $[\alpha]_D$ 0 (conc. 0.008 g/mL, 20ºC, $CHCl_3$).

Following General Procedure B, 4-methoxyphenethylamine (73.3 µL, 0.5 mmol, 1.0 equiv.), (+)-(*S*)-2-(6-methoxynaphthalen-2-yl)propanoic acid (115.1 mg, 0.5 mmol, 1.0 equiv), **MOF-808-py-Nox** (34 mg, 0.025 mmol, 0.05 equiv.), and toluene (5 mL) were added to a screw-cap reaction tube containing a stir bar and flame-activated 4 Å molecular sieves. Then, the reaction mixture was stirred in a 110 ˚C silicone oil bath for 24 h. The crude product was purified by silica gel flash chromatography using a Biotage Isolera instrument (gradient of 10 → 100% CH_2Cl_2 in hexanes containing 1% Et_3N, followed by a gradient of 0 → 5% MeOH in CH_2Cl_2) to afford **29** (43 mg, 24%) as a white solid. $[\alpha]_D$ +10 (conc. 0.01 g/mL, 20ºC, $CHCl_3$).

A control experiment was performed to further validate that the MOF-808 catalyst does not induce epimerization. Following General Procedure B, (+)-(*S*)-2-(6-methoxynaphthalen-2-yl)propanoic acid (115.1 mg, 0.5 mmol, 1.0 equiv), **MOF-808-py-Nox** (34 mg, 0.025 mmol, 0.05 equiv.), and toluene (5 mL) were added to a screw-cap reaction tube containing a stir bar and flame-activated 4 Å molecular sieves. Then, the reaction mixture was stirred in a 110 ˚C silicone oil bath for 24 h. The starting material was fully recovered and subsequently analyzed. $[\alpha]_D$ +64 (conc. 0.01 g/mL, 20 ºC, $CHCl_3$). The optical rotation data is consistent with reported data of the enantiopure compound.[30]

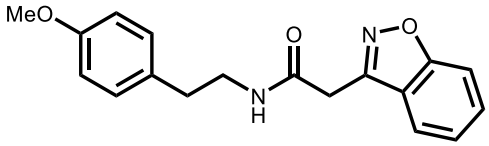

2-(benzo[d]58soxazole-3-yl)-N-(4-methoxyphenethyl)acetamide (30)

Following General Procedure B, 4-methoxyphenethylamine (146.5 µL, 1.0 mmol, 2.0 equiv.), 2-(1,2-benzisoxazol-3-yl)acetic acid (88.6 mg, 0.5 mmol, 1.0 equiv), **MOF-808-py-Nox** (34 mg, 0.025 mmol, 0.05 equiv.), and toluene (5 mL) were added to a screw-cap reaction tube containing a stir bar and flame-activated 4 Å molecular sieves. Then, the reaction mixture was stirred in a 110 ˚C silicone oil bath for 24 h. The crude product was purified by silica gel flash chromatography using a Biotage Isolera instrument (gradient of 10 → 100% CH_2Cl_2 in hexanes containing 1% Et_3N, followed by a gradient of 0 → 5% MeOH in CH_2Cl_2) to afford **30** (79.0 mg, 51%) as a yellow solid. ^{1}H NMR (500 MHz, $CDCl_3$): δ 7.74 (dt, J = 7.9, 1.0 Hz, 1H), 7.64–7.49 (m, 2H), 7.39–7.29 (m, 1H), 7.01–6.83 (m, 2H), 6.80–6.62 (m, 2H), 6.07 (s, 1H), 3.92 (s, 2H), 3.76 (s, 3H), 3.47 (q, J = 6.6 Hz, 2H), 2.69 (t, J = 6.9 Hz, 2H); ^{13}C NMR (126 MHz, $CDCl_3$): δ 166.61, 163.26, 158.25, 153.72, 130.40, 130.34, 129.57, 123.93, 121.84, 121.16, 113.99, 109.91, 55.23, 41.20, 34.54, 33.67 ppm; HRMS (DART) exact mass calculated for [$C_{18}H_{19}N_2O_3^+$]: 311.13902, found 311.14245; Melting point: 126.0–128.0 ˚C; IR (neat, cm^{-1}): 3291, 3102, 3021, 2960, 2931, 2832, 2281, 1645,

1611, 1566, 1509, 1457, 1439, 1409, 1384, 1339, 1301, 1242, 1196, 1176, 1111, 1056, 1026, 946, 899, 860, 823, 757, 706, 621, 580, 553, 522.

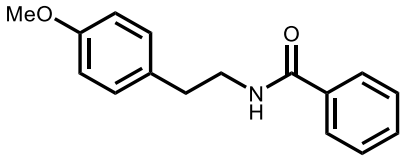

***N*-(4-methoxyphenethyl)benzamide (31)**

Following General Procedure B, 4-methoxyphenethylamine (146.5 μL, 1.0 mmol, 2.0 equiv.), methyl benzoate (62.8 μL, 0.5 mmol, 1.0 equiv), **MOF-808-py-Nox** (34 mg, 0.025 mmol, 0.05 equiv.), and toluene (5 mL) were added to a screw-cap reaction tube containing a stir bar and flame-activated 4 Å molecular sieves. Then, the reaction mixture was stirred in a 110 ˚C silicone oil bath for 24 h. The crude product was purified by silica gel flash chromatography using a Biotage Isolera instrument (gradient of 10 → 50% EtOAc in hexanes containing 1% Et_3N) to afford **31** (47.0 mg, 37%) as a yellow solid. ^{1}H NMR (500 MHz, $CDCl_3$): δ 7.72–7.66 (m, 2H), 7.52–7.45 (m, 1H), 7.41 (dd, J = 8.4, 7.1 Hz, 2H), 7.16 (d, J = 8.0 Hz, 2H), 6.90–6.85 (m, 2H), 6.14 (s, 1H), 3.80 (d, J = 1.3 Hz, 3H), 3.69 (q, J = 6.6 Hz, 2H), 2.88 (t, J = 6.9 Hz, 2H); ^{13}C NMR (126 MHz, $CDCl_3$): δ 167.43, 158.30, 134.65, 131.44, 130.84, 129.80, 128.55, 126.83, 126.77, 114.11, 55.33, 55.24, 41.30, 34.77. The NMR data are consistent with the reported data.[31]

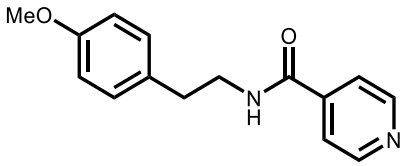

***N*-(4-methoxyphenethyl)isonicotinamide (32)**

Following General Procedure B, 4-methoxyphenethylamine (146.5 μL, 1.0 mmol, 2.0 equiv.), isonicotinic acid (61.5 mg, 0.5 mmol, 1.0 equiv), **MOF-808-py-Nox** (34 mg, 0.025 mmol, 0.05 equiv.), and toluene (5 mL) were added to a screw-cap reaction tube containing a stir bar and flame-activated 4 Å molecular sieves. Then, the reaction mixture was stirred in a 110 ˚C silicone oil bath for 24 h. The crude product was purified by silica gel flash chromatography using a Biotage Isolera instrument (gradient of 10 → 100% CH_2Cl_2 in hexanes containing 1% Et_3N, followed by a gradient of 0 → 5% MeOH in CH_2Cl_2) to afford **32** (76.5 mg, 60%) as a faint yellow solid. ^{1}H NMR (500 MHz, $CDCl_3$): δ 8.68 (d, J = 4.9 Hz, 2H), 7.61–7.57 (m, 2H), 7.17–7.12 (m, 2H), 6.89–6.83 (m, 2H), 6.82 (s, 1H), 3.79 (s, 3H), 3.72–3.65 (m, 2H), 2.89 (t, J = 7.0 Hz, 2H); ^{13}C NMR (126 MHz, $CDCl_3$): δ 165.51, 158.38, 150.46, 141.77, 130.60, 129.73, 120.98, 114.15, 55.29, 52.97, 41.48, 34.57 ppm; HRMS (DART) exact mass calculated for [$C_{15}H_{17}N_2O_2^+$]: 257.12845, found 257.13097; Melting point: 122.0–124.0 ˚C; IR (neat, cm^{-1}): 3301, 3068, 3027, 2980, 2944, 2892, 2859, 2833, 1637, 1613, 1583, 1538, 1510, 1486, 1456, 1435, 1405, 1299, 1246, 1215, 1189, 1174, 1159, 1112, 1068, 1052, 1027, 989, 865, 847, 814, 753, 687, 660, 576, 523.

11. Copies of NMR spectra

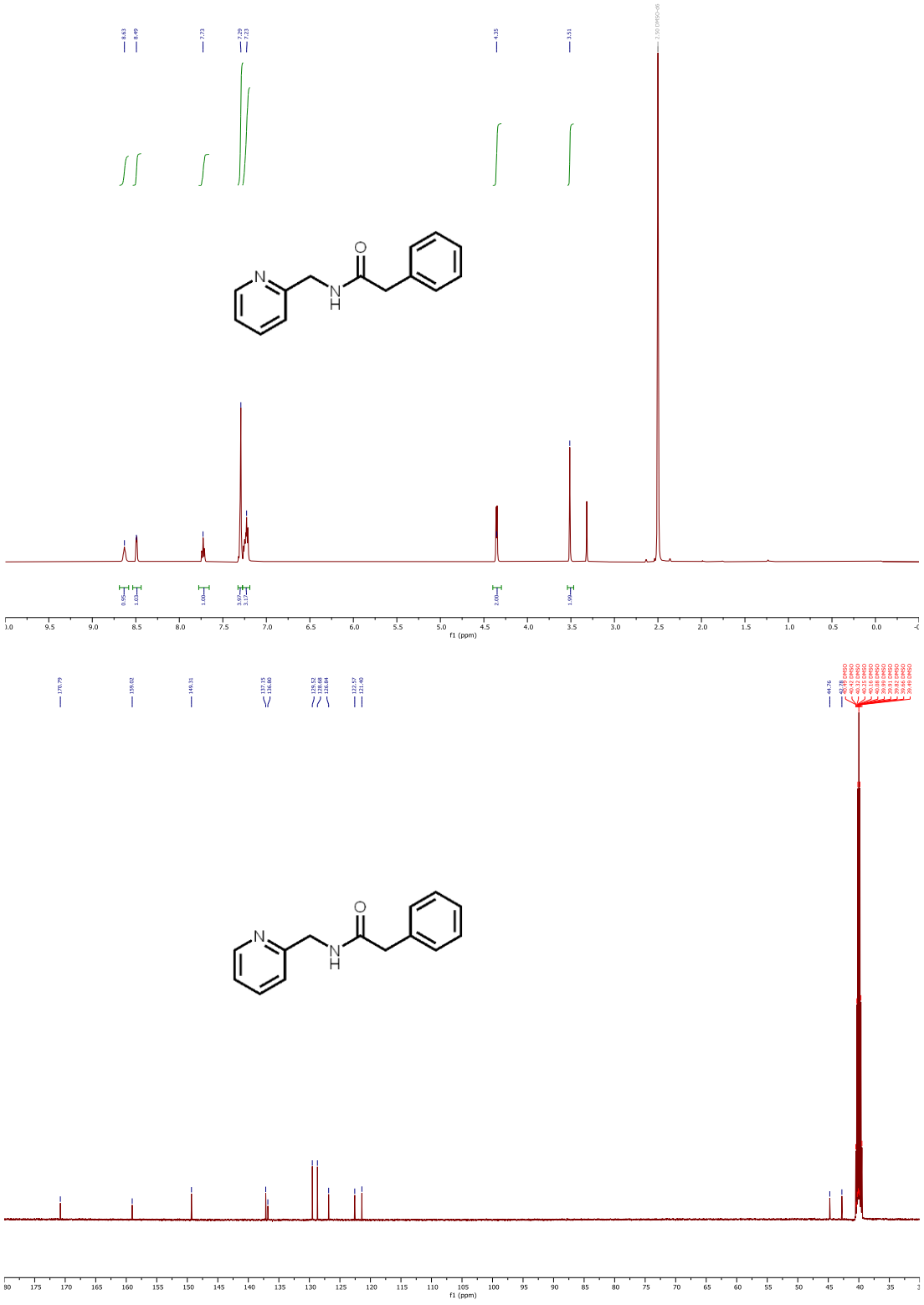

Figure S43. ^{1}H (500 MHz, DMSO-d_6) and ^{13}C (126 MHz, DMSO-d_6) NMR spectra of **5**.

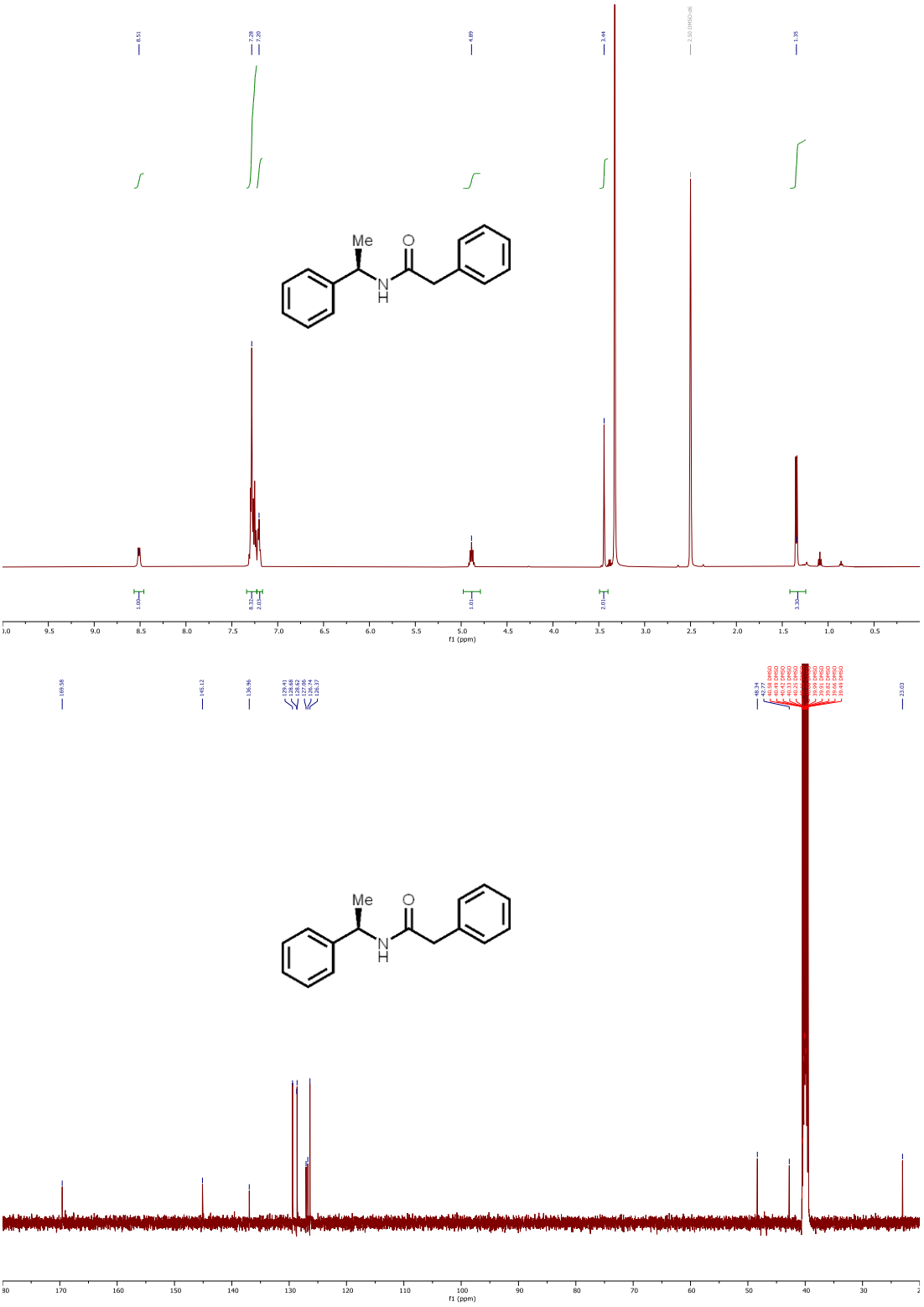

Figure S44. ^{1}H (500 MHz, DMSO-d_6) and ^{13}C (126 MHz, DMSO-d_6) NMR spectra of **6**.

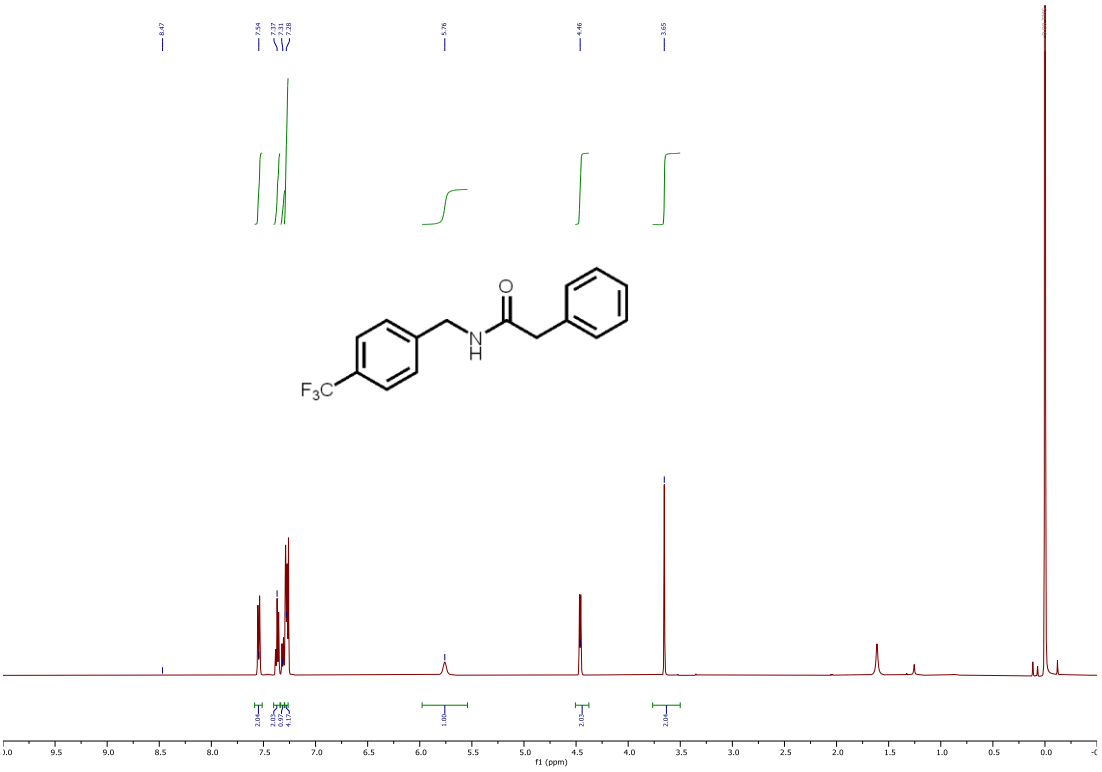
8.47
7.54
7.37
7.31
7.28
5.76
4.46
3.65
O
N
H
F3C
f1 (ppm)

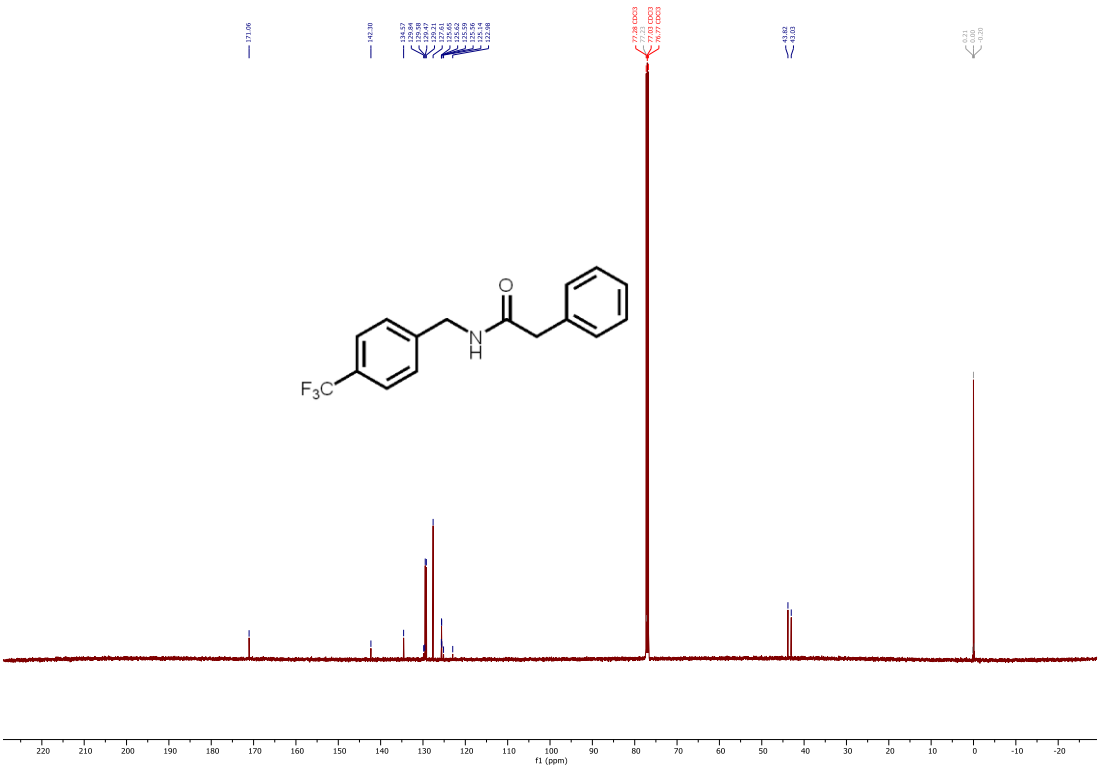
171.06
142.30
134.57
129.84
129.39
129.47
129.21
127.61
125.65
125.62
125.56
125.54
125.14
123.98
77.28 CDCl3
77.03 CDCl3
76.77 CDCl3
43.60
43.63
O
N
H
F3C
f1 (ppm)

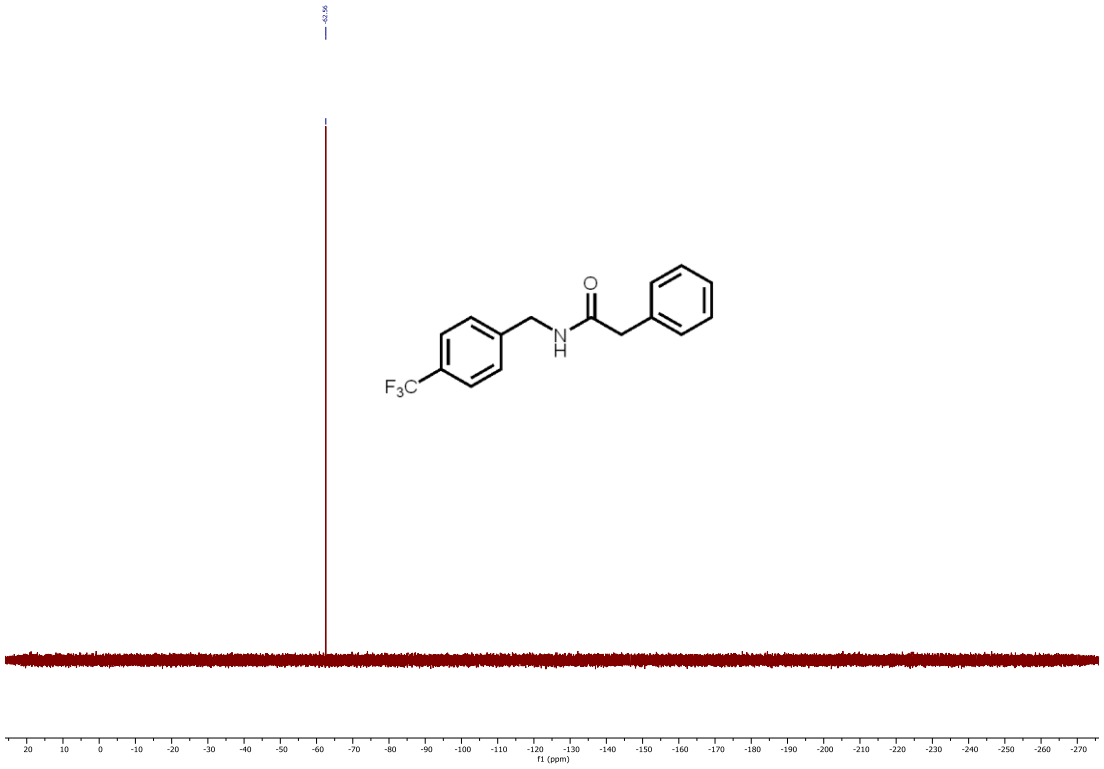

Figure S45. ^{1}H (500 MHz, $CDCl_3$), ^{13}C (126 MHz, $CDCl_3$), and ^{19}F (376 MHz, $CDCl_3$) NMR spectra of **7**.

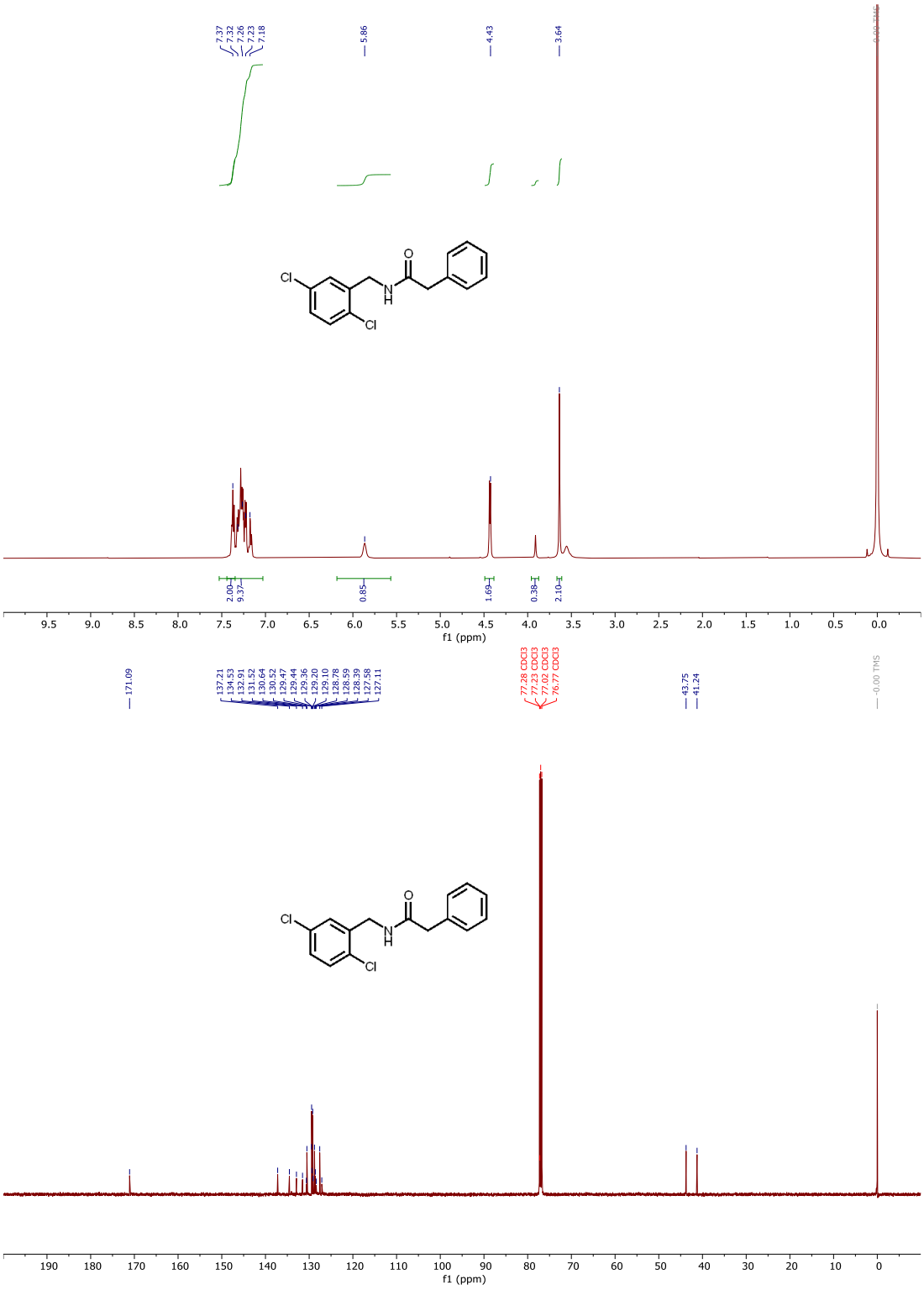

Figure S46. ^{1}H (500 MHz, $CDCl_3$) and ^{13}C (126 MHz, $CDCl_3$) NMR spectra of **8**.

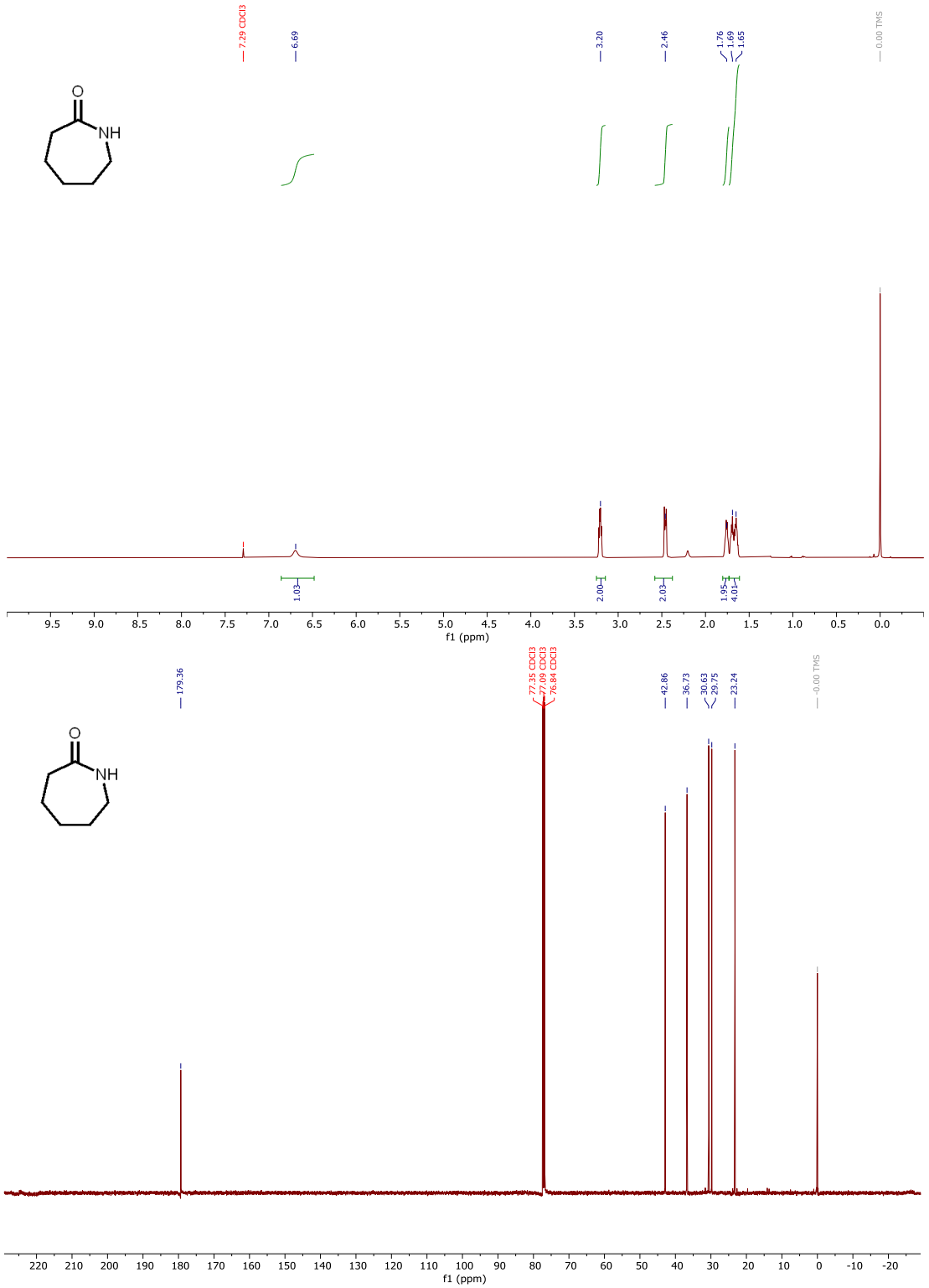

Figure S47. ^{1}H (500 MHz, $CDCl_3$) and ^{13}C (126 MHz, $CDCl_3$) NMR spectra of **9**.

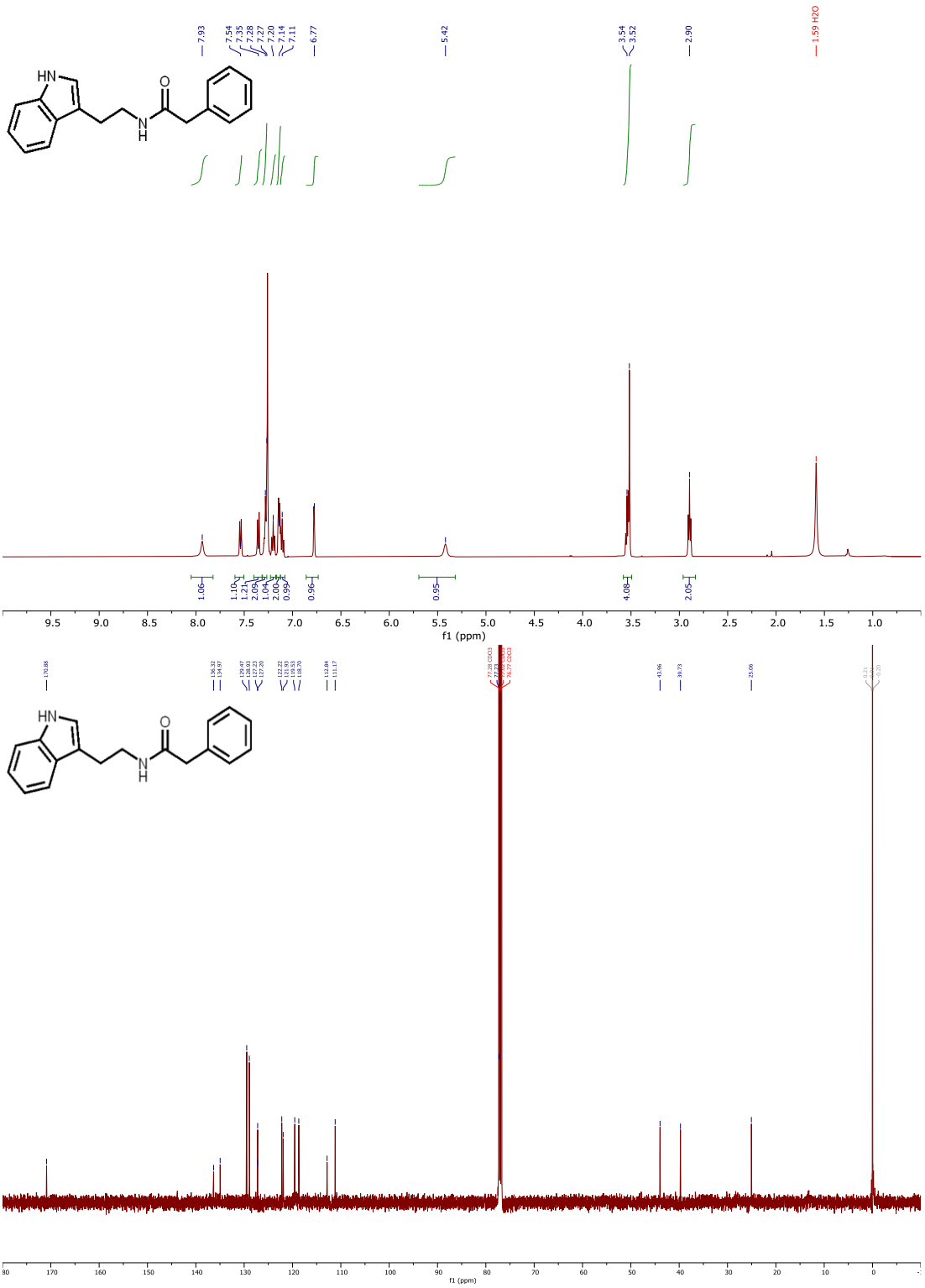

Figure S48. ^{1}H (500 MHz, $CDCl_3$) and ^{13}C (126 MHz, $CDCl_3$) NMR spectra of **10**.

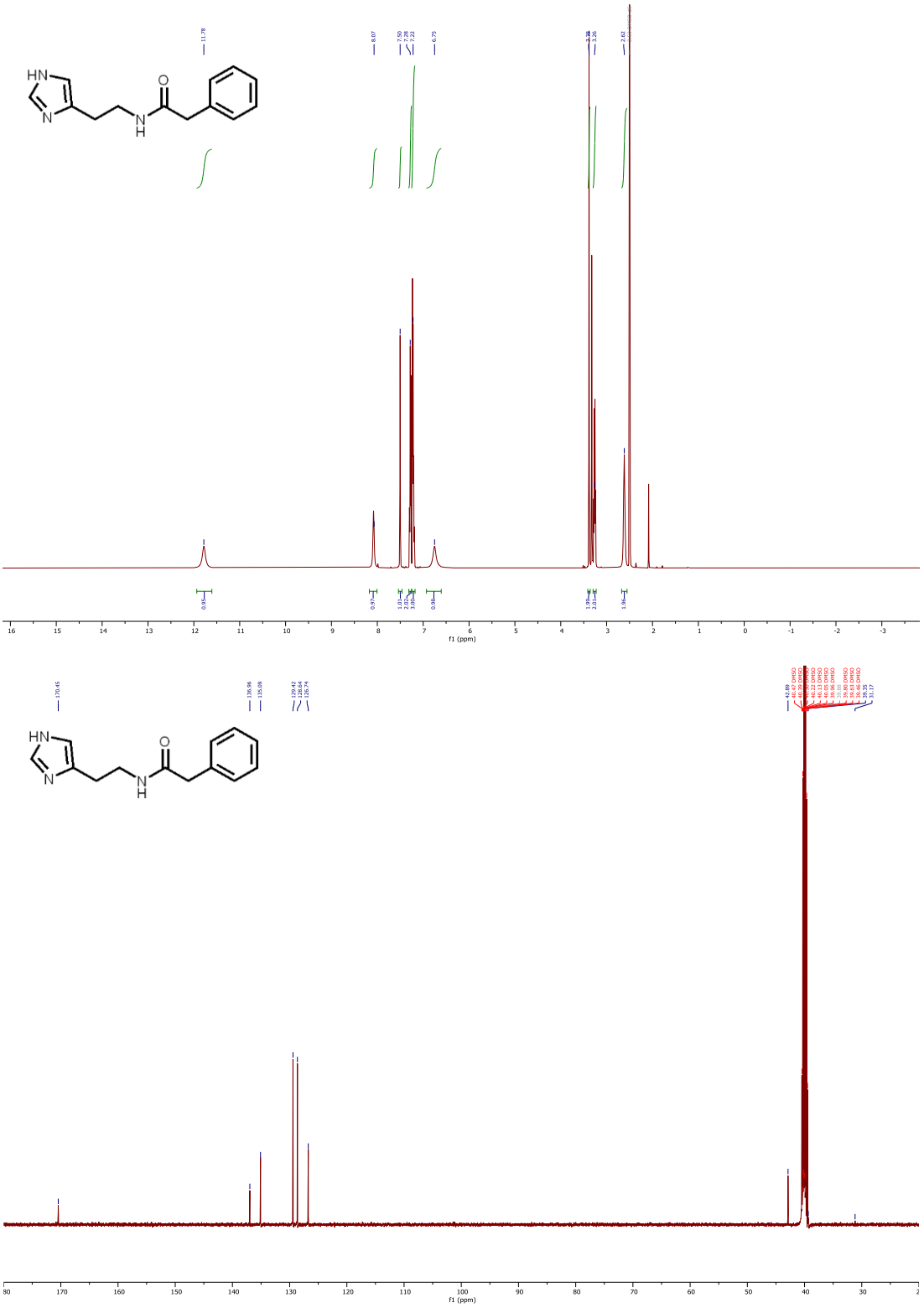

Figure S49. ^{1}H (500 MHz, DMSO-d_6) and ^{13}C (126 MHz, DMSO-d_6) NMR spectra of **11**.

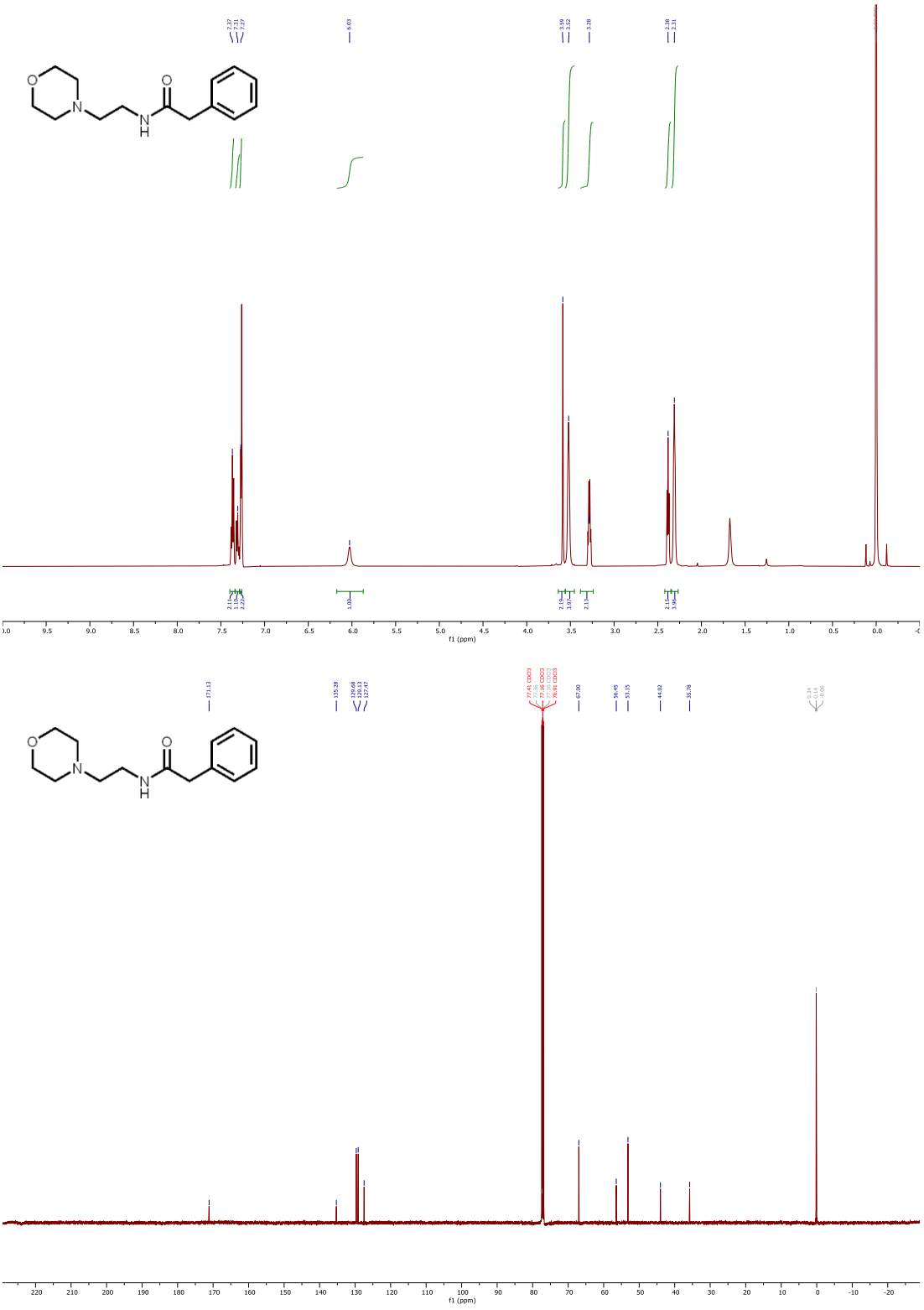

Figure S50. ^{1}H (500 MHz, $CDCl_3$) and ^{13}C (126 MHz, $CDCl_3$) NMR spectra of **12**.

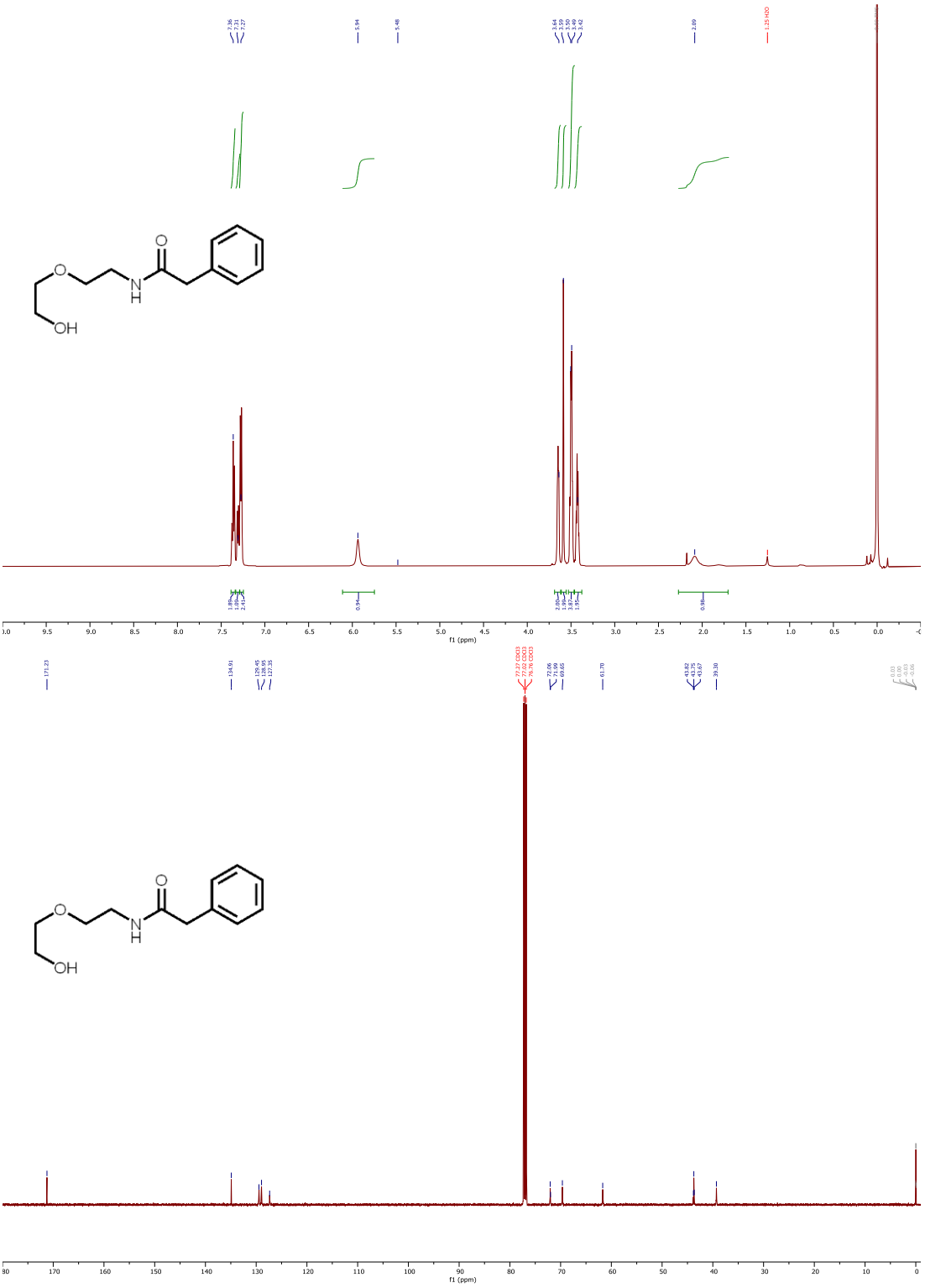

Figure S51. ^{1}H (500 MHz, $CDCl_3$) and ^{13}C (126 MHz, $CDCl_3$) NMR spectra of **13**.

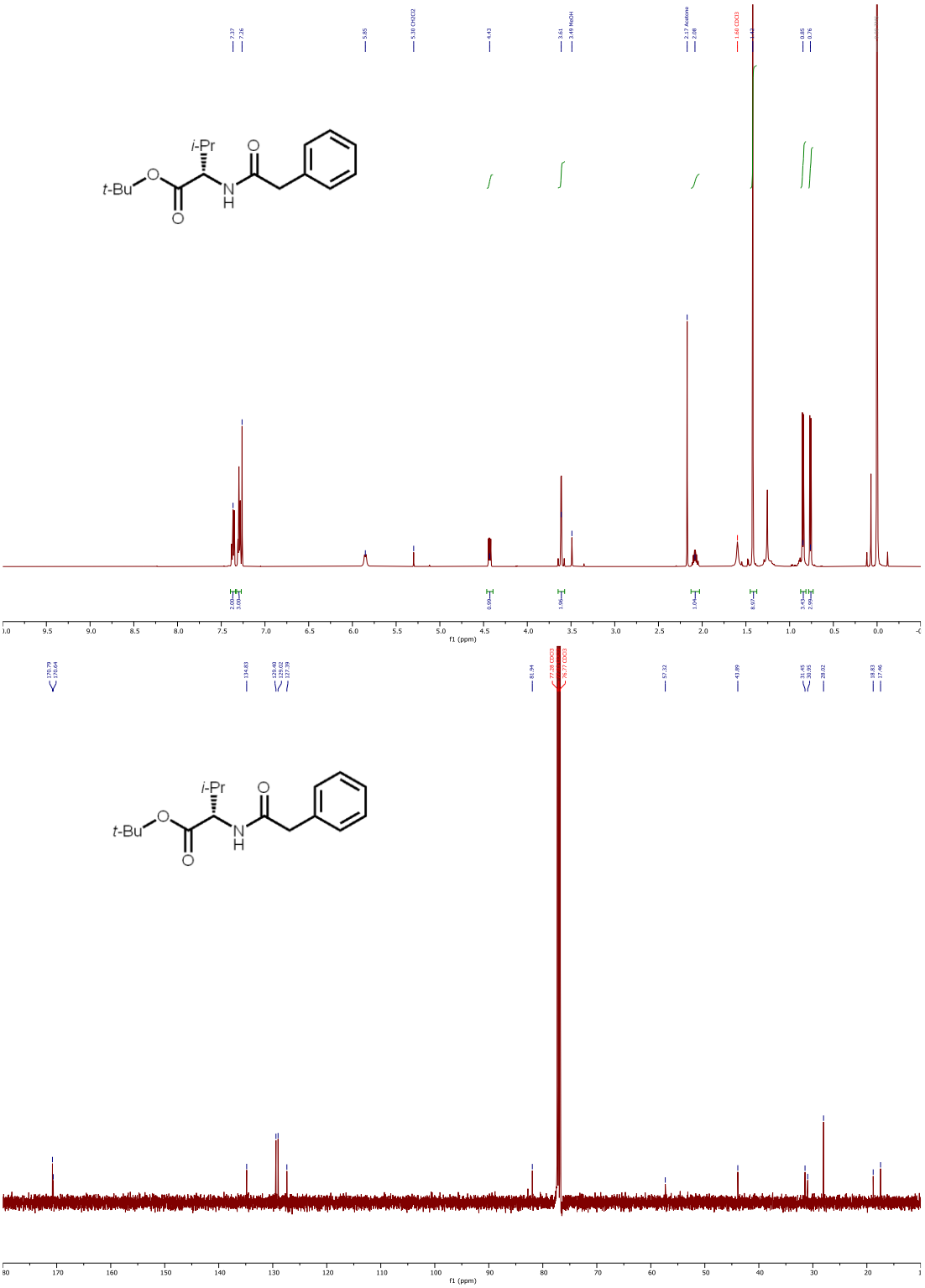

Figure S52. ^{1}H (500 MHz, $CDCl_3$) and ^{13}C (126 MHz, $CDCl_3$) NMR spectra of **14**.

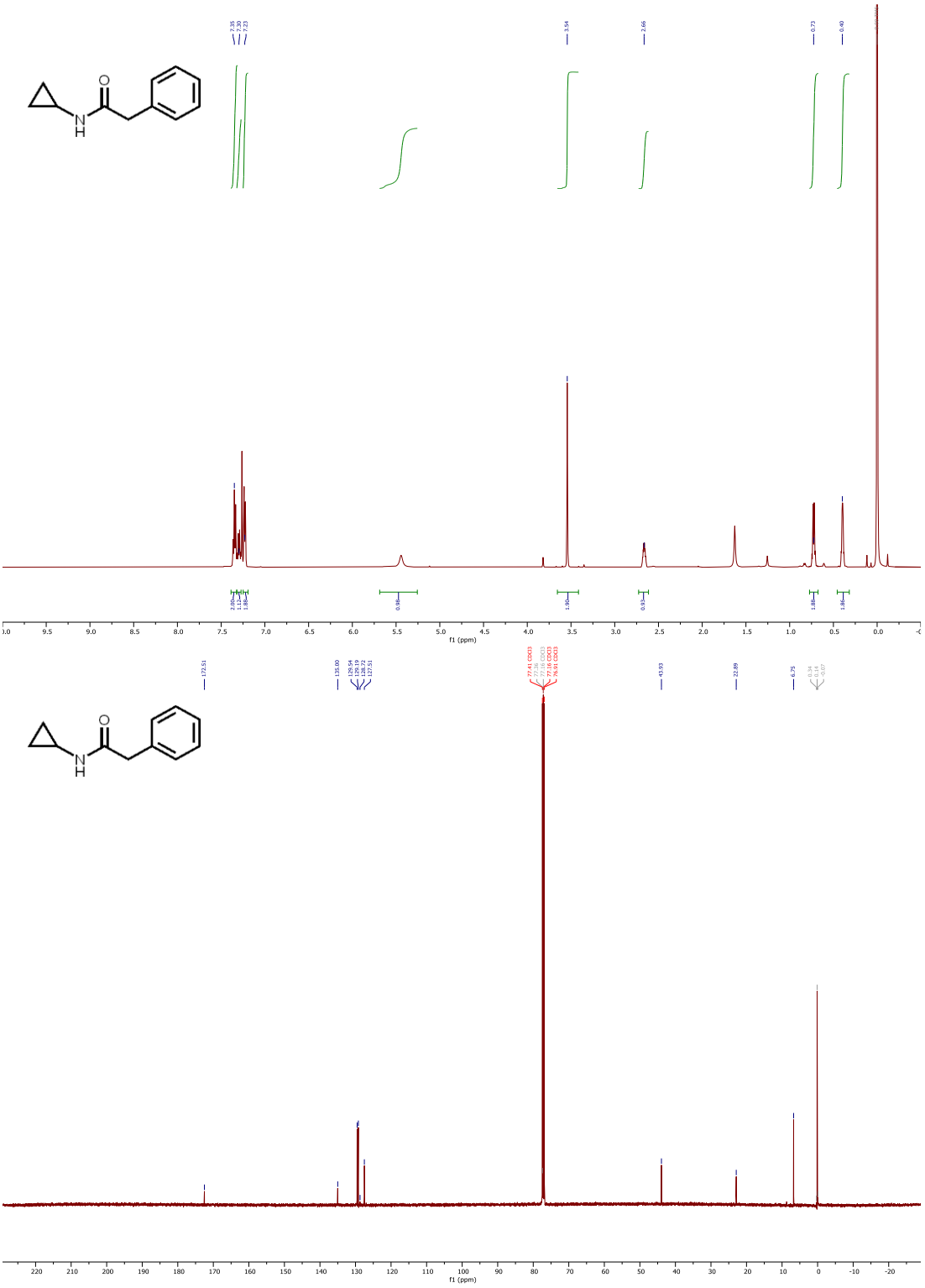

Figure S53. ^{1}H (500 MHz, $CDCl_3$) and ^{13}C (126 MHz, $CDCl_3$) NMR spectra of **15**.

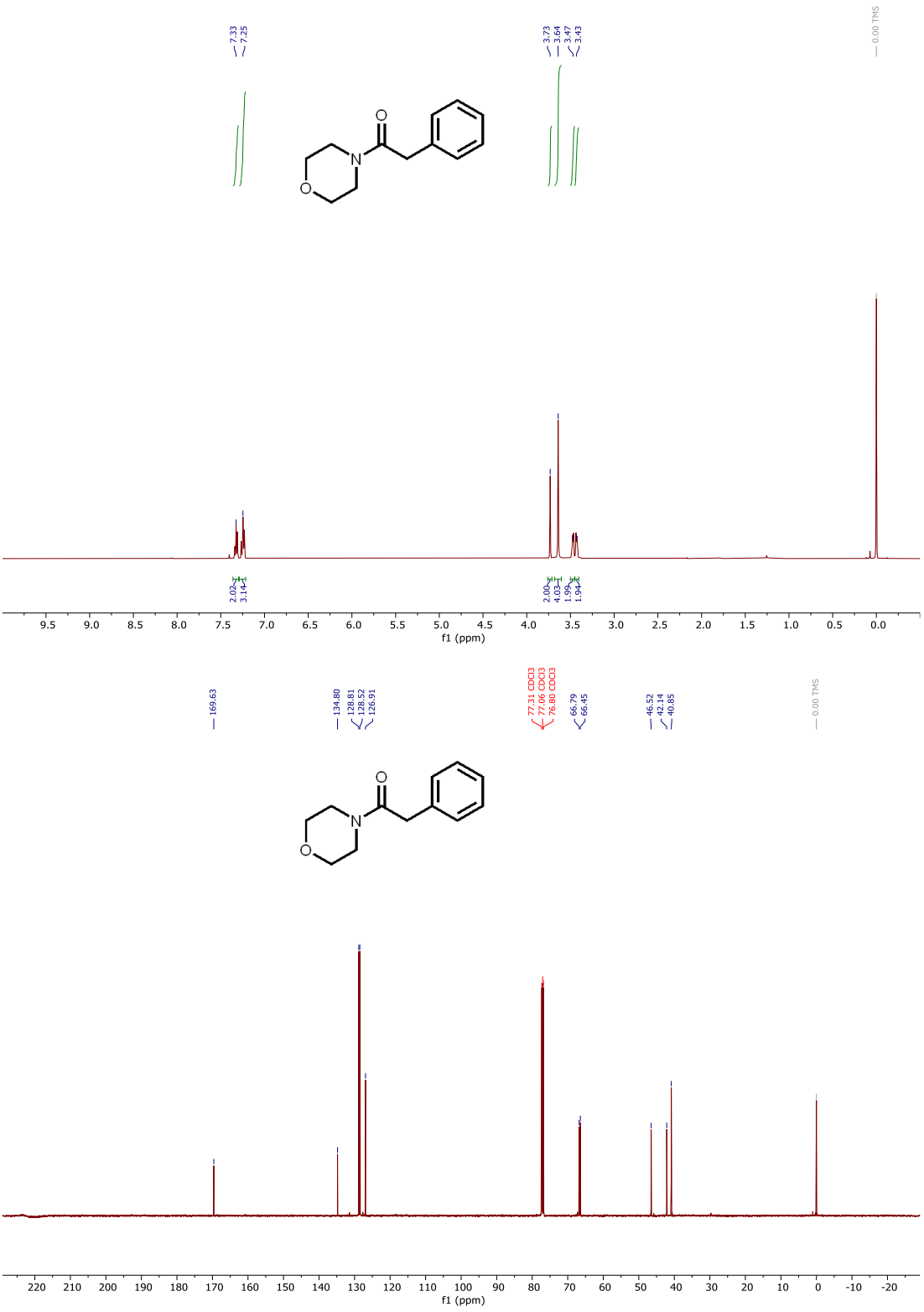

Figure S54. ^{1}H (500 MHz, $CDCl_3$) and ^{13}C (126 MHz, $CDCl_3$) NMR spectra of **16**.

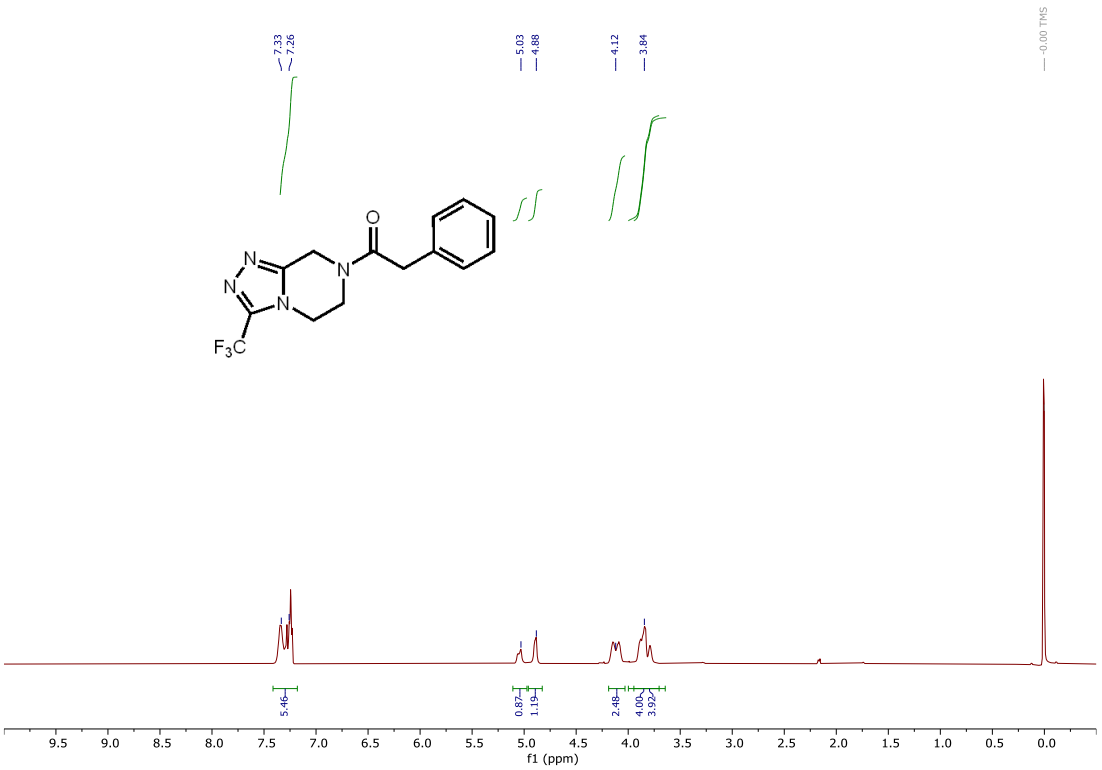
7.33
7.26
5.03
4.88
4.12
3.84
0.00 TMS
O
N
N
N
F3C
5.46
0.87
1.19
2.48
4.00
3.92
9.5 9.0 8.5 8.0 7.5 7.0 6.5 6.0 5.5 5.0 4.5 4.0 3.5 3.0 2.5 2.0 1.5 1.0 0.5 0.0
f1 (ppm)

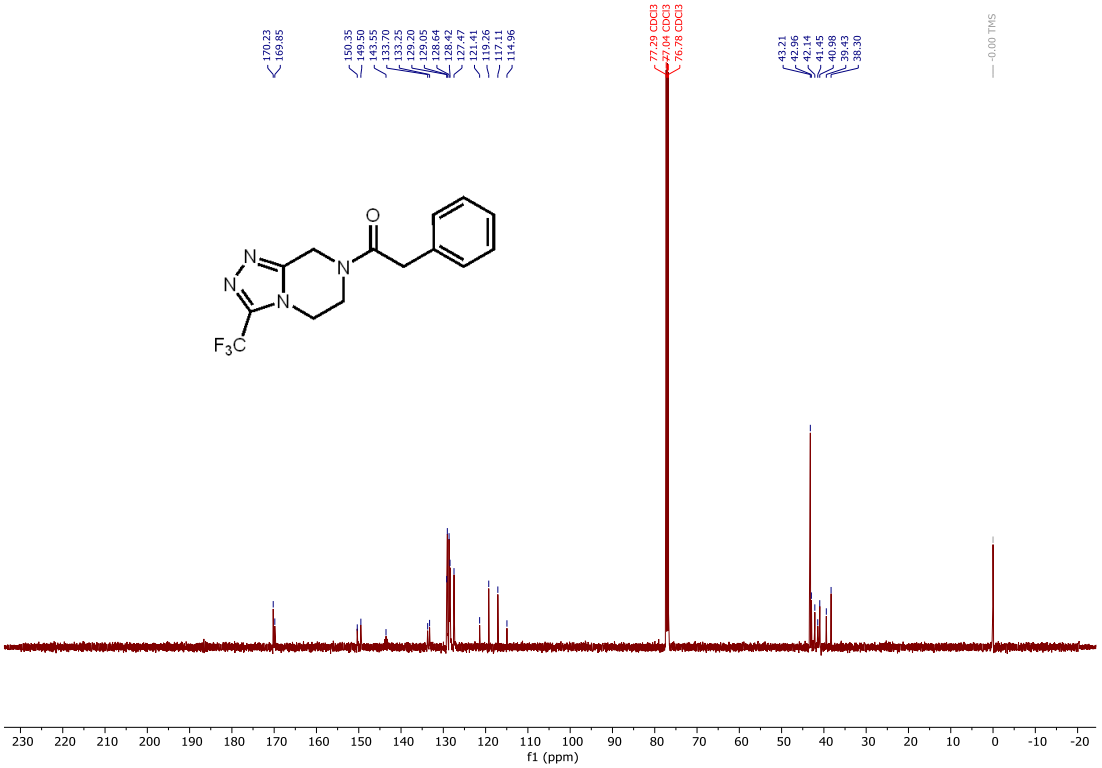
170.23
169.85
150.35
149.50
143.55
133.70
133.25
129.20
129.05
128.64
128.42
127.47
121.41
119.26
117.11
114.96
77.29 CDCl3
77.04 CDCl3
76.78 CDCl3
43.21
42.96
42.14
41.45
40.98
39.43
38.30
0.00 TMS
O
N
N
N
F3C
230 220 210 200 190 180 170 160 150 140 130 120 110 100 90 80 70 60 50 40 30 20 10 0 -10 -20
f1 (ppm)

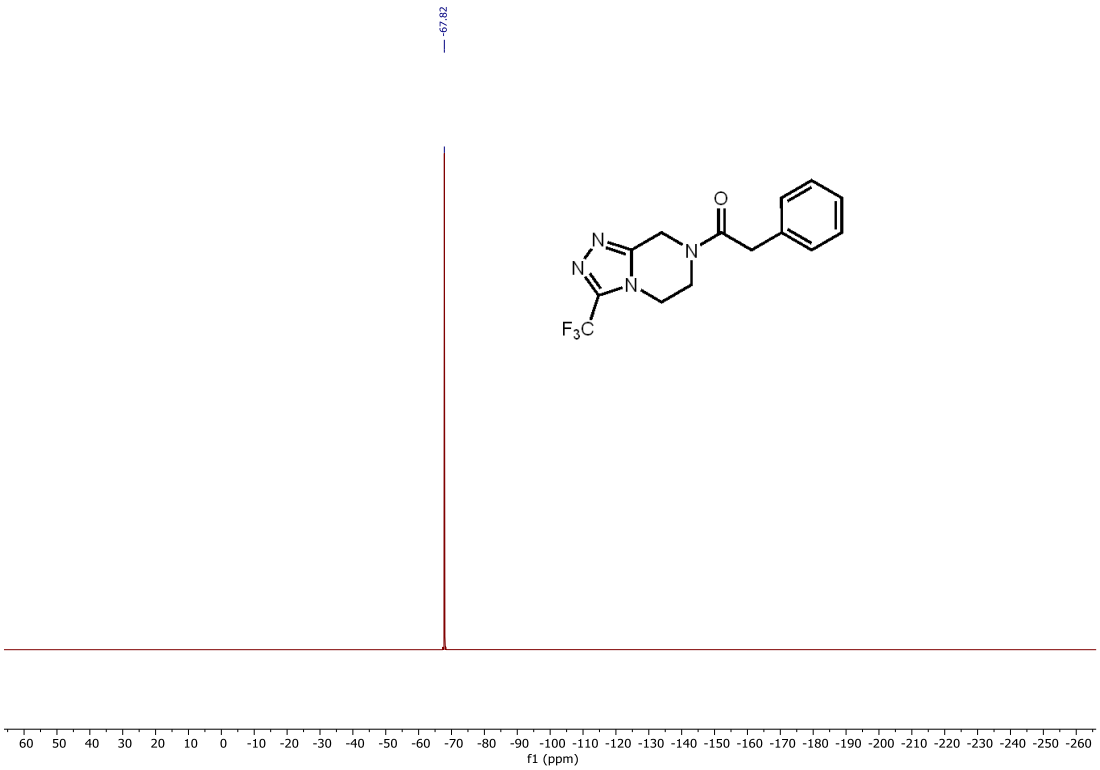

Figure S55. ^{1}H (500 MHz, $CDCl_3$), ^{13}C (126 MHz, $CDCl_3$), and ^{19}F (470 MHz, $CDCl_3$) NMR spectra of **17**.

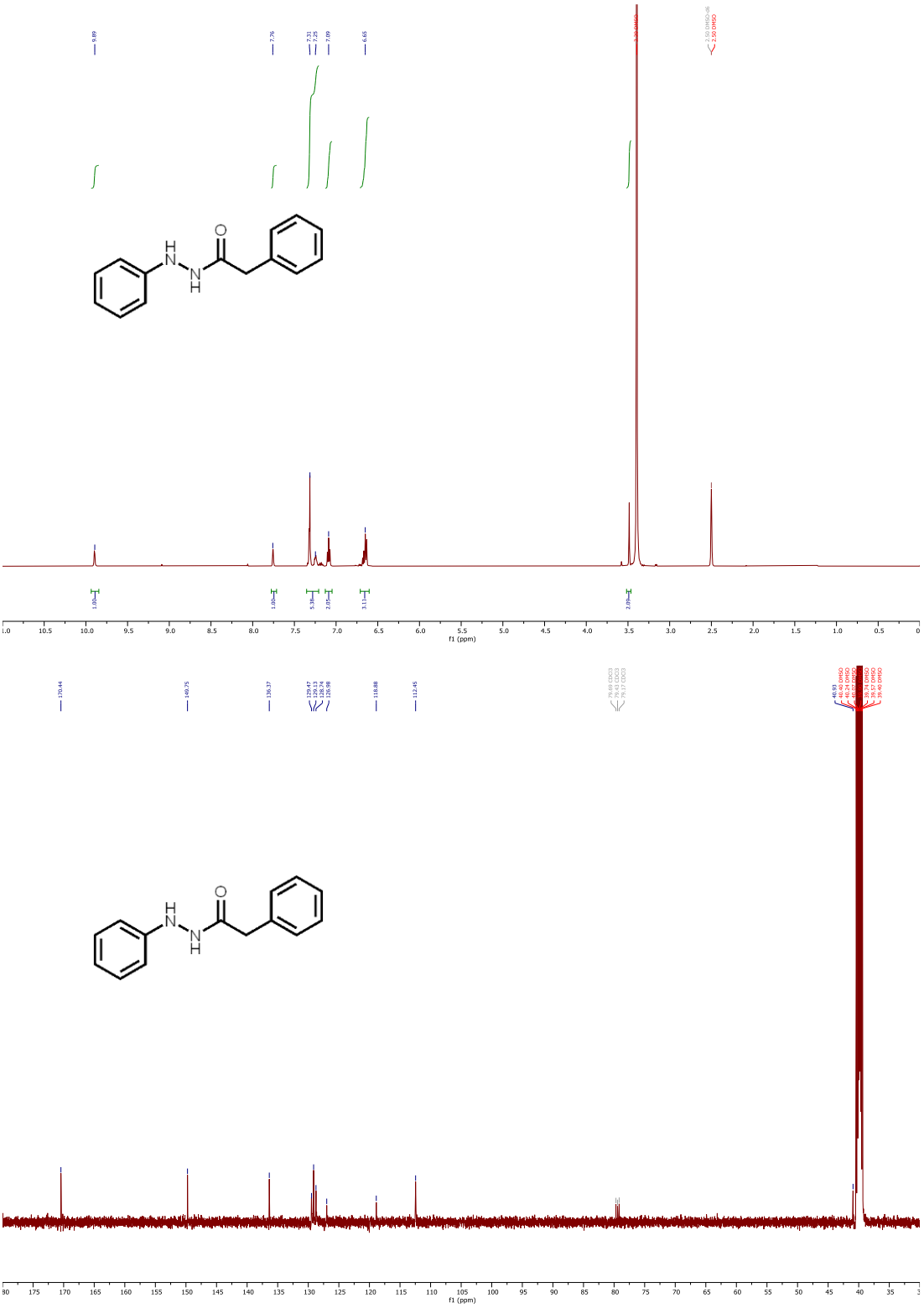

Figure S56. ^{1}H (500 MHz, DMSO-d_6) and ^{13}C (126 MHz, DMSO-d_6) NMR spectra of **18**.

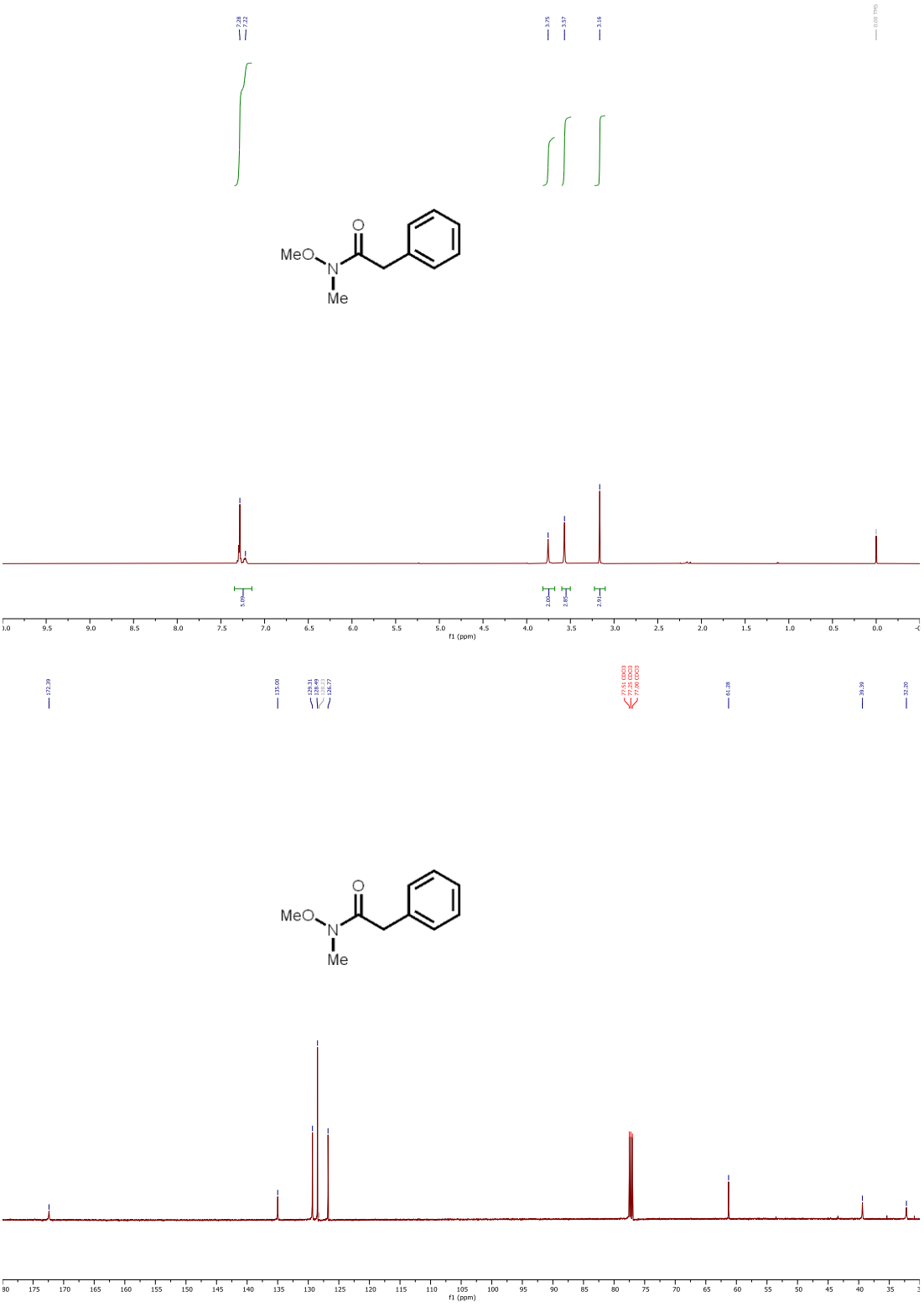

Figure S57. ^{1}H (500 MHz, $CDCl_3$) and ^{13}C (126 MHz, $CDCl_3$) NMR spectra of **19**.

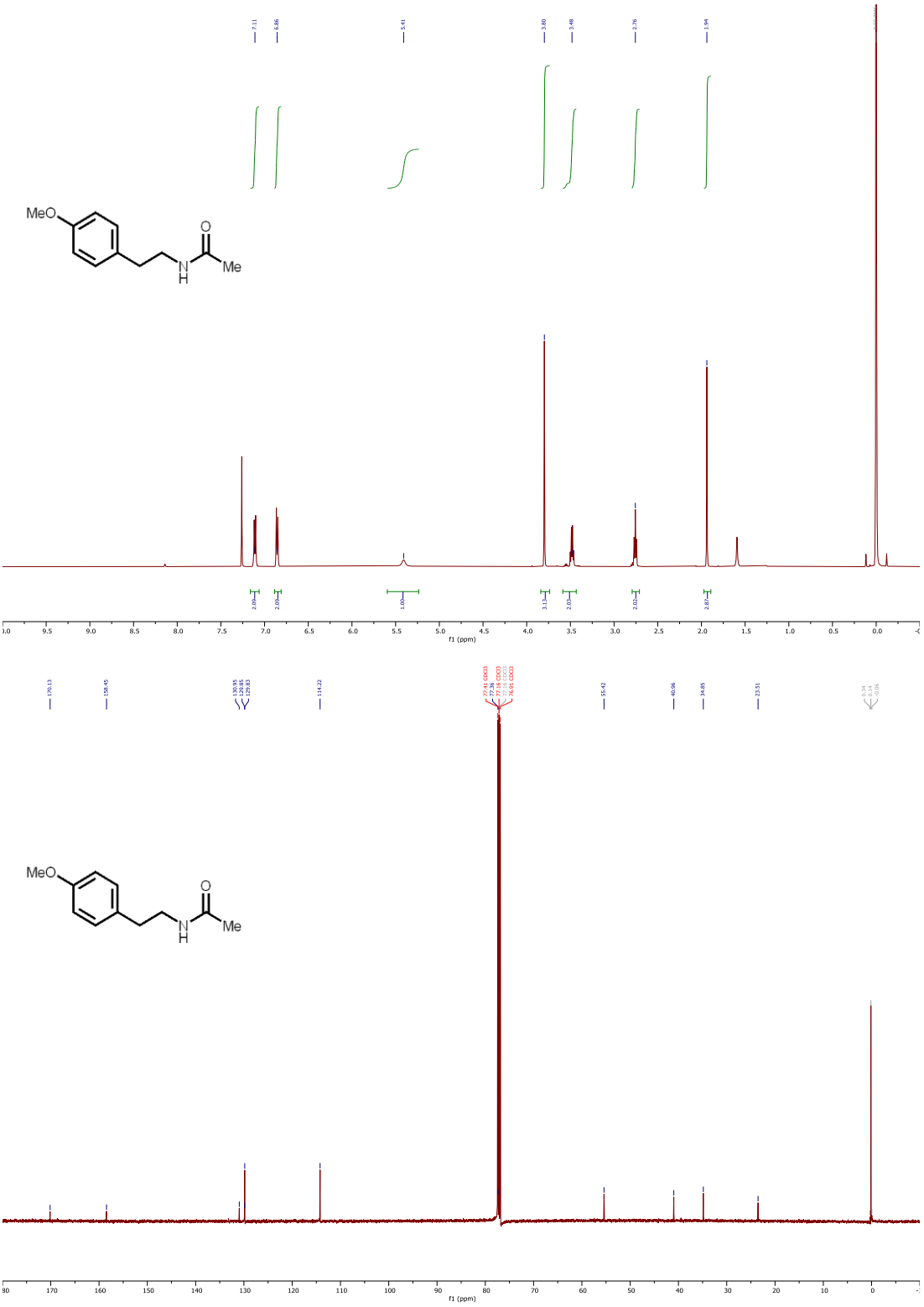

Figure S58. ^{1}H (500 MHz, $CDCl_3$) and ^{13}C (126 MHz, $CDCl_3$) NMR spectra of **2**.

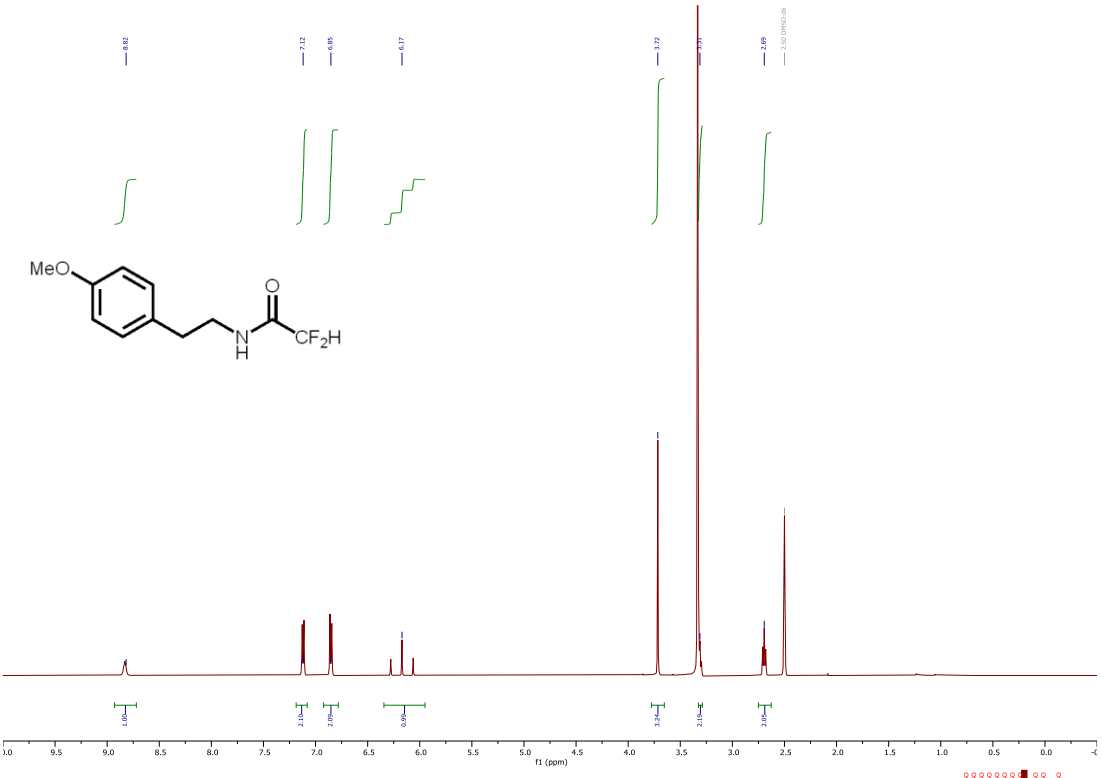
MeO
O
N
H
CF2H
f1 (ppm)

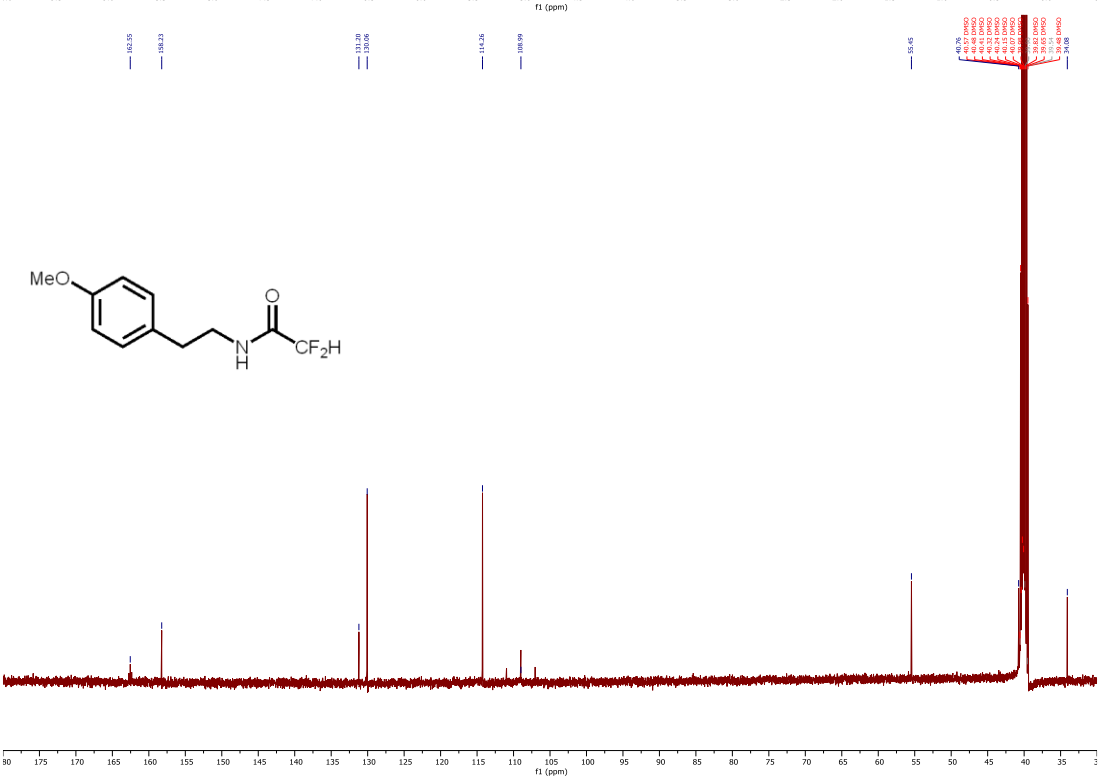
MeO
O
N
H
CF2H
f1 (ppm)

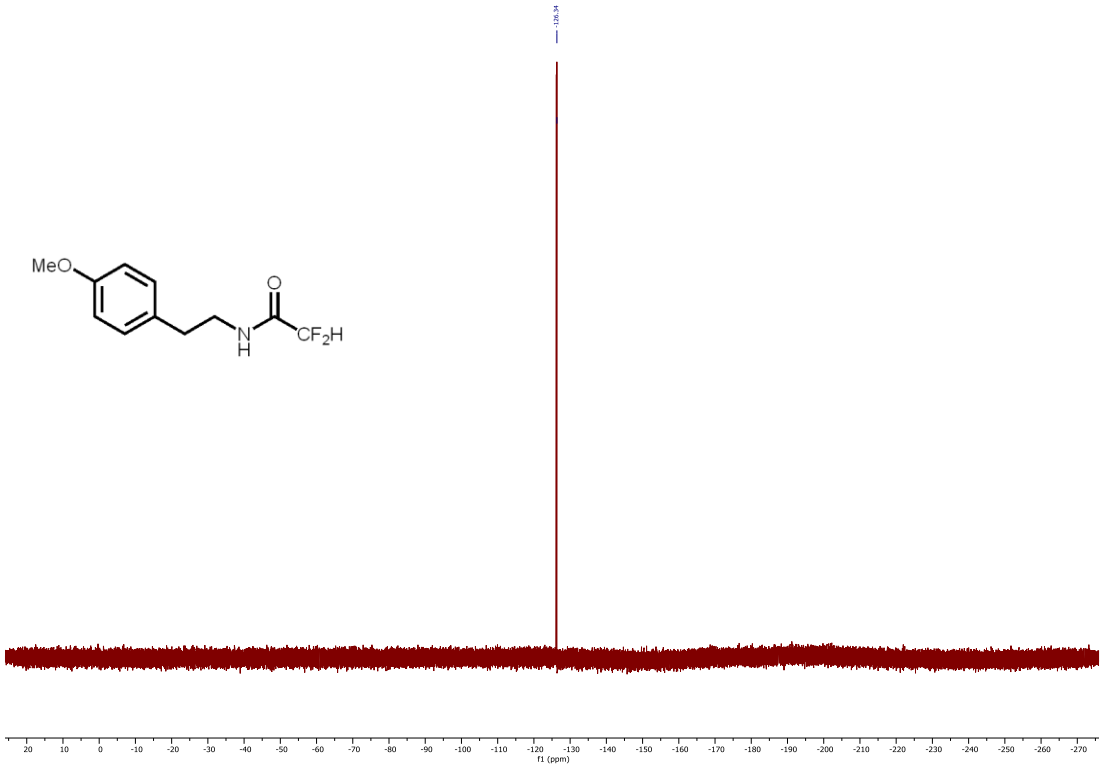

Figure S59. ^{1}H (500 MHz, DMSO-d_6), ^{13}C (126 MHz, DMSO-d_6), and ^{19}F (376 MHz, $CDCl_3$) spectra of **20**.

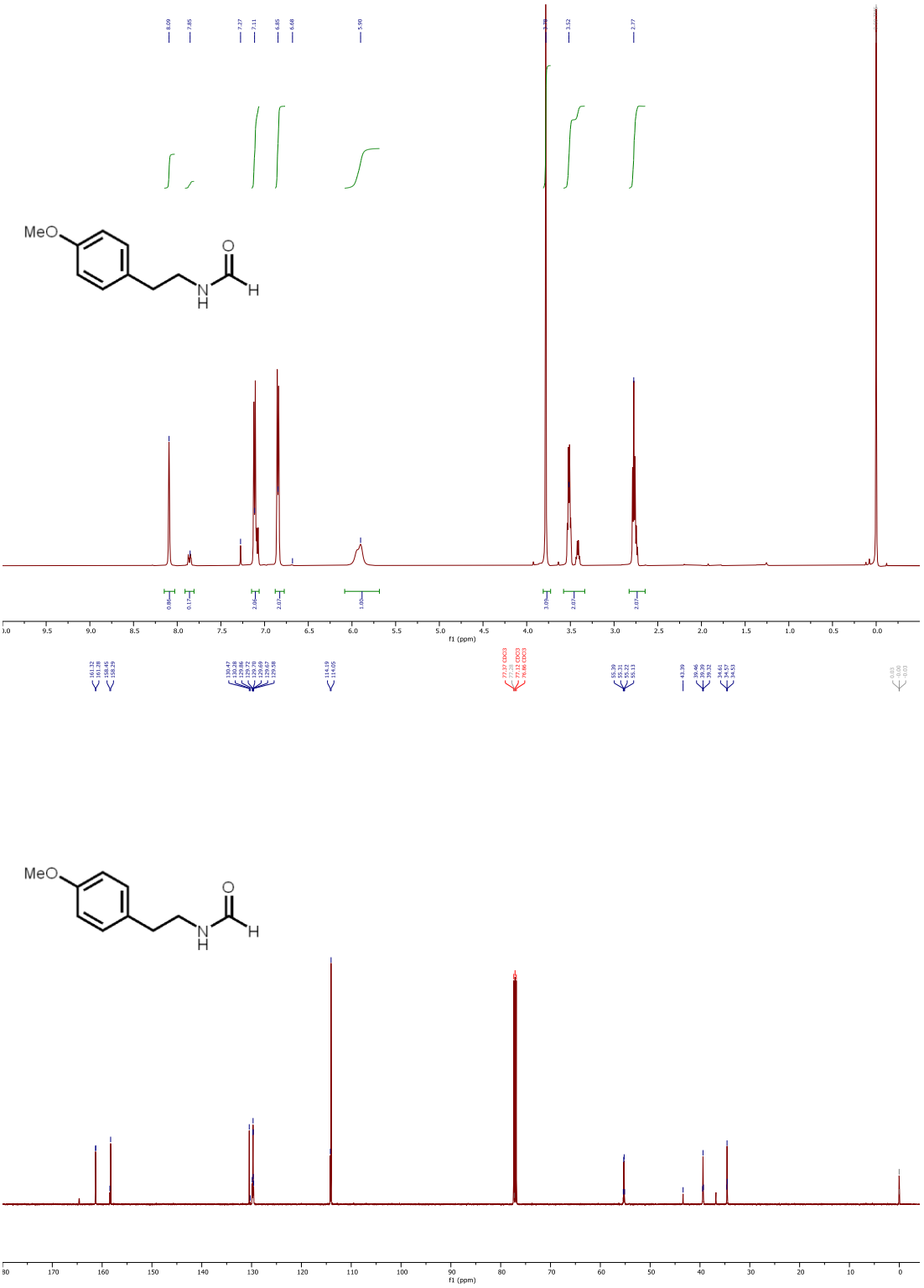

Figure S60. ^{1}H (500 MHz, $CDCl_3$) and ^{13}C (126 MHz, $CDCl_3$) NMR spectra of **4**.

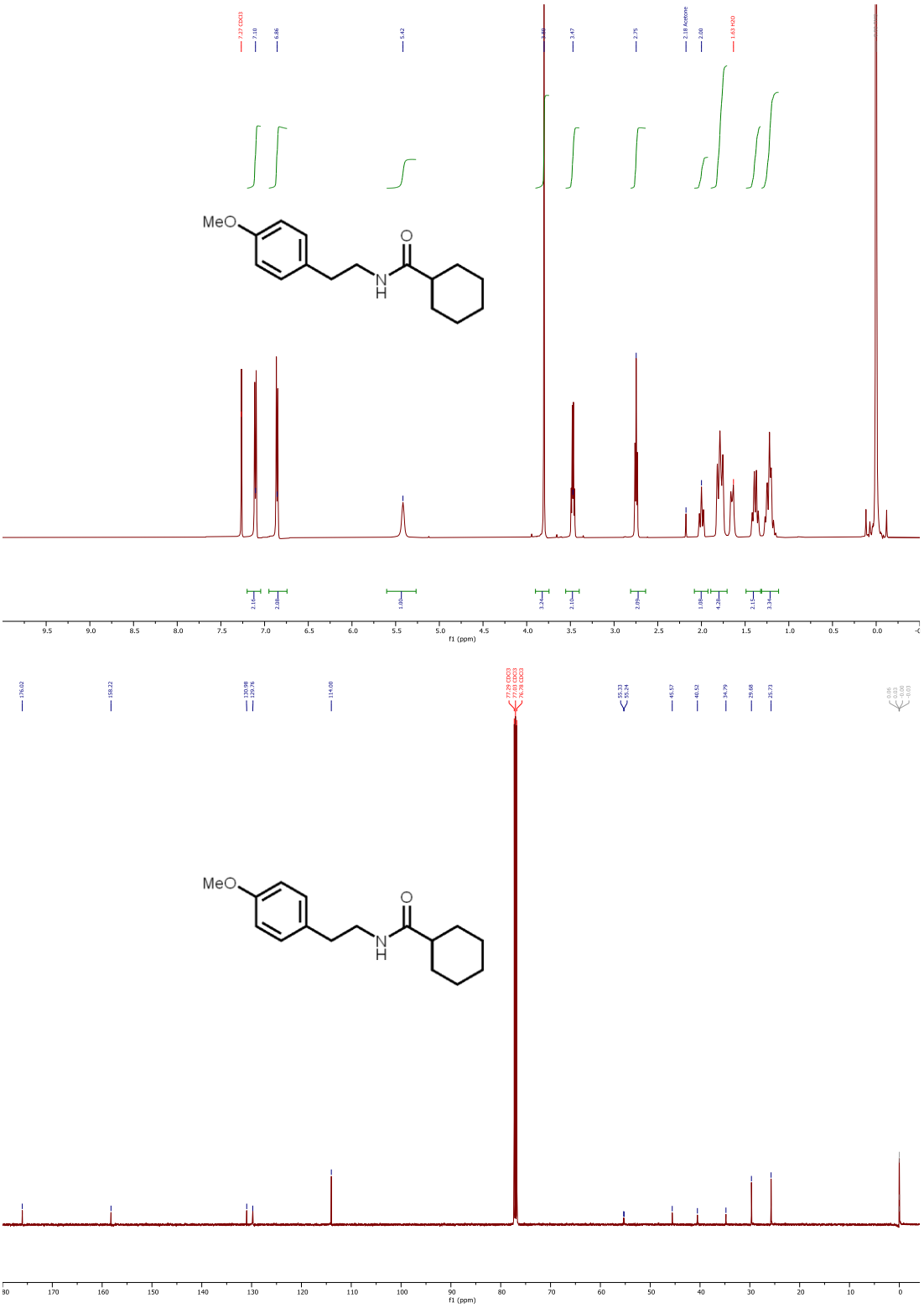

Figure S61. ^{1}H (500 MHz, $CDCl_3$) and ^{13}C (126 MHz, $CDCl_3$) NMR spectra of **21**.

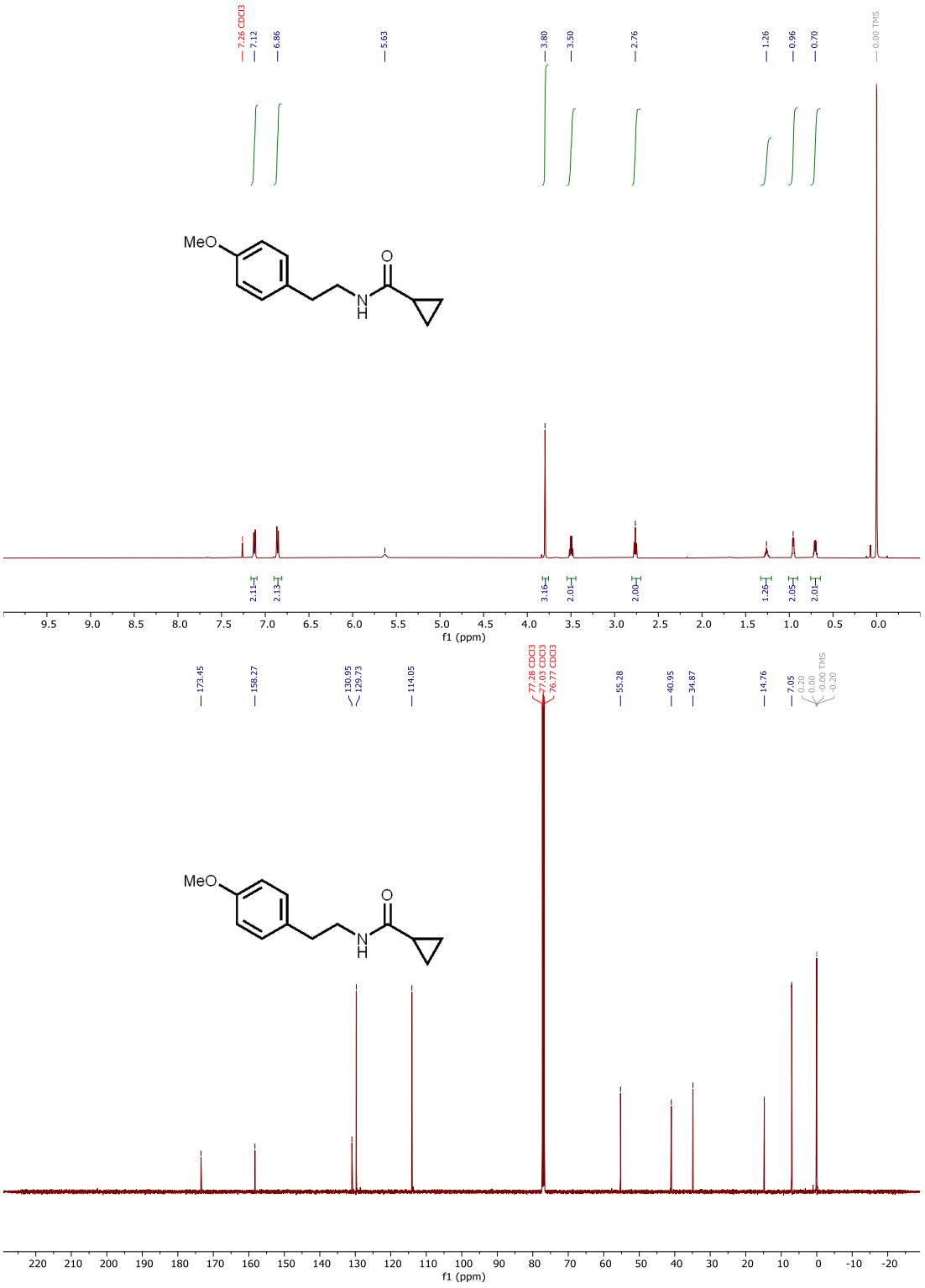

Figure S62. ^{1}H (500 MHz, $CDCl_3$) and ^{13}C (126 MHz, $CDCl_3$) NMR spectra of **22**.

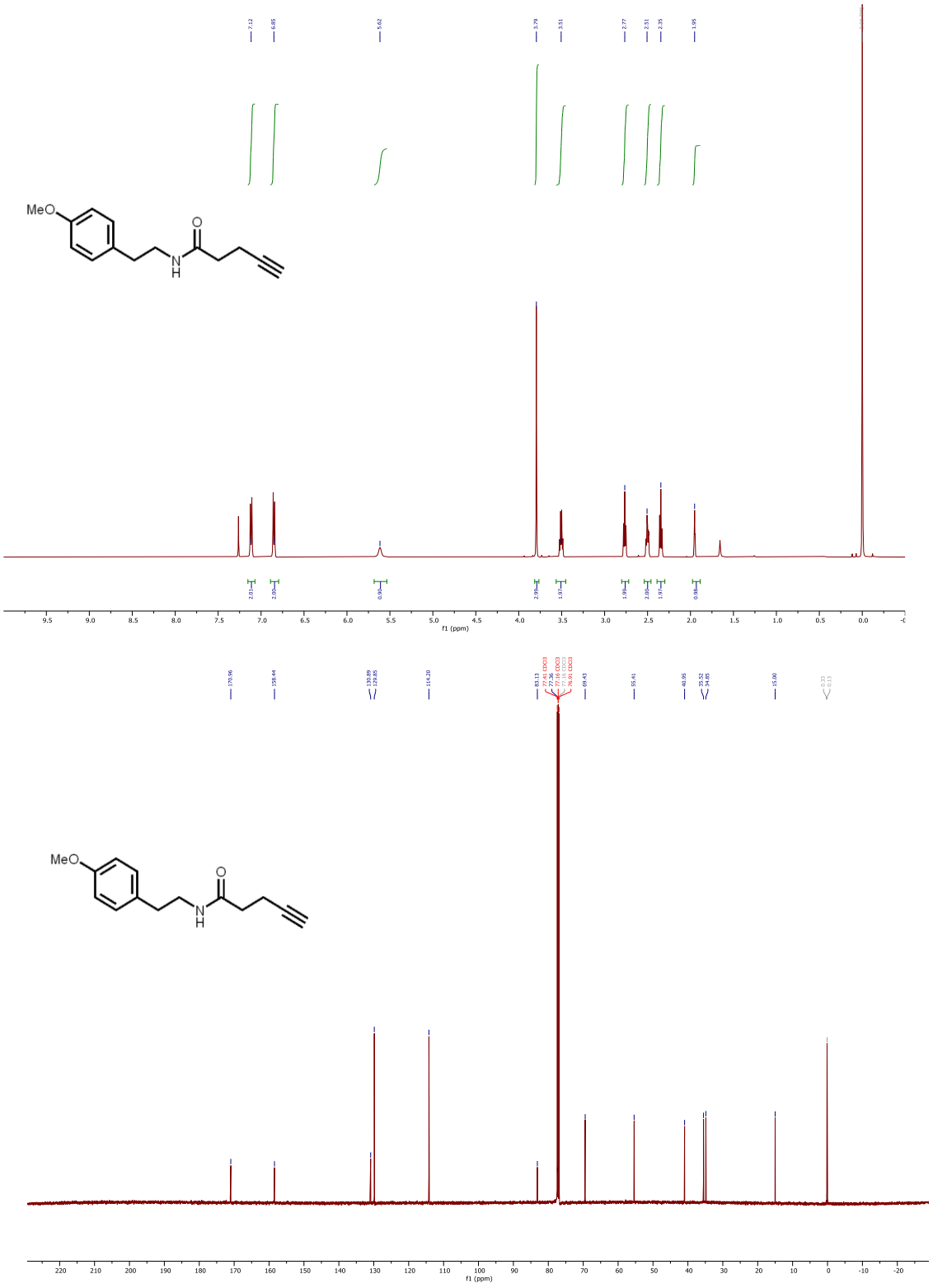

Figure S63. ^{1}H (500 MHz, $CDCl_3$) and ^{13}C (126 MHz, $CDCl_3$) NMR spectra of **23**.

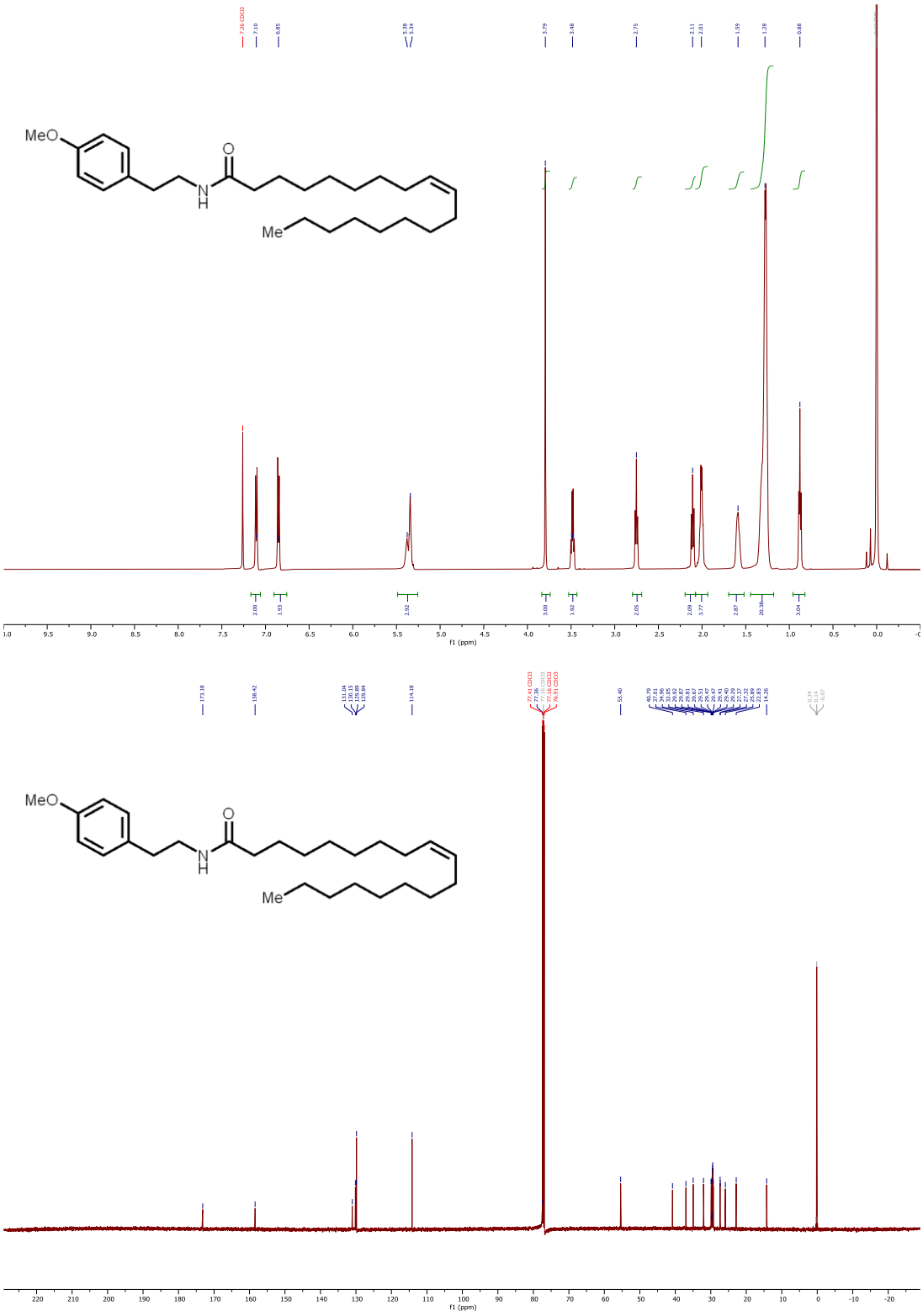

Figure S64. ^{1}H (500 MHz, $CDCl_3$) and ^{13}C (126 MHz, $CDCl_3$) NMR spectra of **24**.

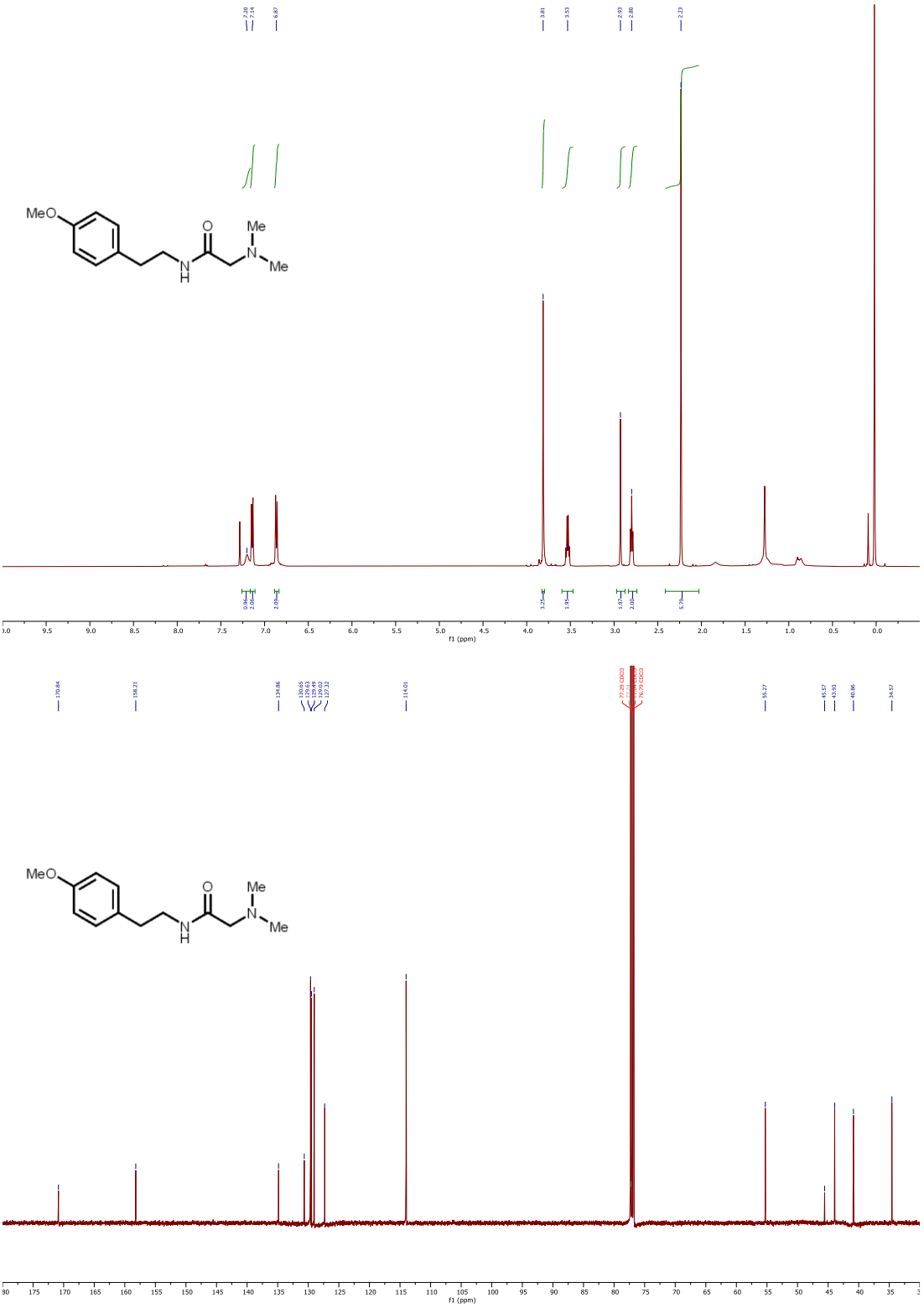

Figure S65. ^{1}H (500 MHz, $CDCl_3$) and ^{13}C (126 MHz, $CDCl_3$) NMR spectra of **25**.

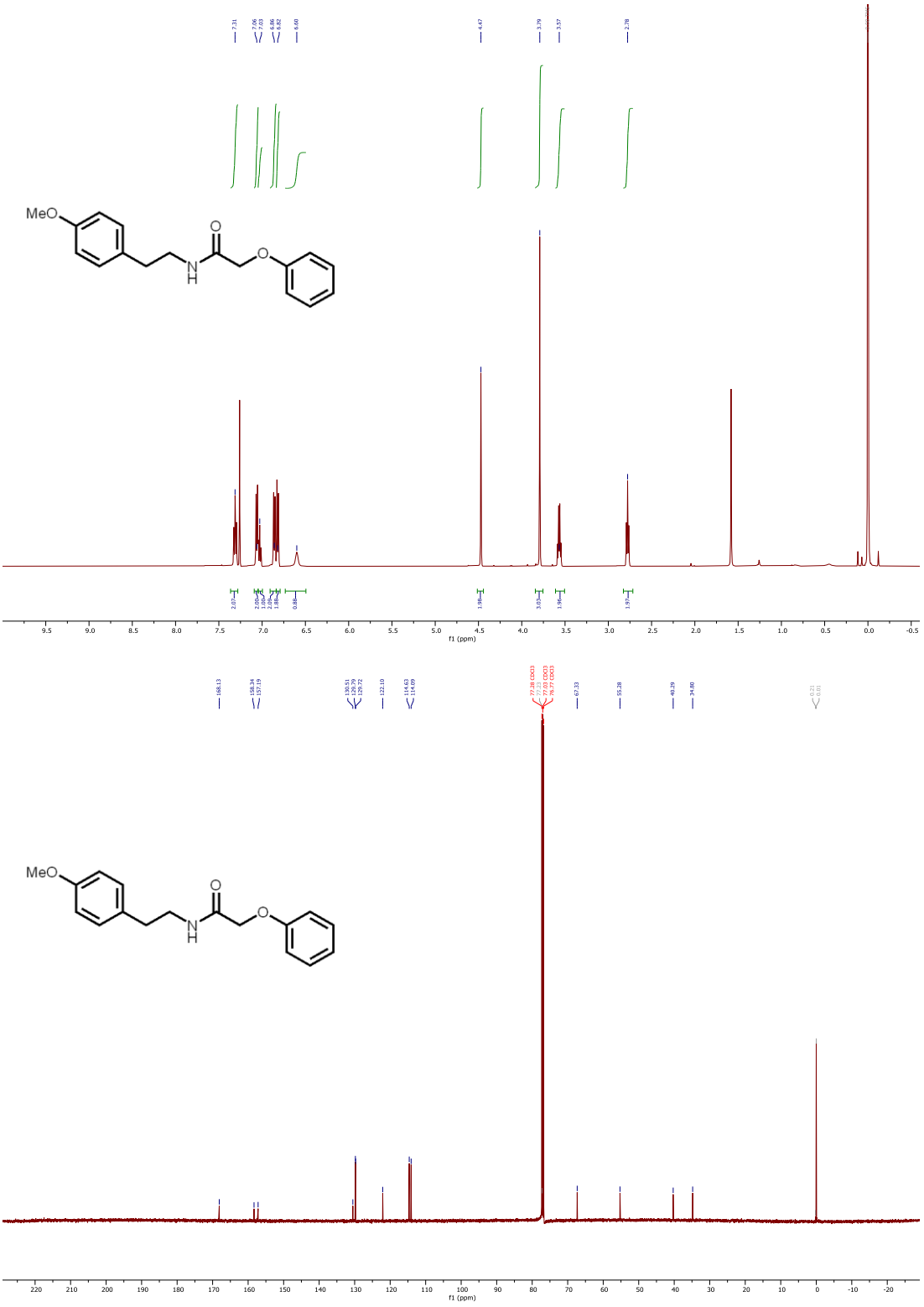

Figure S66. ^{1}H (500 MHz, $CDCl_3$) and ^{13}C (126 MHz, $CDCl_3$) NMR spectra of **26**.

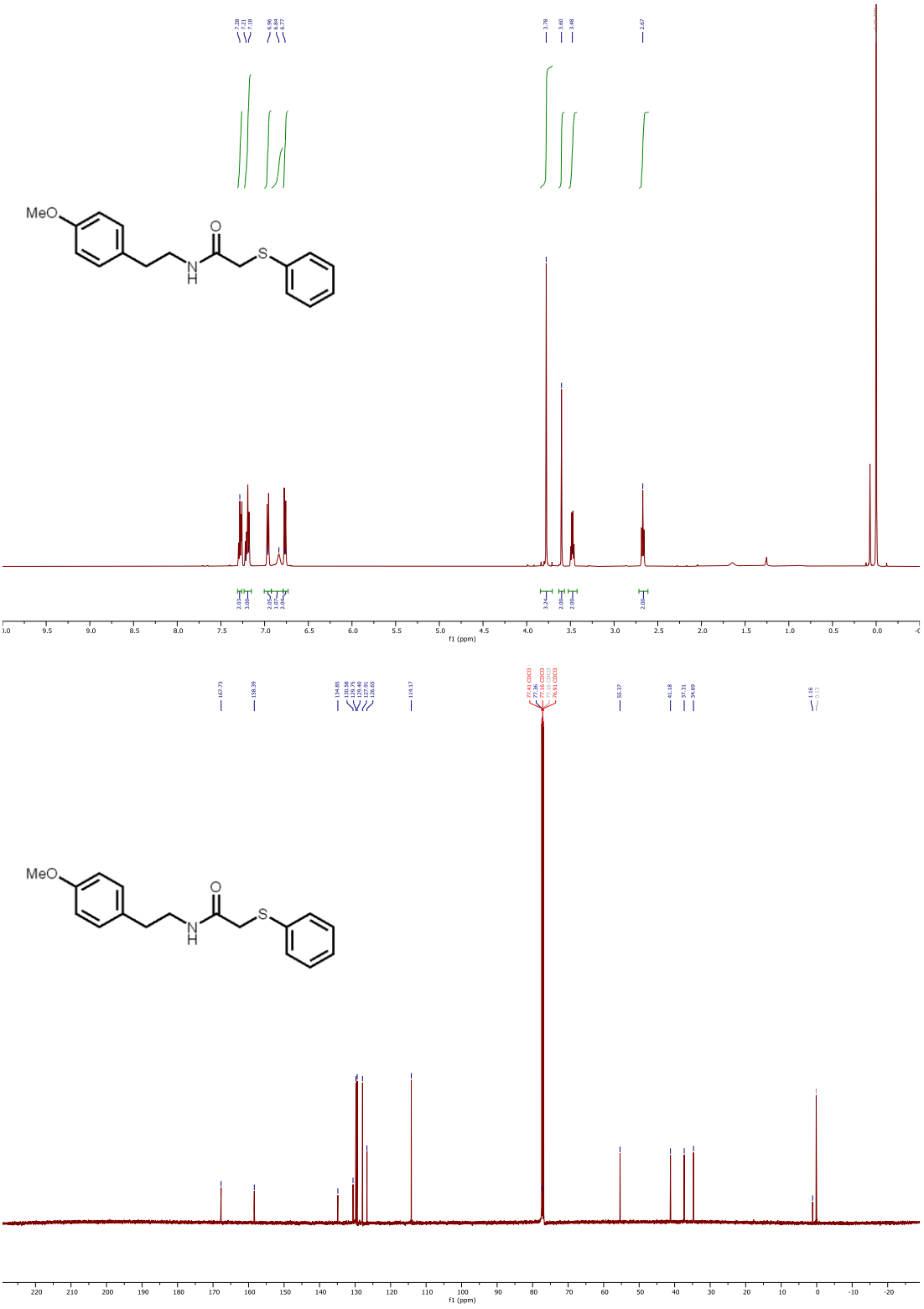

Figure S67. ^{1}H (500 MHz, $CDCl_3$) and ^{13}C (126 MHz, $CDCl_3$) NMR spectra of **27**.

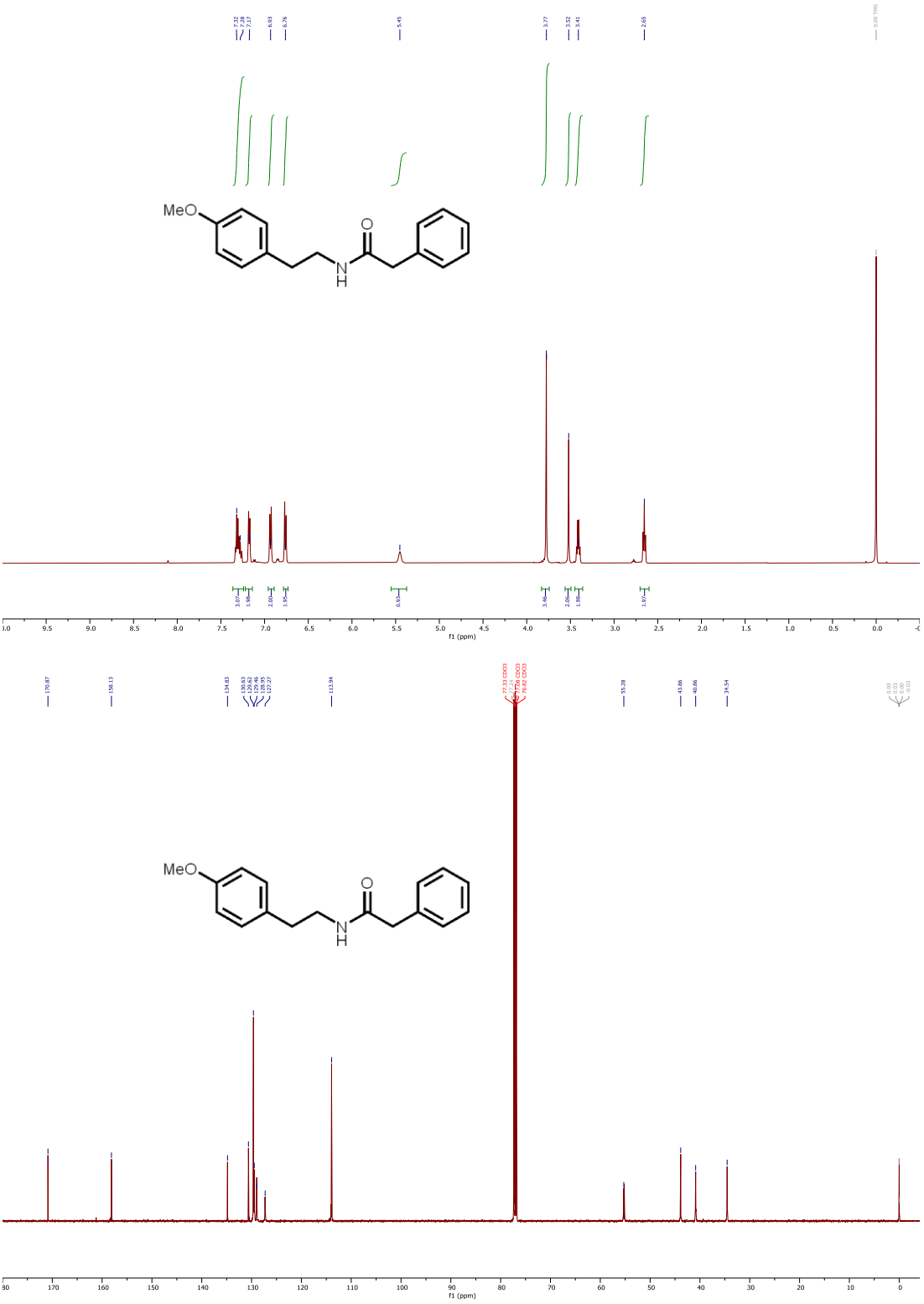

Figure S68. ^{1}H (500 MHz, $CDCl_3$) and ^{13}C (126 MHz, $CDCl_3$) NMR spectra of **28**.

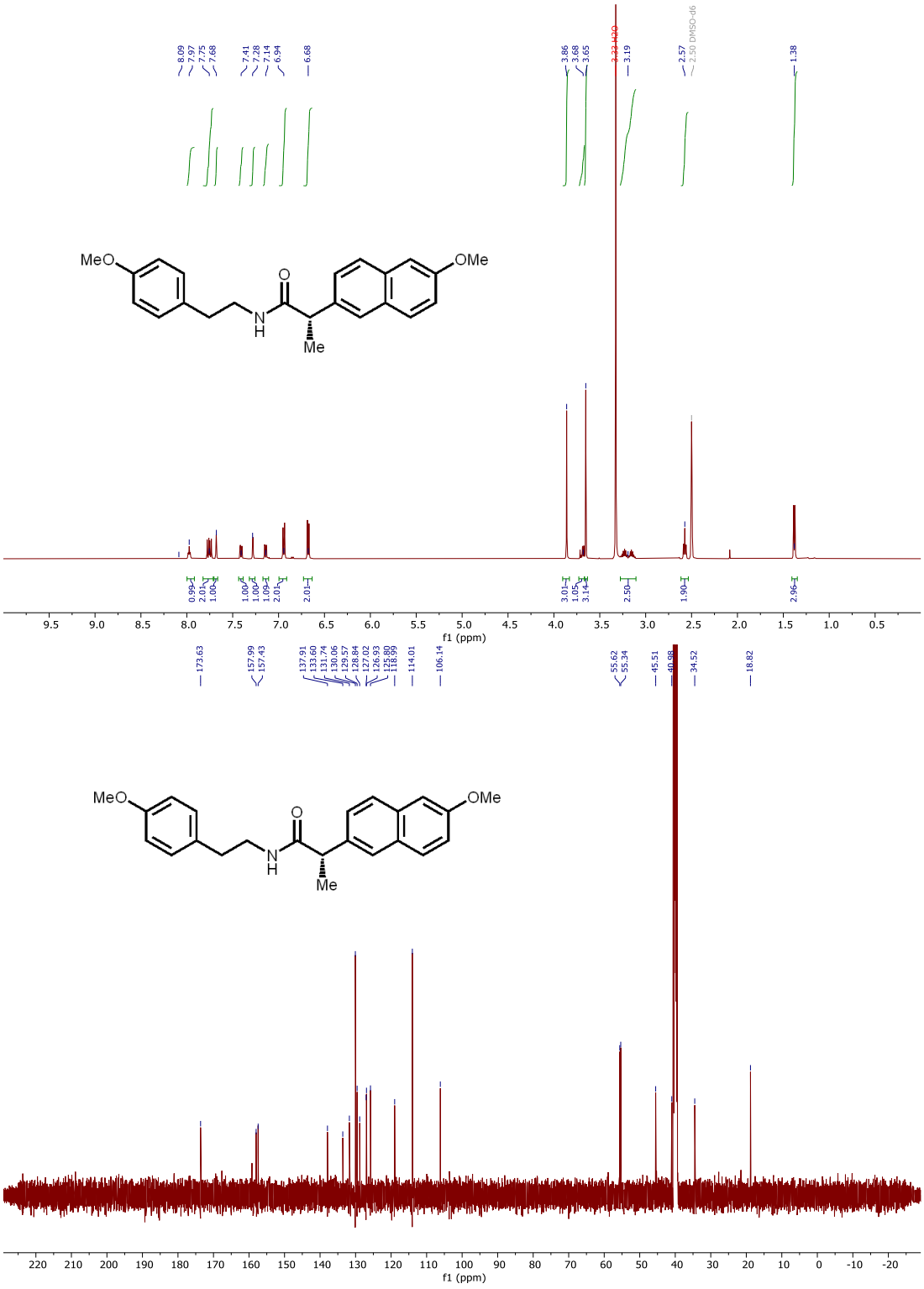

Figure S69. ^{1}H (500 MHz, $CDCl_3$:DMSO-d_6) and ^{13}C (126 MHz, DMSO-d_6) NMR spectra of **29**.

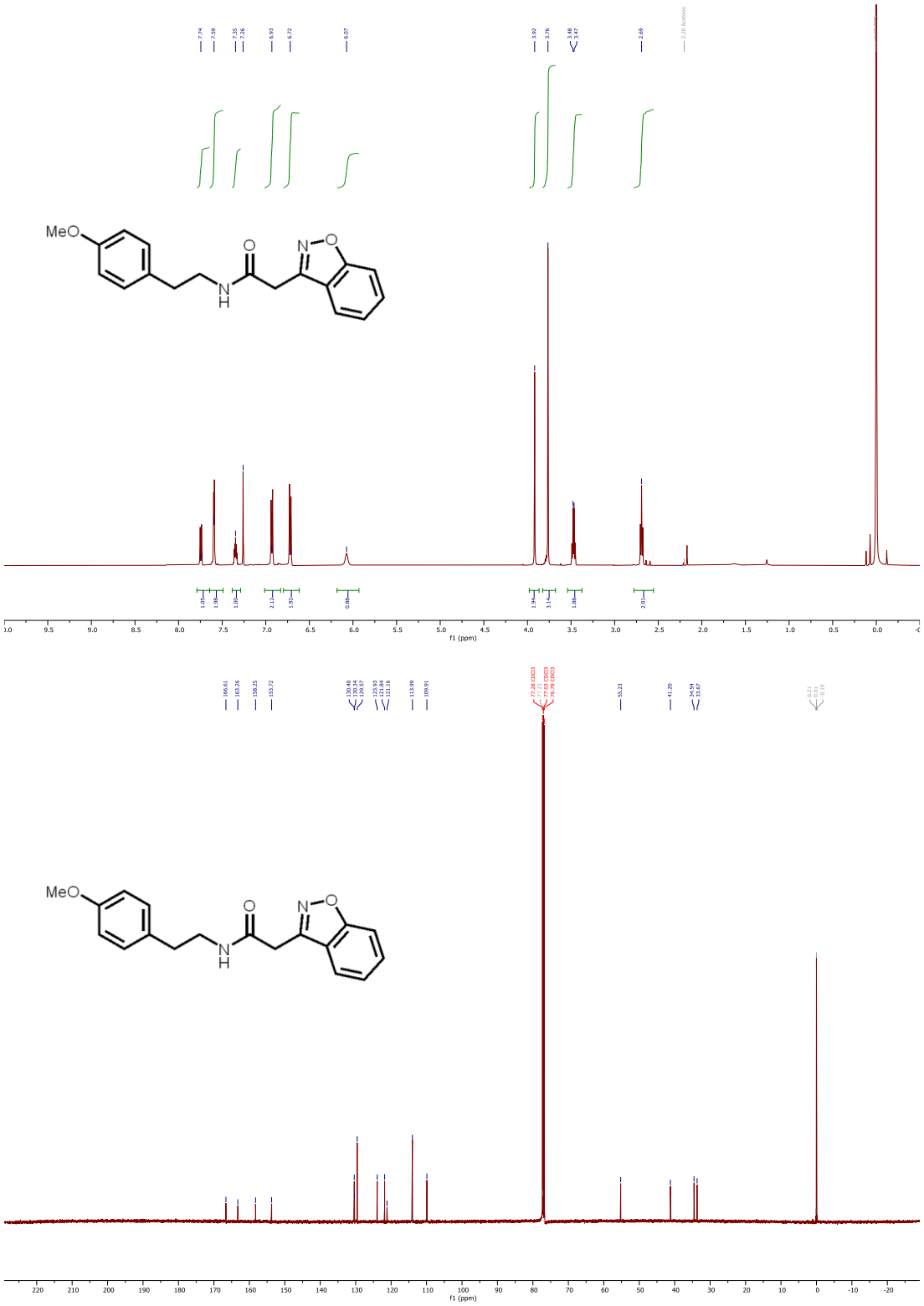

Figure S70. ^{1}H (500 MHz, $CDCl_3$) and ^{13}C (126 MHz, $CDCl_3$) NMR spectra of **30**.

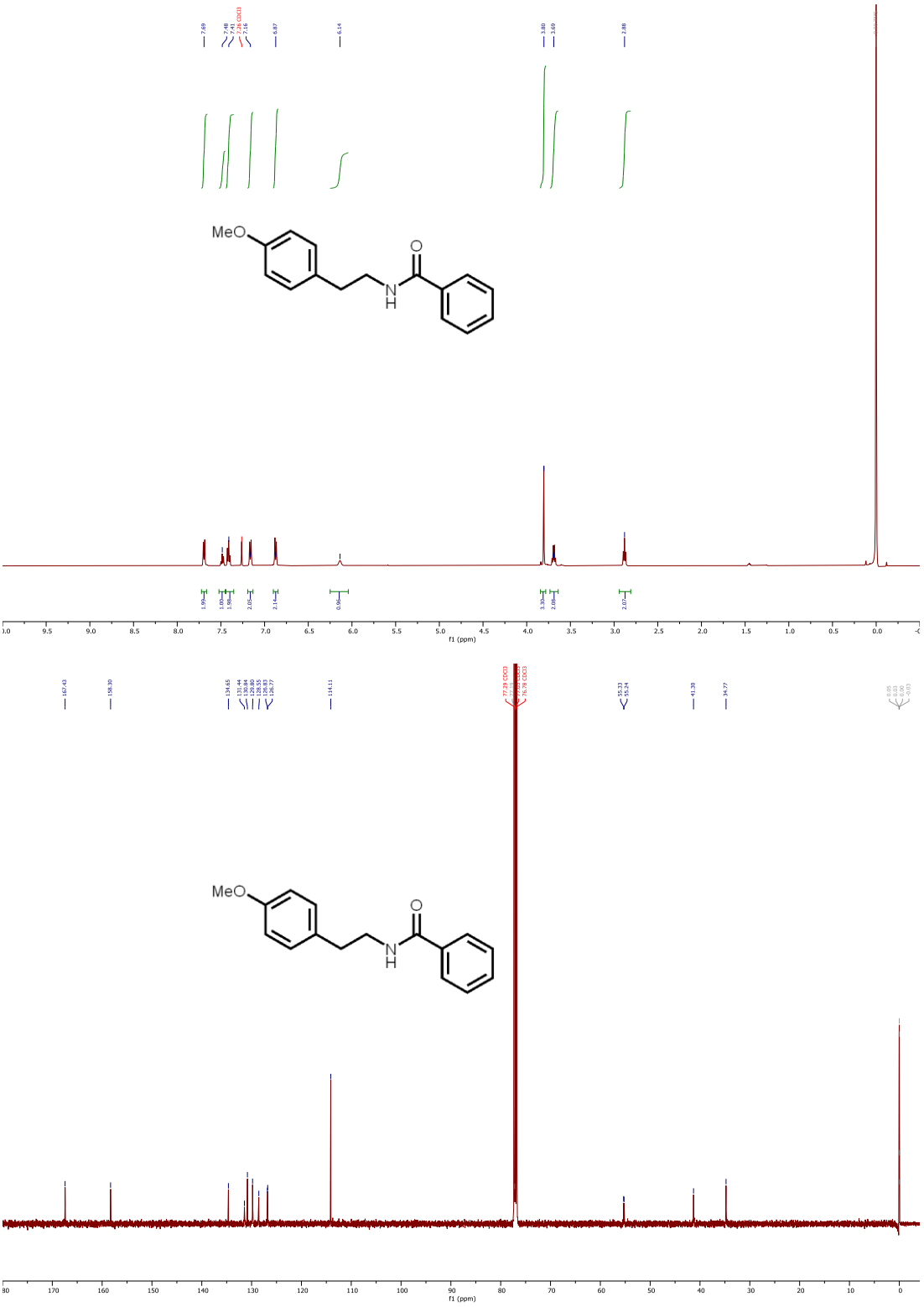

Figure S71. ^{1}H (500 MHz, $CDCl_3$) and ^{13}C (126 MHz, $CDCl_3$) NMR spectra of **31**.

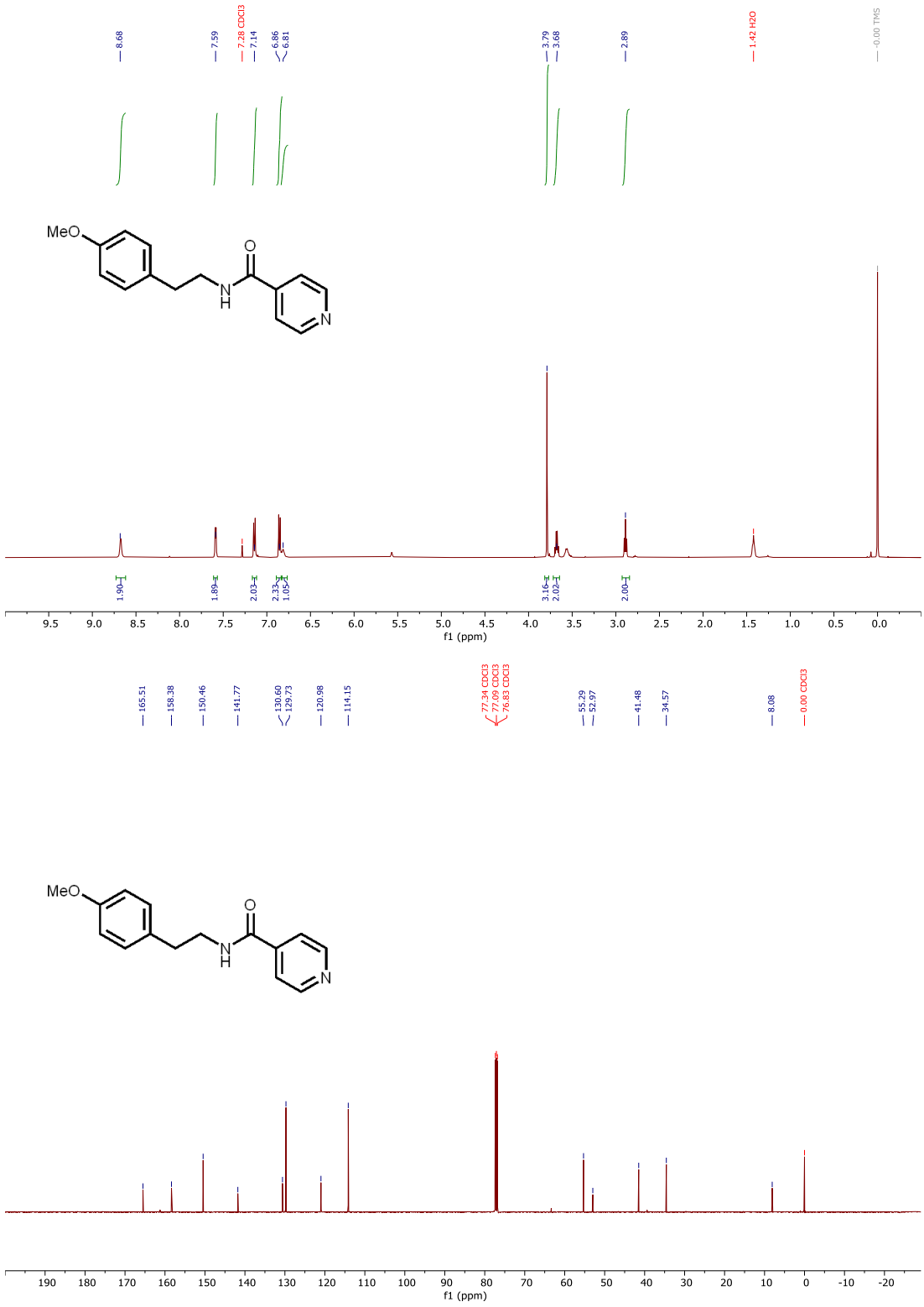

Figure S72. ^{1}H (500 MHz, $CDCl_3$) and ^{13}C (126 MHz, $CDCl_3$) NMR spectra of **32**.

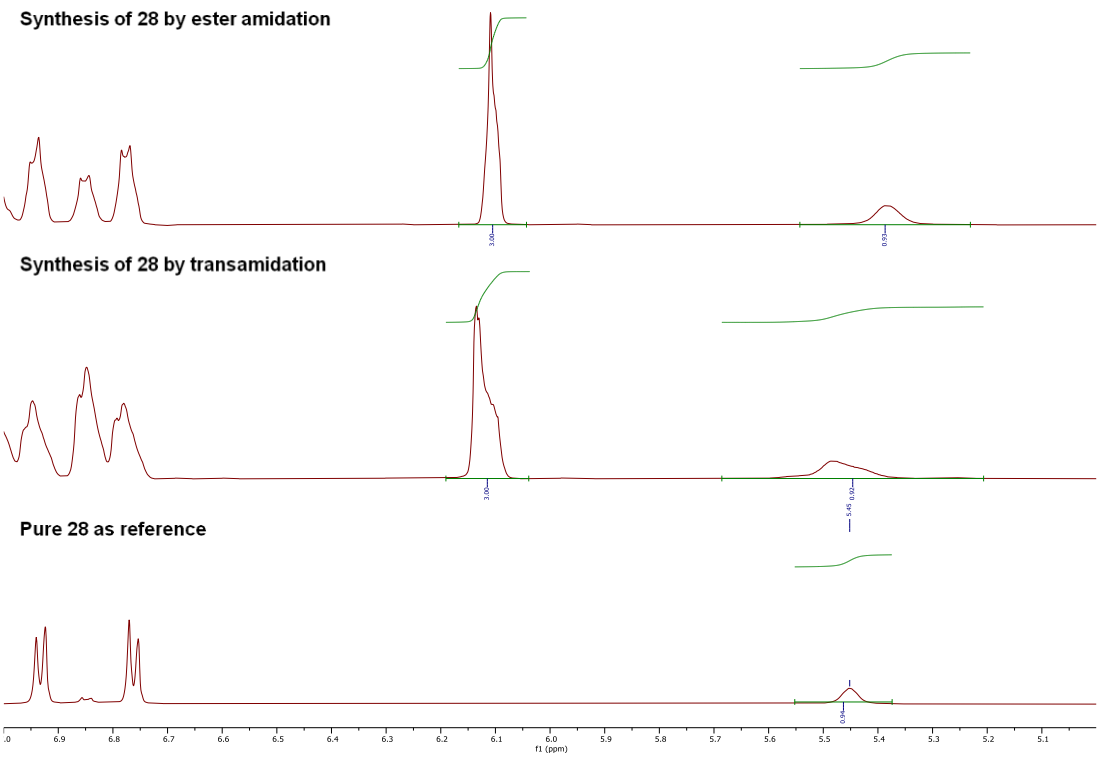

Figure S73. ^{1}H (500 MHz, $CDCl_3$) NMR spectra of **28** synthesized by transamidation and ester amidation compared to pure **28** as reference. The peak at 6.1 ppm corresponds to the internal standard of 1,3,5-trimethoxybenzene, and the peak at 5.4 ppm corresponds to the N–^{1}H of **28**.

References

(1) Shearer, G. C.; Chavan, S.; Bordiga, S.; Svelle, S.; Olsbye, U.; Lillerud, K. P. Defect Engineering: Tuning the Porosity and Composition of the Metal–Organic Framework UiO-66 via Modulated Synthesis. *Chem. Mater.* **2016**, *28* (11), 3749–3761. https://doi.org/10.1021/acs.chemmater.6b00602.

(2) Chen, F. E.; Pitt, T. A.; Okong'o, D. J.; Wetherbee, L. G.; Fuentes-Rivera, J. J.; Milner, P. J. A Structure–Activity Study of Aromatic Acid Modulators for the Synthesis of Zirconium-Based Metal–Organic Frameworks. *Chem. Mater.* **2022**, *34* (7), 3383–3394. https://doi.org/10.1021/acs.chemmater.2c00241.

(3) Noro, S.; Ochi, R.; Kubo, K.; Nakamura, T. Reversible Structural Changes of Strong Hydrogen Bond-Supported Organic Networks Using Neutral 3,5-Pyridinedicarboxylic Acid N-Oxide through Solvent Release/Uptake. *BCSJ* **2016**, *89* (12), 1503–1509. https://doi.org/10.1246/bcsj.20160266.

(4) Mautschke, H.-H.; Drache, F.; Senkovska, I.; Kaskel, S.; Llabrés i Xamena, F. X. Catalytic Properties of Pristine and Defect-Engineered Zr-MOF-808 Metal Organic Frameworks. *Catal. Sci. Technol.* **2018**, *8* (14), 3610–3616. https://doi.org/10.1039/C8CY00742J.

(5) Furukawa, H.; Gándara, F.; Zhang, Y.-B.; Jiang, J.; Queen, W. L.; Hudson, M. R.; Yaghi, O. M. Water Adsorption in Porous Metal–Organic Frameworks and Related Materials. *J. Am. Chem. Soc.* **2014**, *136* (11), 4369–4381. https://doi.org/10.1021/ja500330a.

(6) Ly, H. G. T.; Fu, G.; Kondinski, A.; Bueken, B.; De Vos, D.; Parac-Vogt, T. N. Superactivity of MOF-808 toward Peptide Bond Hydrolysis. *J. Am. Chem. Soc.* **2018**, *140* (20), 6325–6335. https://doi.org/10.1021/jacs.8b01902.

(7) Jerozal, R. T.; Pitt, T. A.; MacMillan, S. N.; Milner, P. J. High-Concentration Self-Assembly of Zirconium- and Hafnium-Based Metal–Organic Materials. *J. Am. Chem. Soc.* **2023**, *145* (24), 13273–13283. https://doi.org/10.1021/jacs.3c02787.

(8) Basu, O.; Mukhopadhyay, S.; Laha, S.; Das, S. K. Defect Engineering in a Metal–Organic Framework System to Achieve Super-Protonic Conductivity. *Chem. Mater.* **2022**, *34* (15), 6734–6743. https://doi.org/10.1021/acs.chemmater.2c00654.

(9) Romero-Muñiz, I.; Romero-Muñiz, C.; del Castillo-Velilla, I.; Marini, C.; Calero, S.; Zamora, F.; Platero-Prats, A. E. Revisiting Vibrational Spectroscopy to Tackle the Chemistry of Zr_6O_8 Metal-Organic Framework Nodes. *ACS Appl. Mater. Interfaces* **2022**, *14* (23), 27040–27047. https://doi.org/10.1021/acsami.2c04712.

(10) Gu, Y.; Ye, G.; Xu, W.; Zhou, W.; Sun, Y. Creation of Active Sites in MOF-808(Zr) by a Facile Route for Oxidative Desulfurization of Model Diesel Oil. *ChemistrySelect* **2020**, *5* (1), 244–251. https://doi.org/10.1002/slct.201903376.

(11) Yang, D.; Bernales, V.; Islamoglu, T.; Farha, O. K.; Hupp, J. T.; Cramer, C. J.; Gagliardi, L.; Gates, B. C. Tuning the Surface Chemistry of Metal Organic Framework Nodes: Proton Topology of the Metal-Oxide-Like Zr_6 Nodes of UiO-66 and NU-1000. *J. Am. Chem. Soc.* **2016**, *138* (46), 15189–15196. https://doi.org/10.1021/jacs.6b08273.

(12) Grün, A.; Milen, M.; Földesi, T.; Ábrányi-Balogh, P.; Drahos, L.; Keglevich, G. Microwave-Assisted Amidation of Arylacetic Acids by Reaction with 2-Aryl-Ethylamines. *Synth. Commun.* **2013**, *43* (11), 1491–1498. https://doi.org/10.1080/00397911.2011.642925.

(13) He, G.; Zhang, S.-Y.; Nack, W. A.; Li, Q.; Chen, G. Use of a Readily Removable Auxiliary Group for the Synthesis of Pyrrolidones by the Palladium-Catalyzed Intramolecular Amination of Unactivated γ C(Sp^3)□H Bonds. *Angew. Chem. Int. Ed.* **2013**, *52* (42), 11124–11128. https://doi.org/10.1002/anie.201305615.

(14) Lundberg, H.; Adolfsson, H. Hafnium-Catalyzed Direct Amide Formation at Room Temperature. *ACS Catal.* **2015**, *5* (6), 3271–3277. https://doi.org/10.1021/acscatal.5b00385.
(15) Nordstrøm, L. U.; Vogt, H.; Madsen, R. Amide Synthesis from Alcohols and Amines by the Extrusion of Dihydrogen. *J. Am. Chem. Soc.* **2008**, *130* (52), 17672–17673. https://doi.org/10.1021/ja808129p.
(16) Kim, K.; Kang, B.; Hong, S. H. N-Heterocyclic Carbene-Based Well-Defined Ruthenium Hydride Complexes for Direct Amide Synthesis from Alcohols and Amines under Base-Free Conditions. *Tetrahedron* **2015**, *71* (26), 4565–4569. https://doi.org/10.1016/j.tet.2015.02.016.
(17) Gao, Y.; Liu, J.; Li, Z.; Guo, T.; Xu, S.; Zhu, H.; Wei, F.; Chen, S.; Gebru, H.; Guo, K. Dichloroimidazolidinedione-Activated Beckmann Rearrangement of Ketoximes for Accessing Amides and Lactams. *J. Org. Chem.* **2018**, *83* (4), 2040–2049. https://doi.org/10.1021/acs.joc.7b02983.
(18) Gernigon, N.; Al-Zoubi, R. M.; Hall, D. G. Direct Amidation of Carboxylic Acids Catalyzed by Ortho-Iodo Arylboronic Acids: Catalyst Optimization, Scope, and Preliminary Mechanistic Study Supporting a Peculiar Halogen Acceleration Effect. *J. Org. Chem.* **2012**, *77* (19), 8386–8400. https://doi.org/10.1021/jo3013258.
(19) Field, R. A.; Haines, A. H.; Chrystal, E. J. T.; Luszniak, M. C. Histidines, Histamines and Imidazoles as Glycosidase Inhibitors. *Biochem. J.* **1991**, *274* (3), 885–889. https://doi.org/10.1042/bj2740885.
(20) Al-Riyami, L.; Pineda, M. A.; Rzepecka, J.; Huggan, J. K.; Khalaf, A. I.; Suckling, C. J.; Scott, F. J.; Rodgers, D. T.; Harnett, M. M.; Harnett, W. Designing Anti-Inflammatory Drugs from Parasitic Worms: A Synthetic Small Molecule Analogue of the Acanthocheilonema Viteae Product ES-62 Prevents Development of Collagen-Induced Arthritis. *J. Med. Chem.* **2013**, *56* (24), 9982–10002. https://doi.org/10.1021/jm401251p.
(21) Tam, E. K. W.; Rita; Liu, L. Y.; Chen, A. 2-Furanylboronic Acid as an Effective Catalyst for the Direct Amidation of Carboxylic Acids at Room Temperature. *Eur. J. Org. Chem.* **2015**, *2015* (5), 1100–1107. https://doi.org/10.1002/ejoc.201403468.
(22) Gockel, S. N.; Hull, K. L. Chloroform as a Carbon Monoxide Precursor: In or Ex Situ Generation of CO for Pd-Catalyzed Aminocarbonylations. *Org. Lett.* **2015**, *17* (13), 3236–3239. https://doi.org/10.1021/acs.orglett.5b01385.
(23) Balalaie, S.; Mahdidoust, M.; Eshaghi-Najafabadi, R. 2-(1H-Benzotriazole-1-Yl)-1,1,3,3-Tetramethyluronium Tetrafluoroborate as an Efficient Coupling Reagent for the Amidation and Phenylhydrazation of Carboxylic Acids at Room Temperature. *JICS* **2007**, *4* (3), 364–369. https://doi.org/10.1007/BF03245987.
(24) Tan, Y.; Yuan, W.; Gong, L.; Meggers, E. Aerobic Asymmetric Dehydrogenative Cross-Coupling between Two C-H Groups Catalyzed by a Chiral-at-Metal Rhodium Complex. *Angew. Chem. Int. Ed.* **2015**, *54* (44), 13045–13048. https://doi.org/10.1002/anie.201506273.
(25) Wright, A. E.; Roth, G. P.; Hoffman, J. K.; Divlianska, D. B.; Pechter, D.; Sennett, S. H.; Guzmán, E. A.; Linley, P.; McCarthy, P. J.; Pitts, T. P.; Pomponi, S. A.; Reed, J. K. Isolation, Synthesis, and Biological Activity of Aphrocallistin, an Adenine-Substituted Bromotyramine Metabolite from the Hexactinellida Sponge Aphrocallistes Beatrix. *J. Nat. Prod.* **2009**, *72* (6), 1178–1183. https://doi.org/10.1021/np900183v.
(26) Neochoritis, C. G.; Zarganes-Tzitzikas, T.; Stotani, S.; Dömling, A.; Herdtweck, E.; Khoury, K.; Dömling, A. Leuckart–Wallach Route Toward Isocyanides and Some Applications. *ACS Comb. Sci.* **2015**, *17* (9), 493–499. https://doi.org/10.1021/acscombsci.5b00066.

(27) Ogiyama, T.; Yonezawa, K.; Inoue, M.; Katayama, N.; Watanabe, T.; Yoshimura, S.; Gotoh, T.; Kiso, T.; Koakutsu, A.; Kakimoto, S.; Shishikura, J. Discovery of an 8-Methoxytetrahydroisoquinoline Derivative as an Orally Active N-Type Calcium Channel Blocker for Neuropathic Pain without CYP Inhibition Liability. *Bioorg. Med. Chem.* **2015**, *23* (15), 4638–4648. https://doi.org/10.1016/j.bmc.2015.05.053.

(28) Urbani, P.; Cavallo, P.; Cascio, M. G.; Buonerba, M.; De Martino, G.; Di Marzo, V.; Saturnino, C. New Metabolically Stable Fatty Acid Amide Ligands of Cannabinoid Receptors: Synthesis and Receptor Affinity Studies. *Bioorg. Med. Chem. Lett.* **2006**, *16* (1), 138–141. https://doi.org/10.1016/j.bmcl.2005.09.023.

(29) Saxena, A. K.; Pandey, G.; Gupta, S.; Singh, A. B.; Srivastava, A. K. Synthesis of Protein Tyrosine Phosphatase 1B Inhibitors: Model Validation and Docking Studies. *Bioorg. Med. Chem. Lett.* **2009**, *19* (8), 2320–2323. https://doi.org/10.1016/j.bmcl.2009.02.058.

(30) Andrus, M. B.; Harper, K. C.; Christiansen, M. A.; Binkley, M. A. Phase-Transfer Catalyzed Asymmetric Arylacetate Alkylation. *Tetrahedron Lett.* **2009**, *50* (31), 4541–4544. https://doi.org/10.1016/j.tetlet.2009.05.090.

(31) Zhu, C.; Wei, W.; Du, P.; Wan, X. Metal Free Amide Synthesis via Carbon–Carbon Bond Cleavage. *Tetrahedron* **2014**, *70* (51), 9615–9620. https://doi.org/10.1016/j.tet.2014.11.003.